Doctoral Dissertation
Doctoral Program in Materials Science and Technology (32nd Cycle)

Advanced joined materials development and their shear strength evaluation for aerospace, energy and structural applications

Stefano De la Pierre des Ambrois
* * * * * *

Supervisor
Prof. Monica Ferraris

Doctoral Examination Committee:
Prof. Daniel Milanese, Referee, Università degli Studi di Parma
Prof. Alberto Ortona, Referee, University of Applied Sciences and Arts of Southern Switzerland

Politecnico di Torino

I hereby declare that, the contents and organisation of this dissertation constitute my own original work and does not compromise in any way the rights of third parties, including those relating to the security of personal data.

Stefano De la Pierre des Ambrois
Turin, April 29, 2020

Summary

- Development of sandwich structures for aerospace applications:

Joining of CFRP honeycombs to glass-ceramic mirrors for satellites and other aerospace components. Joining material selection, characterization and optimization, based on the aerospace environment requirements. Scale-up of the joining process from small samples to large sandwich structures. Mechanical characterization of joined components with shear tests and tensile tests, before and after ageing in relevant conditions. Surface modification of the substrates to improve their joint strength.

- Torsion test: a method to measure the shear strength of joined components.

Torsion test of glass ceramic sealant materials for solid oxide fuel/electrolysis cells (SOFCs/SOECs), at room and application relevant temperatures. Torsion test of adhesively bonded steel, steel-to-glass and ceramic joined components for structural applications. Comparison between torsion test and other lap shear tests.

Keywords: Joining, Torsion test, Shear Strength, Sandwich Structure, Adhesive, Glass-ceramic.

Acknowledgment

The results of the PhD thesis have been carried out in collaboration with:

GLANCE, DISAT, Politecnico di Torino: Monica Ferraris, Milena Salvo, Valentina Casalegno, Federico Smeacetto, Marco Sangermano, Stefano Rizzo, Antonio Favero and all the people from GLANCE group

DIMEAS, Politecnico di Torino: Luca Goglio, Davide Paolino

Università di Palermo: Antonino Valenza, Tommaso Scalici

Thales Alenia Space, Cannes (France): Olivier Damiano, Laurence Cornillon

Forschungszentrum Jülich (Germany): Jürgen Malzbender

Slovak Academy of Sciences (Slovakia): Peter Tatarko and all the people from the Institute of Material Research (Kosice)

University of Perugia: Andrea Terenzi

Department of Chemistry, UniTo: Ingrid Corazzari

Valentin Giglia and Julien Burdloff-Berain

DTU (Denmark): Ilaria Ritucci

TABLE OF CONTENTS

1. Introduction

1.1. Sandwich structures for aerospace applications

1.1.1. Joining of sandwich structures

In aerospace applications, a growing demand is to make structures lighter, while optimizing the stiffness and strength. To do so, the sandwich architecture appears to be the most efficient design, and the main objective is then to develop ultra-stable and low weight structures, based on such architecture. For this reason, key aspects for materials employed are light-weight, high-strength, high-stiffness and fatigue resistance.

Carbon based composite materials, and more precisely sandwich structures, have always been widely used in the space industry to build satellites, thanks to their unique mass/properties ratio [1]. In the last years Carbon/carbon composites (C/C) have been selected as key materials for space instruments because of their excellent properties, such as thermal expansion coefficient close to zero, very high thermo-elastic stability, low density and moisture insensitivity [2].

A promising alternative to C/C are Carbon Fiber Reinforced Polymers composites (CFRPs). CFRPs honeycomb (HC) could replace C/C in sandwich structures with ultrastable glass-ceramic skins such as Zerodur™ [3]. CFRPs are a recent introduction in the aerospace industry to build satellite components, thanks to their unique mass/properties ratio: however, performances of satellite components are highly dependent from the adhesives used to assembly the sandwich structure.

For satellite applications, environmental conditions can be extreme and severe thermal cycling can occur with exposure and non-exposure to the sun light, thus the main requirement for the whole structure is an excellent thermal stability to avoid signal distortions.

To fully benefit the potential given by Zerodur™ and CFRP, it is important to select a joining material having low thermal expansion coefficient, together with a sound mechanical strength and a curing temperature suitable for both CFRP and Zerodur™. Last but not least, the adhesive should be easy to apply in a cleanroom environment and on square meter size components.

The multiple advantages of adhesives as joining material are, to cite a few, the overall joined structure weight reduction, the absence of holes for bolts/screws, etc. Moreover, bonding is required not only during manufacturing, but also during components' repair: the use of adhesives facilitates the removal of damaged parts and their replacing.

Inorganic solutions applicable to these sandwiches structures (i.e. lead/bismuth based low temperature glasses, cements such as Vubonite™ (phosphate cement, University of Brussels) and Keraflex (cement, MAPEI) were not suitable, mainly due to the high processing temperature in case of selected glasses and to the low adhesion and consequently low mechanical strength of joints in case of cements.

Existing solutions (i.e. commercial adhesives) have some drawbacks too: first of all they are not specifically designed to join CFRP and Zerodur™, but they are rather developed for joining of aluminum honeycombs to carbon/epoxy or C/C skins [4].

For this specific case, the existing adhesives, for the aerospace applications, have curing temperatures too high and detrimental for the mechanical properties of both CFRP and Zerodur™. Moreover their CTE, higher than those of CFRP and Zerodur™, may cause distortions of the sandwich structure due to thermal and/or moisture expansion effects. [5, 6]

The objective of this work was to develop an advanced and high performant adhesive, able to provide suitable mechanical strength to the Zerodur™ - CFRP - Zerodur™ sandwich structures, coupled with a suitable thermo-mechanical

stability within the operative range and feasibility of the joint on large flat and curved surfaces.

1.1.2. CFRP surface modification

The following text, data and images are an adaptation of the results that were submitted in the article: [7]

CFRPs (Carbon Fiber Reinforced Plastics) are widely used in several applications ranging from sporting goods such as golf club, tennis racket and fishing rod, to aerospace, racing cars, drones, unmanned autonomous vehicles and other transportation fields because of their unparalleled mechanical strength coupled to low density [8]. Their joining and integration is a key issue and a wide range of solutions, mainly based on adhesive bonding, are available in the literature [9].

Adhesive bonding is the most popular option, first of all because adhesives can be used at temperatures compatible with CRFP matrices (about 150-200 °C), but also because of the robustness of the procedure, the possibility of disassembly in case of maintenance and their excellent fatigue life [10]. The use of adhesive allows saving weight by eliminating fasteners and introducing a more uniform load transfer: stress distribution is more uniform than with other conventional methods of joining [11], the load is transmitted from one CFRP to the other one through the adhesive layer in the overlap region, therefore the adhesive works as a medium for load transmission, which is important to achieve high strength joints.

There are different strategies to enhance the joint strength, starting from the proper selection of the adhesives [12], the adhesive thickness [13], and the surface preparation [14], among others.

The surface preparation is the most important parameter to improve the joint strength: mechanical abrasion is one of the most widely used surface treatment

[15], while a totally new approach is the chemical etching of the CFRP surface to promote the adhesive penetration into it, thus improving the interaction adhesive/CFRP, also by changing the CFRP surface tension. Other methods to reinforce joints have been also proposed, among them Comeld™ and other similar options from TWI [16], or bio-mimetical approaches [17].

In this work, we propose an original method to increase the mechanical strength of adhesive joined CFRP by etching of their surface: the idea is to chemically remove only a few microns of the matrix while keeping the carbon fibers unaffected.

The chemical etching proposed here was inspired by some works aimed to recycle CFRP by dissolving their polymeric matrix [18] and by the international standards UNI EN 2564 [19] and ASTM D 3171 – 99 [20], used to completely dissolve the CFRP matrix in order to measure their fiber content. In [18] authors used potassium phosphate tribasic (K_3PO_4) as a catalyst and benzyl alcohol as a solvent to depolymerize cured epoxy resin and unsaturated polyester resin in CFRP: e.g. it took up to 8 hours to completely dissolve a tennis racket.

In ASTM D 3171 – 99 [20] and UNI EN 2564 [19], methods based on sulfuric acid (96-98 %) and hydrogen peroxide (30-50%), nitric acid (70%), ethylene glycol/potassium hydroxide or hydrochloric acid (5-10%), heated up to 160 °C, according to the given procedures, were proposed to measure the composites' fiber content.

The original etching procedure described in the following parts of this thesis is based on controlled sulfuric acid etching on the surface of CFRP. After surface etching the CFRP were joined and the effect of etching time and temperature on joint strength was evaluated [7].

References

(1.1. Sandwich structures for aerospace applications)

1. C. Scarponi. Carbon–carbon composites in aerospace engineering, Advanced Composite Materials for Aerospace Engineering, 2016, Pages 385-412.

2. Z.S. Toor, Space Applications of Composite Materials, Journal of Space Technology, Vol. 8, No. 1, 2018

3. R. Edeson, G.S. Aglietti, A.R.L. Tatnall. Conventional stable structures for space optics: The state of the art. Acta Astronautica. Vol. 66, 2010, Pages 13-32

4. A. Pramanik, A. K. Basak, Y. Dong, P. K. Sarker, M. S. Uddin, G. Littlefair, A. R. Dixit, S. Chattopadhyaya. Joining of carbon fibre reinforced polymer (CFRP) composites and aluminium alloys – A review. Composites Part A Volume 101, 2017, Pages 1-29

5. J Wang , H Jiang , Q Guo , L Liu , J Song , S Bai, S Qiao. High-Temperature Joining of Carbon/Carbon Composites by an Organic Resin Adhesive. Journal of Adhesion Science and Technology 23 (2009) 115–123;

6. M Wang, X Hu, X Xu, Z Yun, J Liu, H Du, A Guo. A user-friendly heat-resistant modified polymer-based adhesive for joining and repair of carbon/carbon composites. Materials and Design, Volume 86, 2015, Pages 709-713

7. S. De La Pierre, V. Giglia, M. Sangermano, L. Cornillon, O. Damiano, M. Ferraris. Etching of Carbon Fiber-Reinforced Plastics to Increase Their Joint Strength. Journal of Materials Engineering and Performance. Vol. 29 (2020), pages 242–250

8. S-S Yao, F-L Jin, K.Y. Rhee, D. Hui, S-J Park. Recent advances in carbon-fiber-reinforced thermoplastic composites: A review. Composites Part B: Engineering, Volume 142, 2018, Pages 241-250.

9. S. Budhe, M.D. Banea, S. de Barros, L.F.M. da Silva, An updated review of adhesively bonded joints in composite materials, International Journal of Adhesion and Adhesives, Volume 72, 2017, Pages 30-42.

10. A. Pramanik, A.K. Basak, Y. Dong, P.K. Sarker, M.S. Uddin, G. Littlefair, A.R. Dixit, S. Chattopadhyaya. Joining of carbon fibre reinforced polymer (CFRP) composites and aluminium alloys – A review, Composites Part A: Applied Science and Manufacturing, Volume 101, 2017, Pages 1-29.

11. J.J. Tierney, J.W. Gillespie, P.-E. Bourban, 2.31 - Joining of Composites, Editor(s): Anthony Kelly, Carl Zweben, Comprehensive Composite Materials, Pergamon, 2000, Pages 1029-1047.

12. Nunes, S.L.S., Campilho, R.D.S.G., da Silva, F.J.G., de Sousa, C.C.R.G., Fernandes T.A.B., Banea M.D., da Silva, L.F.M. (2016) Journal of Adhesion 92(7-9): 610-634.

13. Banea, M.D., da Silva, L.F.M., Campilho, R.D.S.G. (2015) Journal of Adhesion 91(5): 331-34.

14. Budhe, S., Ghumatkar, A., Birajdar, N., Banea, M.D. (2015) Applied Adhesion Science 3: 1-10.

15. Hunter, R., Ibacache, N., Moller, J., Betancourt, R., Mora, T., Diez, E., Pavez, B. (2012) Adhesion of Single Lap Joints, Journal of Adhesion 88: 376-390.

16. Faye Smith. Comeld™: An Innovation in Composite to Metal Joining, Materials Technology, (2005) 20:2, 91-96.

17. Avgoulas 2016, "Biomimetic-inspired CFRP to perforated steel joints" Composite Structures 152 (2016) 929–938

18. M. Nakagawa, H. Kuriya, K. Shibata "Characterization of CFRP Using Recovered Carbon Fibers from Waste CFRP", Hitachi Chemical Co., Ltd., Ibaraki - Proceedings of the 5th ISFR (October 11-14, 2009, Chengdu, China).

19. UNI EN 2564: Aerospace series, carbon Fiber laminates, determination of the fiber, resin and void contents. 1998.

20. ASTM D 3171 – 99: Standard test methods for constituent content of composite materials. ASTM Int. (1999).

1.2. Torsion Test

Shear tests are difficult to be done in a correct way, in particular on joined ceramics, due to the several issues related to the proper use of the only international standard, i.e. asymmetric four point bending (A4PB), (ASTM C1469-10, 2005), thoroughly discussed in [1-4] and briefly summarized here: samples for A4PB tests need precise alignment during preparation and testing; they should not be prepared one by one; A4PB is suitable if the bond strength is lower than 50% of the adherend bending strength, and "U" or "V" notches are required in the joined region if the bond strength is higher than 25% of the adherend bending strength.

The presence of several "in house" alternative tests to avoid using A4PB makes the comparison of results impossible, with negative impact on the use of joined ceramics, composites and their integration with other materials such as metals and polymers. Most of the in house tests are lap tests which should, in general, be used only for comparative studies and not to evaluate the shear strength for design purposes, unless the stress at failure can be precisely ascertained. On this respect, it must be underlined that ASTM D905-08 "Standard Test Method for Strength Properties of Adhesive Bonds in Shear by Compression Loading" caveat on the use of lap joint tests (ASTM D905-08, 2013).

Recently, torsion has been proposed as a suitable alternative to A4PB to provide reliable shear strength values for joined components: advantages of torsion have been reported in [2-6] and are mainly due to the pure (even if not uniform) shear stress for circular samples under torsion, the possibility given by the hourglass geometry to reduce the joined section to ensure failure in the bond, and a precise way to calculate stress concentration factor (K_t) for a given hourglass geometry [5].

However, torsion test can provide sound results only if the experimental results are correctly used.

1.2.1. Glass-ceramic sealants for SOFC/SOEC applications

The interest in solid oxide fuel/electrolysis cells (SOFCs/SOECs) as electrochemical devices to convert chemical energy of fuels into electricity and vice versa has increased in recent years [7, 8, 9]. Main focus of works has been the planar design due to its higher power output, where typically individual cells are connected together in series to form a stack [10]. Typical temperature ranges are 650 °C to 850 °C [11], where recently long term operation times exceeding 70000 h have been verified [12].

The ceramic cell and metallic interconnects are joined by sealant materials [13, 14], where, although in some cases metallic materials have been used [15], mostly glasses and in particular glass-ceramic materials are being used [10, 11, 16, 17, 18]. As a consequence of thermal and chemical strains, normal and/or shear stresses arise: this also happens in case of thermal gradients during thermal cycling and even in case of steady state operation [19]. These stresses as well as additional clamping loads [15] can lead to damage and failure, where mobile applications appear to be more critically affected, due to the associated larger number of in-operational thermal cycles [20].

The sealing materials have been identified as a critical component in various studies, since they have to join components and warrant hermetically separation of fuel and oxygen [21]. Therefore, mechanical issues of the sealant material have a serious impact on performance and degradation rate [17]. Although a number of works have been dedicated to evaluate the sealants under tensile- and/or bending-dominant loading condition [22, 23, 24], extensive experimental work has been conducted to evaluate the fracture toughness [13, 25], fracture strength [26,

27] and creep behavior [28, 29, 30], however, only a limited number of studies exist on shear strength evaluation, which appears to be the most application relevant loading condition [31, 32], where especially the application relevant elevated temperature behavior received only minor attention [33, 34].

According to literature, the mechanical properties of the joints, such as the strength significantly depend on the testing method. For example, Selçuk et al. [35] investigated the shear strength of glass–ceramic sealants by single lap offset (SLO) under compression, single lap (SL) under compression and asymmetrical 4-point bending tests (A4PB). The three different testing methods resulted in a significant variation in the apparent shear strength, in particular, in case of the SLO configuration a relatively lower strength was obtained due to the higher normal tensile stresses applied perpendicular to the joint.

The mechanical stability of such glass-ceramic based joints well be critical in particular at high temperatures, especially during cooling cycle once the temperature is lower than Tg. Different groups have analyzed mechanical properties of glass-ceramics at room and high temperatures. For instance, Stephens et al. [36] tested a barium–calcium–aluminosilicate-based glass-sealing material (G18) under tensile and torsion conditions, to analyze the interfacial shear strength between the G18 glass and the Crofer22APU. A noticeable reduction (50%) in the mechanical strength of joint was observed with an increase in temperature from 25 °C to 800 °C.

The torsion test on hourglass-shaped specimens appears to be a convenient and promising method to assess the shear strength with only a minor effect of unwanted addition stress components [21, 22, 37, 38], hence, in the current work shear stresses are measured by torsion test for two different sealants by measuring their behavior at room temperature and at application relevant temperatures. The results are supported by extensive post-operation characterizations by using electron microscopy and compositional analysis on the fracture surfaces.

1.2.2. Structural adhesives

Glass as building material offers several unparalleled advantages with respect to other materials, such as: durability, unlimited aesthetic options, and transparency coupled with good stiffness and strength [39]. Nevertheless, the possibility to fully exploit its advantages in primary load-carrying structures (e.g. floors, facades, columns etc.) strictly depends on the combination with other structural elements made of other common materials such as steel [40].

Mechanical joints are usually used to attach glass panels to the load-bearing structure. However, the discontinuities caused by the holes as well as the drilling process may induce cracks and/or residual stresses in the glass. Fiore et al. [41] have recently shown that holes induce local stress concentration that can cause the premature failure, thus leading to safety concerns, oversized structures and the need of accurate and expensive monitoring program able to prevent fatigue failures.

To overcome these problems, adhesive joining techniques are preferred, in order to guarantee structural continuity, a more efficient and homogeneous load transmission between different elements of the structure, and to lower or suppress the stress concentration [42, 43]. Moreover, adhesive joints can contribute to cost and weight saving due to their higher strength-to-weight ratio, better fatigue behaviour and ease of application. Notwithstanding the advantages presented above, the applications are still limited due to their sensitivity to manufacturing defects, harsh conditions and to difficulties in the assessment of their mechanical behaviour [44, 45].

In the particular context of mechanical behaviour, several different tests have been proposed for the shear strength characterization of joined components, such as lap shear [46], modified transverse crack tensile [47], end-notched flexure [48] and end-loaded split tests [49]. However, all these tests evaluate different in-plane

and out-of-plane shear failure modes or a combination of them and therefore they do not effectively measure the pure shear strength of a joined component.

Moreover, all lap shear tests should, in general, be used for comparative studies only and not to provide the shear strength of joined components for design purposes: it is worth noticing that ASTM D905-08 [50] has a *caveat* on the use of lap joint tests.

Also loading rate and strain-rate effects may significantly influence the shear strength of the joint and they should be considered for dynamic applications where the joint is subject to rapidly varying loading conditions [51, 52].

The only available standard to measure the (non-lap) shear strength of joined (*ceramic*) samples is the asymmetric four-point bending (A4PB) test (ASTM C1469) [53]. This test was designed to give pure shear loading and zero bending moment in the joined area. However, Ferraris et al. [54] pointed out the difficulty of performing this test in a correct manner, because: (a) joined samples for this test should not be prepared one by one; (b) even a slight misalignment provides unreliable results; (c) if the joint bending strength is higher than 50% of the non-joined material, this test cannot be used.

Torsion tests on hourglass shaped joined components have been proposed by some authors and used by several other research groups to obtain the pure shear strength of joined samples [54-59]. If correctly performed, this torsion test has the main advantage of inducing fracture by torsion in the reduced hourglass shaped joined section, thus providing pure shear strength of the joined components with limited stress concentration nearby.

However, the brittle or ductile nature of the joining material itself has to be carefully taken into account: if the joining material is purely brittle, such as glasses or glass-ceramics, results obtained by using the maximum (and final) point of the torsion curve (torsional moment *versus* torsion angle) to calculate the shear strength are correct.

On the contrary, if the joining material is ductile, such as adhesives or brazing alloys, shear strength results obtained as above are wrong: the torsion curves may

be very different when fully joined or ring-shaped hourglass joined samples are tested. A difference of about 100% was measured with torsion tests on Araldite AV119 fully joined samples compared to ring-shaped ones [53]. The difference is due to the wrong use of the maximum torsional moment in the torsion curve to calculate the shear strength of these joined samples: in the case of ductile joining materials, the curve shows a nonlinear-plastic behaviour. In order to use the torsion curve maximum point to calculate shear strength, the curve must be linear elastic only.

The aim of this study is two-fold: first, to provide designers with reliable, pure shear strength and elastic properties (elastic modulus and Poisson's ratio) for an epoxy joined glass-to-steel component; second, to propose a method to obtain these important data in case of an unknown brittle or plastic behaviour of the adhesive.

An example of glass-to-steel adhesive joined component used in buildings is shown in Figure 1: a structure including glass panels was built in 2015 at the University of Palermo, Italy, by adhesive joining of glass to steel, with a joint configuration similar to the one subject of this work.

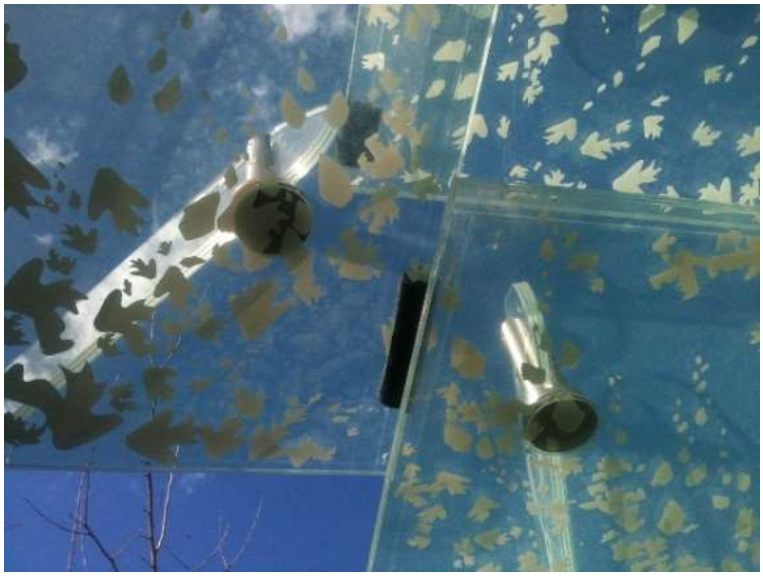

Figure 1: Example of building with glass and steel: particular of the glass panel with the adhesive joint glass/steel.

References

(1.2. Torsion test)

1. Ferraris, M., Ventrella, A., Salvo, M., Avalle, M., Pavia, F., Martin E., 2010. Comparison of Shear Strength Tests on AV119 Epoxy-Joined Carbon/ Carbon Composites. Compos. Part B-Eng. 41, 182–191.

2. Ferraris, M., Salvo, M., Casalegno, V., Ventrella, A., Avalle, M., 2012. Torsion Tests on AV119 Epoxy-Joined SiC. Int. J. Appl. Ceram. Technol. 9, 795-807.

3. Ferraris, M., Ventrella, A., Salvo, M., Gross, D., 2014. Shear strength measurements of AV119 epoxy-joined SiC by different torsion tests. Int. J. Appl. Ceram. Technol. 11, 394-401.

4. Ferraris, M., Ventrella, A., Salvo, M., Katoh, Y. Gross, D., 2015. Torsional Shear Strength Tests for Glass-Ceramic Joined Silicon Carbide. Int. J. Appl. Ceram. Technol. 12:693-699.

5. Goglio L., Ferraris, M., 2016. Bonding of ceramics: An analysis of the torsion hourglass specimen. Int. J. Adh. Adh. 70, 46-52.

6. Fakouri Hasanabadi, M., Faghihi-Sani, M.A., Kokabi, A.H., Malzbender ,J., 2017. The analysis of torsional shear strength test of sealants for solid oxide fuel cells. Ceram. Inter. 43, 12546-12550.

7. A. Choudhury, H. Chandra, A. Arora, Application of solid oxide fuel cell technology for power generation—A review, Renewable and Sustainable Energy Reviews 20 (2013) 430-442.

8. M.A. Laguna-Bercero, Recent advances in high temperature electrolysis using solid oxide fuel cells: A review, J. Power Sources 203 (2012) 4-16.

9. A. Pandiyan, A. Uthayakumar, R. Subrayan, S.W. Cha, S.B. Krishna Moorthy, Review of solid oxide electrolysis cells: a clean energy strategy for hydrogen generation, Nanomaterials and Energy. 8 (2019) 2–22.

10. L. Blum, W.A. Meulenberg, H. Nabielek, R. Steinberger-Wilckens, Worldwide SOFC technology overview and benchmark, I. J. Appl. Cer. Technol. 2 (2005), 482-492

11. L. Blum, Q. Fang, L.G.J. de Haart, J. Malzbender, N. Margaritis, N.H. Menzler, SOC development at Forschungszentrum Jülich, ECS Transactions 78 (2017) 1791-1804.

12. L. Blum, L.G.J. De Haart, J. Malzbender, N. Margaritis, N.H. Menzler, Anode-supported solid oxide fuel cell achieves 70 000 hours of continuous operation, Energy Technol. 4 (2016) 939-942.

13. J.W Fergus, Sealants for solid oxide fuel cells, J. Power Sources 147 (2005) 46-57.

14. N. Mahato, A. Banerjee, A. Gupta, S. Omar, K. Balani, Progress in material selection for solid oxide fuel cell technology: A review, Prog. Mater. Sci. 72 (2015) 141-337.

15. B. Kuhn, E. Wessel, J. Malzbender, R.W. Steinbrech, L. Singheiser, Effect of isothermal aging on the mechanical performance of brazed ceramic/metal joints for planar SOFC-stacks, Int. J. Hydrogen Energy 35 (2010) 9158-9165.

16. M.K. Mahapatra, K. Lu, Glass-based seals for solid oxide fuel and electrolyzer cells - A review, Mater. Sci Eng. Rep. 67 (2010) 65-85.

17. Y. Zhao, J. Malzbender, S.M. Groß. The effect of room temperature and high temperature exposure on the elastic modulus, hardness and fracture toughness of glass ceramic sealants for solid oxide fuel cells, J. Euro. Ceram. Soc. 31 (2011) 541-548.

18. F. Smeacetto, M. Salvo, M. Santarelli, P. Leone, G.A. Ortigoza-Villalba, A. Lanzini , L.C. Ajitdoss, M. Ferraris, Performance of a glass-ceramic sealant in a SOFC short stack, Int. J. Hydrogen Energy 38 (2013) 588-596.

19. M. Peksen, 3D transient multiphysics modelling of a complete high temperature fuel cell system using coupled CFD and FEM, Int. J. Hydrogen Energy 39 (2014) 5137-5147.

20. A. Al-Masria, M. Peksen, K. Khanafer, 3D multiphysics modeling aided APU development for vehicle applications: A thermo-structural investigation, Int. J. Hydrogen Energy 44 (2019) 12094-12107.

21. L. Blum, S.M. Groß, J. Malzbender, U. Pabst, I.C. Vinke, Investigation of solid oxide fuel cell sealing behavior under stack relevant conditions at Forschungszentrum Jülich, J. Power Sources 196 (2011) 7175-7181.

22. S. Rodríguez-López, J. Wei, K. C. Laurenti, I. Mathias, M. J. Pascual, Mechanical properties of solid oxide fuel cell glass-ceramic sealants in the system BaO/SrO-MgO-B2O3-SiO2, J. Euro. Ceram. Soc. 37 (2017) 3579-3594.

23. S.R. Choi, N.P. Bansal, A. Garg, Mechanical and microstructural characterization of boron nitride nanotubes-reinforced SOFC seal glasscomposite, Mater. Sci. Eng. A 460–461 (2007) 509–515

24. H. Abdoli, P. Alizadeh, D. Boccaccini, K. Agersted, Effects of thermal aging on thermo-mechanical behavior of a glass sealant for solid oxide cell applications, J. Eur. Ceram. Soc. 34 (2014) 2525–2534.

25. L. Han, B. Talic; K. Kwok, P. Vang Hendriksen, H.L. Frandsen, Interface Fracture Energy of Contact Layers in a Solid Oxide Cell Stack, ACS Appl. Energy Mater. 3 (2020) 2372-2385

26. M. Fakouri Hasanabadi, M. A. Faghihi-Sani, A. H. Kokabi, S. M. Groß-Barsnick, J. Malzbender, Room- and high-temperature flexural strength of a stable solid oxide fuel/electrolysis cell sealing material, Ceram. Int. 45 (2019) 733-739.

27. F. Heydari, A. Maghsoudipour, Z. Hamnabard, S. Farhangdoust, Mechanical properties and microstructure characterization of zirconia nanoparticles glasscomposites for SOFC sealant, Mater. Sci. Eng. A 552 (2012) 119–124, http://dx.doi.org/10.1016/j.msea.2012.05.019

28. C.K. Lin, K.L. Lin, J.H. Yeh, W.H. Shiu, C.K. Liu, R.Y. Lee, Aging effects on high-temperature creep properties of a solid oxide fuel cell glass-ceramic sealant, J. Power Sources 241 (2013) 12–19, http://dx.doi.org/10.1016/j.jpowsour.2013.04.088.

29. J. Milhans, M. Khaleel, X. Sun, M. Tehrani, M. Al-Haik, H. Garmestani, Creep properties of solid oxide fuel cell glass-ceramic seal G18, J. Power Sources 195(2010) 3631–3635

30. J. Malzbender, Y. Zhao, T. Beck, Fracture and creep of glass–ceramic solid oxide fuel cell sealant materials, J. Power Sources 246 (2014) 574-580.

31. L. Goglio, M. Ferraris, Bonding of ceramics: An analysis of the torsion hourglass specimen, Int. J. Adhesion and Adhesives, 70 (2016) 46-52.

32. M. Fakouri Hasanabadi, M. A. Faghihi-Sani, A. H. Kokabi, J. Malzbender, The analysis of torsional shear strength test of sealants for solid oxide fuel cells, Ceram. Int. 43 (2017) 12546-1255.

33. M. Fakouri Hasanabadi, A. H. Kokabi, M. A. Faghihi-Sani, S. M. Groß-Barsnick, J. Malzbender, Room- and high-temperature torsional shear strength of solid oxide fuel/electrolysis cell sealing material, Ceram. Int. 45, (2019) 2219-2225.

34. H.T. Chang, C.K. Lin, C.K. Liu, S.H. Wu, High-temperature mechanical properties of a solid oxide fuel cell glass sealant in sintered forms, J. PowerSources 196 (2011) 3583–3591

35. A. Selçuk, A. Atkinson, Measurement of mechanical strength of glass-to-metal joints. Fuel Cells 15 (2015) 595–603.

36. E.V. Stephens, J.S. Vetrano, B.J. Koeppel, Y. Chou, X. Sun, M.A. Khaleel, Experimental characterization of glass–ceramic seal properties and their constitutive implementation in solid oxide fuel cell stack models. J. Power Sources, 193 (2009) 625–631.

37. B. Cela Greven, S. Gross-Barsnick, T. Koppitz, R. Conradt, F. Smeacetto, A. Ventrella, M. Ferraris, Torsional shear strength of novel glass-ceramic composite

sealants for solid oxide fuel cell stacks, Int. J. Appl. Ceram. Technol. 15 (2018) 286-295.

38. F. Smeacetto, A. De Miranda, A. Ventrella, M. Salvo, M. Ferraris, Shear strength tests of glass ceramic sealant for solid oxide fuel cells applications, Adv. Appl. Ceram. 114 (2015) S70-S75.

39. Pariafsai F. A review of design considerations in glass buildings. Front Archit Res 2016;5:171–93.

40. Marchione F, Munafò P. Experimental strength evaluation of glass/aluminum double-lap adhesive joints. J Build Eng 2020; 30:101284.

41. Fiore V, Calabrese L, Proverbio E, Galtieri G, Scalici T, Lo Presti V.M, et al. Pull-off adhesion of hybrid glass-steel adhesive joints in salt fog environment. J Adhes Sci Technol 2016;30.

42. Vinson J.R. Adhesive bonding of polymer composites. Polym Eng & Sci. 1989;29:1325–31.

43. Sarrado C, Turon A, Costa J, Renart J. On the validity of linear elastic fracture mechanics methods to measure the fracture toughness of adhesive joints. Int J Solids Struct 2016; 81: 110–6.

44. Heshmati M, Haghani R, Al-Emrani M. Dependency of cohesive laws of a structural adhesive in Mode-I and Mode-II loading on moisture, freeze-thaw cycling, and their synergy, Mater Des 2017; 122:433-447.

45. González Ramírez F.M, Garpelli F.P, Sales R.C.M, Candido G.M, Arbelo M.A, Shiino M.Y, Donadon M.V. Experimental characterization of Mode I fatigue delamination growthonset in composite joints: A comparative study. Mater Des 2018; 160: 906–914.

46. Machalická K, Eliášová M. Adhesive joints in glass structures: effects of various materials in the connection, thickness of the adhesive layer, and ageing. Int J Adhes Adhes 2017; 72: 10-22

47. Scalici T, Pitarresi G, Catalanotti G, van der Meer F.P, Valenza A. The Transverse Crack Tension test revisited: An experimental and numerical study. Compos Struct 2016;158.

48. ASTM. ASTM D7905/7905M - 14 - Standard Test Method for Determination of the Mode II Interlaminar Fracture Toughness of Unidirectional Fiber-Reinforced Polymer Matrix Composites 2014.

49. International Organization for Standardization. ISO 15114:2014 - Fibre-reinforced plastic composites – Determination of the mode II fracture resistance for unidirectionally reinforced materials using the calibrated end-loaded split (C-ELS) test and an effective crack length approach 2014.

50. ASTM. ASTM D905-08(2013) - Standard Test Method for Strength Properties of Adhesive Bonds in Shear by Compression Loading.

51. Viana G, Machado J, Carbas R, Costa M, da Silva L.F.M, Vaz M, Banea M.D. Strain rate dependence of adhesive joints for the automotive industry at low and high temperatures, J Adhes Sci Technol 2018; 32:19, 2162-2179.

52. Gupta S.K, Shukla D.K. Effect of stress rate on shear strength of aluminium alloy single lap joints bonded with epoxy/nanoalumina adhesives. Int J Adhes Adhes 2020; 99:102587.

53. ASTM. ASTM C1469-10(2015) - Standard Test Method for Shear Strength of Joints of Advanced Ceramics at Ambient Temperature 2015.

54. Ferraris M, Ventrella A, Salvo M, Avalle M, Pavia F, Martin E. Comparison of shear strength tests on AV119 epoxy-joined carbon/carbon composites. Compos Part B Eng 2010;41:182–91.

55. Osipova T, Wei J, Pećanac G, Malzbender J. Room and elevated temperature shear strength of sealants for solid oxide fuel cells. Ceram Int 2016;42:12932–6.

56. Ferraris M, Salvo M, Casalegno V, Avalle M, Ventrella A. Torsion tests on AV119 epoxy - Joined SiC. Int J Appl Ceram Technol 2012;9:795–807.

57. Goglio L, Ferraris M. Bonding of ceramics: An analysis of the torsion hourglass specimen. Int J Adhes Adhes 2016;70:46–52.

58. Nozawa T, Ogiwara H, Kannari J, Kishimoto H, Tanigawa H. Torsion test technique for interfacial shear evaluation of F82H RAFM HIP-joints. Fusion Eng Des 2011;86:2512–6.

59. Ferraris M, Ventrella A, Salvo M, Gross D. Shear strength measurement of AV119 epoxy-joined SiC by different torsion tests. Int J Appl Ceram Technol 2014;11:394–401.

2. Materials and methods

2.1. Sandwich structures for aerospace applications

2.1.1. Joining of sandwich structures

The CFRP plates and honeycombs (HC)CFRP used in this study were supplied by Thales Alenia Space (TAS - Cannes, France) and produced by North Thin Ply Technology (NTPT, Switzerland), from composite pre-impregnated (prepreg) made of carbon fibers having a diameter of about 7 microns and a cyanate ester matrix (NTPT ThinPreg™ 380CE). They are manufactured by using proprietary spread tow technology. This involves the spreading of untwisted fibre tows into thin, flat unidirectional tapes which are then combined with resin to obtain prepreg tapes of 40 microns and 47% fiber volume fraction; the CFRP plies layout for plates and honeycombs is (0°/+60°/-60°, top layer in 0° direction) with an ILSS (Interlaminar Shear Strength) of about 33 MPa [1].

The HC(CFRP) have 10 mm or 20 mm cell size, each honeycomb wall is built with 6 plies (0°/+60°/-60°), and an overall thickness of 0.21 mm, the same fiber volume fraction (47%) as above.

Zerodur™ (Schott, Germany) is an extremely low expansion glass-ceramic with CTE (0-50 °C) 0 ± 0.100 10^{-6}/K, Young's Modulus 90.3 GPa and Density 2.53 g/cm^3 [2]. It has been supplied by Thales Alenia Space (TAS - Cannes, France) in 2.5 mm thick slabs.

A commercially available adhesive suggested for joining carbon based materials, Graphi-Bond™ 551-RN from AREMCO Products, Inc. (USA) (referred to as GB in this work) was used in this work: the main components are graphite and graphite fibres in a phenolic resin, with a CTE = 7.4 10^{-6}/K, according to data sheet [3]

Cured bulk GB samples (50 mm x 20 mm x 5 mm) have been prepared by a curing cycle of 0.3°C/min heating to 130°C followed by 4 hours dwelling at 130°C and 2 hours at 260°C (in air), as reported in [4] for the analyses described in the following paragraphs.

A phenolic based adhesive (referred to as PH in this work) and one cyanate ester based adhesive (referred to as CY in this work), already proven effective for joining of C/C, were both prepared by M.D.P Materials Design & Processing S.r.l. - Italy, and their characteristics reported in [5], and briefly summarised here.

Their compositional range (wt %) is:

- 55 – 75 wt % phenolic resin (Hexion - Resole based Bakelite 1211, Germany), 1-4 wt % Carbon black (Cabot, grade Vulcan 7H, UK), 1-4 wt % Milled Carbon Fibres (SIGRAFIL C10 M250 UNS by SGL Carbon, UK), 5-20 wt % Graphite (Cecchi, grade A20 microshield, Italy), 10-25 wt % ethanol as a solvent.

- 65 – 85 wt % cyanate ester (Lonza PT 30, Germany), the same fillers as above, no solvent added.

The typical curing cycle for the phenolic adhesive is done by heating at 0.3 °C/min up to 130 °C, dwell time 4 hours followed by heating to 260 °C at 0.3 °C/min , dwell time 2 hours, then cooling (referred to as PH260 in this work).

The phenolic adhesive was also cured with a lower temperature curing cycle (referred to as PH150 in this work): 4 hours at 130°C followed by 10 hours at 150°C, C (heating rate: 0,3°C/min) in order to avoid detrimental effects of curing at 260 °C on CFRP.

The curing for cyanate ester adhesive is faster, done by heating up to 150 °C, dwell time 1 hour followed by heating to 200 °C at 10 °C/min, dwell time 3 hours and a last step at 270 °C, dwell time 3 hours.

The curing processes were done in a muffle furnace (Nabertherm LH 60/40, Germany) in air with different thermal cycles according to the adhesive's composition.

The commercial adhesive (GB), the phenolic one with both curing cycles (PH260 and PH150) and the cyanate ester (CY) adhesives where cured inside molds in order to obtain bulk cured adhesives (175 mm x 50 mm x 3 mm) for dilatometry (Netzsch, DIL 402 PC/4) and thermogravimetric analysis (TGA) with differential thermo-gravimetry (DTG) and Thermo-Gravimetric-Evolved Gas analysis (TGA-EGA).

For the TGA-EGA, an ultra-microbalance (sensitivity 0.1 µg) connected with a time/temperature-resolved FTIR (Spectrum 100, Perkin Elmer) was employed. the gas evolved from the sample during the main degradative process was automatically collected (ca. 100 µL) and injected into a Clarus 500S gas chromatograph (Perkin Elmer) equipped with a standard non-polar fused silica capillary column Elite 5MS (Perkin Elmer).

The substances eluted were identified with an integrated Clarus 560S mass spectrometer (PerkinElmer) as detector. Total Ion Count (TIC) chromatograms were reported. Analyses of the average mass spectra identified at the chromatographic peak middle height were carried out with NIST MS Search Software.

For comparison purposes, CFRP HC has been tested by TGA-EGA as above.

Zerodur™ slabs were joined by the commercial adhesive GB and phenolic adhesive cured with both high (PH260) and low (PH150) temperature curing processes to measure the indentation elastic modulus by nano-indentation inside the joints, using the continuous stiffness measurement (CSM) method with a Berkovich indenter (Nano Indenter G200, Agilent Technologies).

CFRP slabs were cleaned with ethanol, sonicated and dried prior to joining. They were joined by the phenolic adhesive cured with both high (PH260) and low (PH150) temperature curing cycle, with about 1 kPa to keep samples in the correct

position. The joint thickness ranges between 140 to 200 microns, measured by difference after joining.

Joints were tested by lap shear test in compression, Single Lap Offset (SLO) shear test (figure 2) [6] (*adapted from ASTM D905-08* [7]). The lap shear of these joints was also tested after thermal history (table 1):

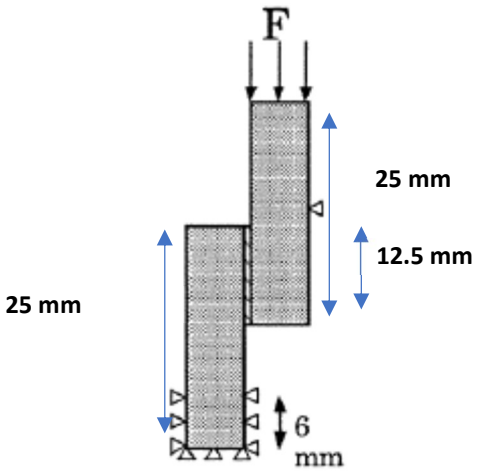

Figure 2: Single Lap Offset (SLO) shear test configuration and sample dimensions

Step 1: **24h at 80°C under Vacuum**	• Vacuum with P<2 x 10^{-5} bar at room temperature • Temperature ramp: between 0,3 et 0,5°C/min until 80 ± 2°C • Step at 80°C during 24h. • Cool-down until RT at 5°C/min maxi
Step 2: **ageing 7 days at 45°C, 93% RH**	• Ageing during 7 days at 45±3 °C and 93±5 %HR (to avoid 100% HR)
Step 3: thermal cycling **64 cycles [-30°C ; 70°C]**	• 64 cycles [-30°C ; 70°C] : • Temperature ramp: 5°C/min (heating and cooling) • Step of 30 min at -30°C and 70°C • first cycle: step at 70°C first

table 1: Ageing conditions for the joined samples

The tests were performed by using a universal mechanical testing machine (SINTEC D/10), with a cross-head speed of 0,5 mm/min.

The average lap shear strength in compression of the adhesive joined CFRP has been calculated dividing the maximum load at failure by the joining area. Joining area for all SLO samples is 25 mm x 12,5 mm = 312.5 mm^2. The tests were carried out on at least five samples.

Zerodur™ - CFRP - Zerodur™ sandwich structures (100 mm x 100 mm; 150 mm x 100 mm) joined by the low temperature cured phenolic adhesive (PH150) have been tested in triplicate, in tensile and lap shear mode, respectively.

To obtain the sandwich structures, the CFRP honeycomb was cut to the Zerodur™ plates size, one side of honeycomb was dipped into the phenolic adhesive PH at room temperature, then the same side was placed on the Zerodur™ plate; the half assembly was turned over and the other honeycomb side was dipped into the phenolic adhesive PH; then the same side was placed on the second Zerodur™ plate; a small load was applied on the obtained assembly (around 1kPa) to keep it in position; the assembly was placed in a furnace for the modified, low temperature curing treatment (PH150).

The tensile and apparent shear values were calculated by dividing the load at fracture by the entire Zerodur™ area or by dividing by the calculated CFRP HC bonded area, as will be discussed below.

The joints polished cross-sections and fracture surfaces after lap shear tests have been observed by Field Emission Scanning Electron Microscopy equipped with Energy Dispersive Spectroscopy (FESEM-EDS SUPRATM 40, Zeiss and Merlin Gemini Zeiss).

2.1.2. CFRP surface modification

CFRP plates and honeycomb are the same described in the previous paragraph.

The CFRP plates were cut by a disc saw to obtain slabs of 25 mm x 25 mm x 4 mm to be used for Single Lap Offset (SLO) shear test [6] (*adapted from ASTM D905-08* [7]) and 25 mm x 12 mm x 3 mm for bending tests [8]. (HC)CFRP were cut by scissors to 50 mm x 50 mm samples (thickness = 12 mm).

2.1.2.1. Etching Procedure

Before etching, all CFRP slabs and (HC)CFRP were cleaned with ethanol in ultrasonic bath for 10 minutes, 40°C, then dried with compressed air. The CFRP slabs sides not to be etched were masked with PTFE tape.

The CFRP slabs (25 mm x 25 mm x 4 mm) were put inside a Petri dish on a hot plate together with a beaker containing concentrated sulfuric acid (H_2SO_4, 96%, Sigma-Aldrich) and heated up to the selected temperature. The CFRP surface in contact with the hot plate was reversed upside-down and a few acid droplets (about 4 mL) were put on the CFRP surface until it was completely covered with a thin film of acid solution, then left on the hot plate for the selected time. (Figure 3 a, b)

The role of acid concentration (96%, 76 %, 33%), etching time (ranging between 5 and 20 minutes, multiple steps of 5 minutes each) and temperature (ranging between 80-150 °C) were investigated.

The etching process was also used on (HC)CFRP to be joined in a sandwich structure between two soda-lime or two CFRP skins (Figure 4) by dipping the

(HC)CFRP 1-2 mm inside the acid 96%: the process was as described above, but with a time of 5 or 10 minutes, at a temperature range of 100 -150 °C.

A *modification* of the etching process was done by preparing a suspension of alumina powder in sulfuric acid: 15 g of alumina (particle size 20-50 µm, Alfa Aesar) added to 18 mL of sulfuric acid and magnetically stirred for 5 min; then about 1 mL of hydrogen peroxide (H2O2 30%, ITW reagents) was slowly added to the stirred suspension and everything was kept at 150 °C (10, 15 and 20 minutes); this modified etching process was used to etch the CFRP *side* faces, as shown in Figure 5 b, c , to obtain the "brush" joints as in Figure 3 (c).

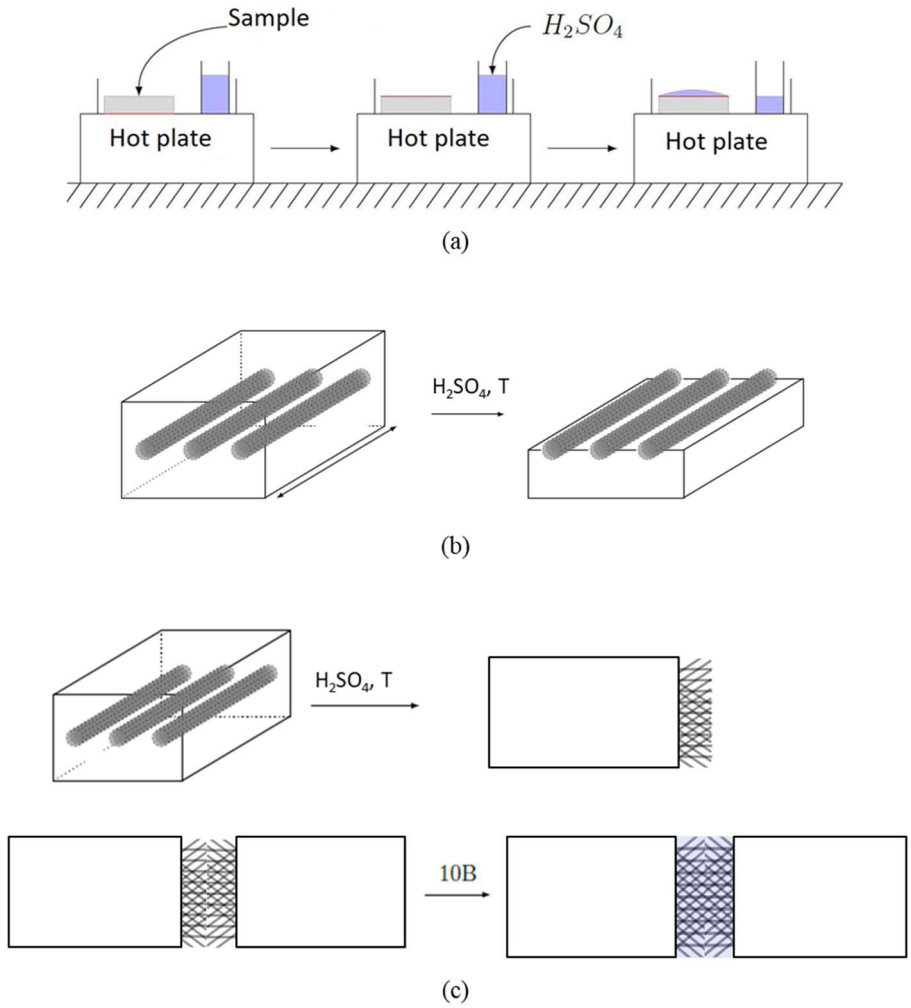

Figure 3: etching process sketch (a), etched CFRP surface (b), etched CFRP side (c)

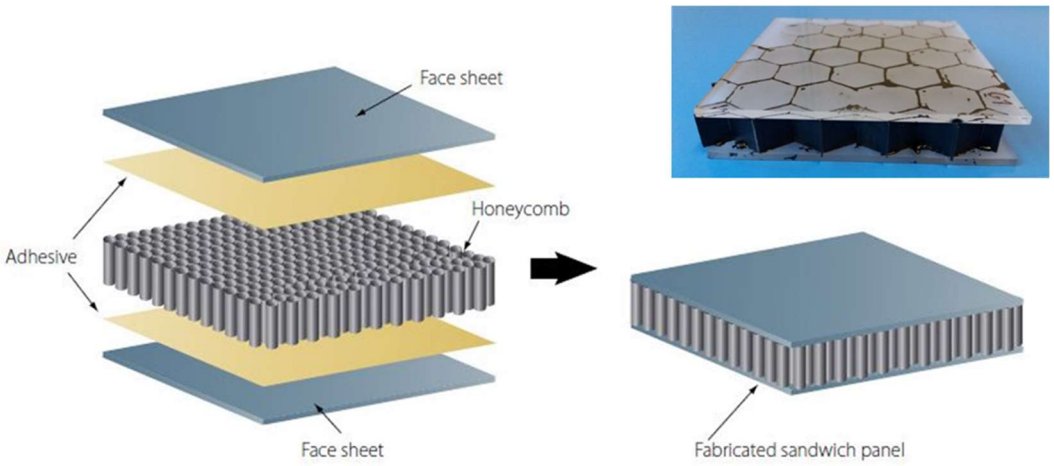

Figure 4: sketch of the sandwich panel made of honeycomb CFRP, (HC)CFRP, core joined to two skins made of CFRP or soda-lime glass slabs (obtained sandwich panel with glass skins, inset)

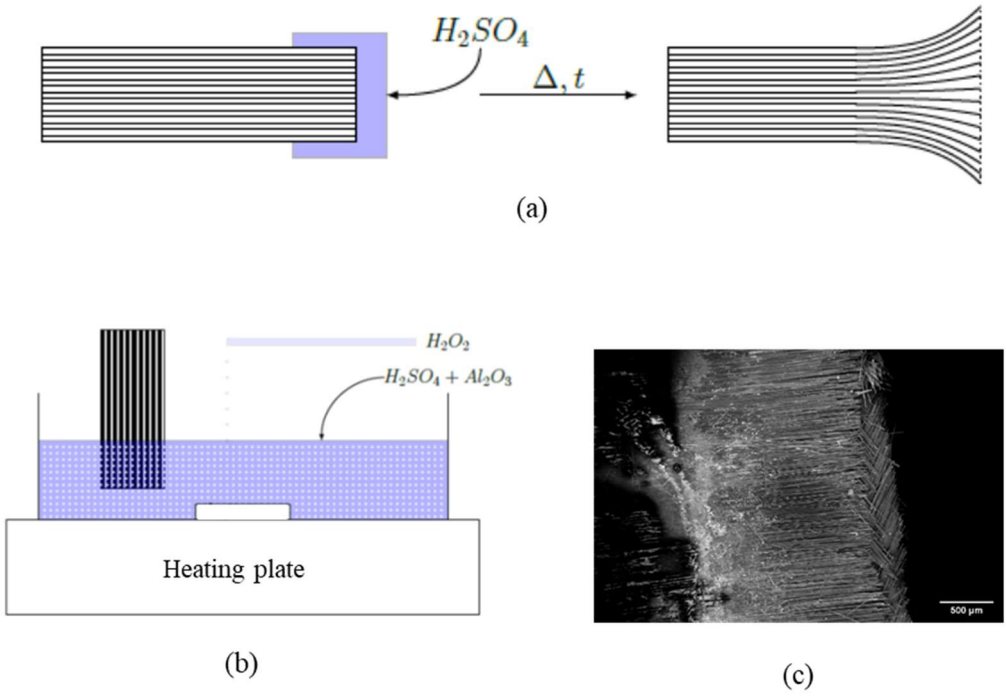

Figure 5: localized CFRP delamination due to excessive acid infiltration and matrix removal (a); etching protocol modified by adding alumina powders and oxygen peroxide to the acid (b); “brush” structure obtained (c) with the modified etching protocol

All the etching processes described above were performed multiple times at steps of 5 minutes each; at the end of each step, the samples were rinsed in distilled water to stop the reaction and ultrasonic cleaned for 10 min, then dried with compressed air. At the end of the whole etching process, samples were cleaned in ethanol in ultrasonic bath for 10 minutes at 40°C, then let dry in air before joining.

Profilometry (FTS Intra with Ultra, Taylor Hobson, Ametek, USA) and mass loss were done on etched samples.

2.1.2.2. Joining

The adhesive used to join CFRP was provided by M.D.P. Materials Design & Processing S.r.l., Italy and labelled as PH150: it is an inorganic loaded phenolic adhesive especially formulated to join carbon based composites: it contains carbon fibers, graphite powders and other fillers. [9]. The curing treatment was set at 130°C (4 hours), followed by another step at 150°C (10 hours), heating rate 0,3 °C/min, in order to preserve the CFRP properties, as these composites cannot be heated at temperature higher than their Tg, 150°C. A minimal pressure (few kPa) was applied on each joined sample to keep them in the correct position during curing. The joint thickness was about 240 ± 40 µm microns, measured ex-post after joining and curing.

2.1.2.3. Mechanical tests

The surface etched CFRP (Figure 3 b) were joined for Single Lap Offset (SLO) tests, with a joined area of 25 mm x 12.5 mm = 312.5 mm^2; the side etched CFRP (figure 3 c) were joined for 4 point bending tests with a joined area of 12 mm x 3 mm = 36 mm^2 [8]; both tests were done on six samples.

The sandwich structures were tested in tensile mode on a (HC)CFRP sandwiched between a soda-lime glass or a CFRP skin, with joined area of 50x50 mm = 2500 mm2 by an in-house build set up (Figure 6 a), which consists in two steel plates

connected to a universal tensile machine by a ball-joint; the sandwich is glued between the two steel plates and tested in tensile mode.

According to an internal TAS standard, tensile strength was calculated dividing the max load at failure by the overall honeycomb wall area, i.e. the area of a single wall multiplied by the total number of walls in the honeycomb. Non-etched CFRP and (HC)CFRP were also joined and tested for comparison purposes.

Joint cross-sections and fracture surfaces after mechanical tests were observed by Field Emission Scanning Electron Microscopy (FESEM- ZEISS Supra 40) with Energy Dispersive Spectroscopy (EDS- SW9100 EDAX).

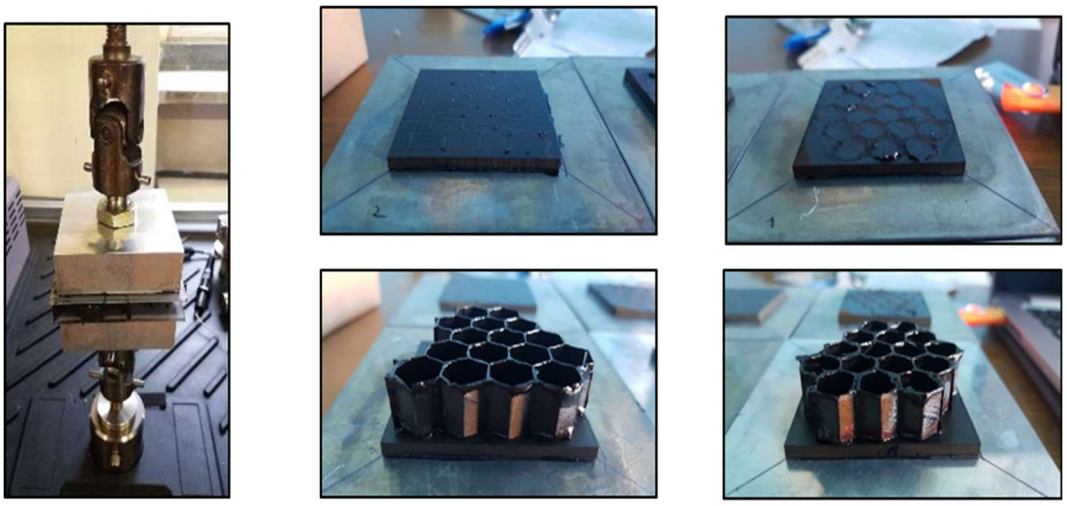

Figure 6: tensile test on the (HC)CFRP sandwich panel with CFRP skins (a); fracture surfaces of the sandwich panel after mechanical tests: adhesive failure for non-etched (HC)CFRP (b); cohesive with partial (HC)CFRP delamination for the etched (HC)CFRP (5 minutes, 125 °C) (c).

References

(2.1. Sandwich structures for aerospace applications)

1. CFRP data sheet, NTPT ThinPreg™ 380CE. North Thin Ply Technology (NTPT, Switzerland) www.thinplytechnology.com

2. Zerodur™ (Schott, Germany) datasheet. www.schott.com/advanced_optics

3. Graphi-Bond™ 551-RN (Aremco, USA) data sheet. http://www.aremco.com/a2.html

4. M. Salvo, V. Casalegno, Y. Vitupier, L. Cornillon, L. Pambaguian, M. Ferraris. Study of joining of carbon/carbon composites for ultra stable structures. Journal of the European Ceramic Society 30 (2010) 1751–1759

5. V. Casalegno, S. De la Pierre, I. Corazzari, F. Turci, P. Tatarko, O. Damiano , L. Cornillon, A. Terenzi , M. Natali, D. Puglia, L. Torre, M. Ferraris. Design, realization and characterization of advanced adhesives for joining ultra-stable C/C based components. 2020. Submitted to Macromolecular Materials and Engineering.

6. D. Amara, F. Levallois, Y. Baziard, J.A. Petit. Study of a single-lap compression-shear test for brittle substrates bonded with a structural adhesive. J Adhes Sci Technol. (1996); 10:1153-1164.

7. ASTM D905-08. Standard Test Method for Strength Properties of Adhesive Bonds in Shear by Compression Loading. ASTM Int. (2013)

8. ASTM D7264 / D7264M Standard Test Method for Flexural Properties of Polymer Matrix Composite Materials. ASTM Int. (2015).

9. M.D.P. patent pending; M.D.P. Materials Design & Processing S.r.l. Italy

2.2. Torsion test

2.2.1. Glass-ceramic sealants for SOFC/SOEC applications

The two sealants (abbreviated as GC1 and GC2) have been prepared by melt-quenching process at 1500 °C, 1 hour; starting products (oxides and carbonates) have been carefully mixed and then melted in air furnaces in platinum-rhodium crucibles. The compositions for both sealants are reported in Table 2; the properties of GC1 have been published elsewhere [1] and also summarized in Table 2. Both sealants have been obtained by casting on a brass plate and the transparent glasses ground to less than 38 microns for the following characterizations. The glass transition temperature (Tg) was measured at a heating rate of 5 °C/min on the powdered as-cast glasses by differential thermal analysis (DTA) (Netzsch, EOS, Selb, Germany). The softening temperature (Ts) and coefficient of thermal expansion (CTE) were measured by hot-stage microscopy (HSM) (Expert System solutions, Modena, Italy) and dilatometry, respectively, on bulk cylindric glass-ceramic samples of 5 mm height obtained by sintering GC1 and GC2 powders with the same thermal treatment used for their joining processes. The crystalline phases in both glass-ceramics were analyzed by X-ray diffraction XRD (Bruker AXS D8 Advance, Karlsruhe, Germany). Both sealants have been powdered and sieved to particle size < 38 microns and mixed with a minimum amount of ethanol to obtain a slurry suitable to be applied by a spatula on the surfaces of the two metallic parts to be joined.

		Glass									Glass ceramic			
Molar %	**SiO_2**	**B_2O_3**	**Al_2O_3**	**CaO**	**BaO**	**Na_2O**	**MgO**	**K_2O**	**Y_2O_3**	**Tg (°C)**	**Ts (°C)**	**CTE 10^{-6} °C^{-1} (200-500 °C)**	**Main crystalline phases**	**Joining process**
GC1 (ref 20)	55.2	0.8	6.7	9.8	0	13.5	12.7	1.1	0.2	605	625	10.9	diopside ($CaMgSi_2O_6$)	Steel oxidation: 950°C, 120 min, air 830 °C, 30 min, Ar
GC2 (ref 21)	55	8	4	7	26	0	0	0	0	677	810	11.4	sanbornite ($BaSi_2O_5$)	950°C, 60 min, air

Table 2: Glass and glass-ceramic sealants GC1 and GC2 composition, characteristic temperatures, coefficient of thermal expansion, crystalline phases and joining process conditions

The hour-glass shape and size of the joined samples are shown Figure 7: two kind of hour-glass shaped samples, both made of the same steel (Crofer 22 APU, ThyssenKrupp VDM GmbH, Germany), have been machined in the hour-glass shape, cut in two parts, then joined by applying the sealant slurry between the two parts: TGH-5 samples, Figure 7 (a), have a joined region diameter of 5 mm, a total height of 3 mm whereas THG-25 samples, Figure 7 (b) have been designed by multiplying the previous diameter and curvature radius by five: the joined region diameter is hence 25 mm and the total height is 11 mm as fixed by the thickness of available material. A tolerance range of ± 0.1 mm is to be considered.

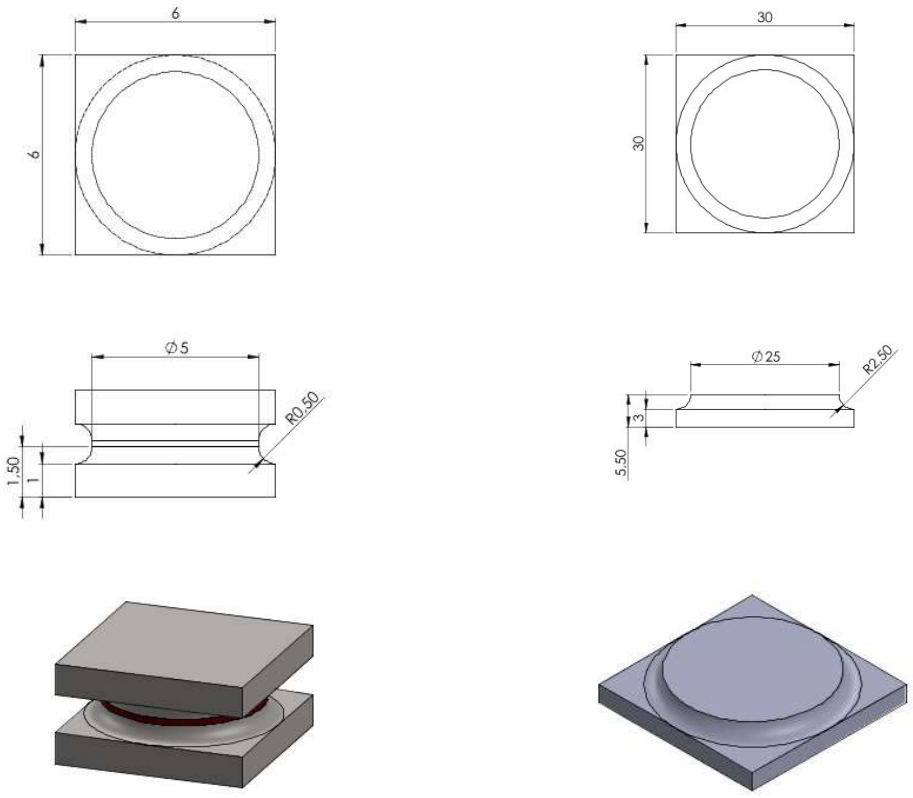

(a) THG-5 (b) THG-25

Figure 7: Size of hourglass shaped samples; both of them are made of steel (Crofer 22 APU), machined in the hourglass shape, cut in two parts, then joined by applying the sealant slurry between the two parts: THG-5 samples (a) have a joined area diameter of 5 mm, a total height of 3 mm; THG-25 samples (b) have been designed by multiplying the previous diameter and curvature radius by five. (half hourglass is shown in figure 7b)

Prior to the joining process with GC1, the half hour-glasses have been pre-oxidized at 950 °C for two hours in a chamber furnace in air to aid bonding onto the oxide scale. Afterwards, they have been then joined by GC1 slurry in a tubular furnace (Carbolite Gero STF 16/180 for THG-5 and GHA 12/300 for THG-25), in Ar atmosphere at temperature of 850°C, joining time 30 min, with the help of a graphite sample holder, to keep the samples in place.

Since pre-oxidation was not necessary for GC2 sealant (because previous tests showed the good compatibility between sealant and steel with a thinner oxide scale), the slurry was used to join as received Crofer22APU half hour-glasses by heat treatment at 950°C, in a muffle furnace, joining time one hour, in air atmosphere: in this case, an alumina sample holder was used to keep samples in place.

Both joining processes have been done without applying any pressure, which appeared not to be necessary for these sealant materials. The thickness of each joint has been characterized based on the thickness difference before and after joining the two half hour-glasses and ranged between 120 and 220 microns; joined hour-glasses have been tested in torsion at room temperature at Politecnico di Torino, Italy (POLITO) (TGH-5 only) and at Forschungszentrum Jülich, Germany (FZJ) (both THG-5 and THG-25); tests at operation relevant elevated temperature (600-800°C) have been done only at Forschungszentrum Jülich (both THG-5 and THG-25) (Figure 8).

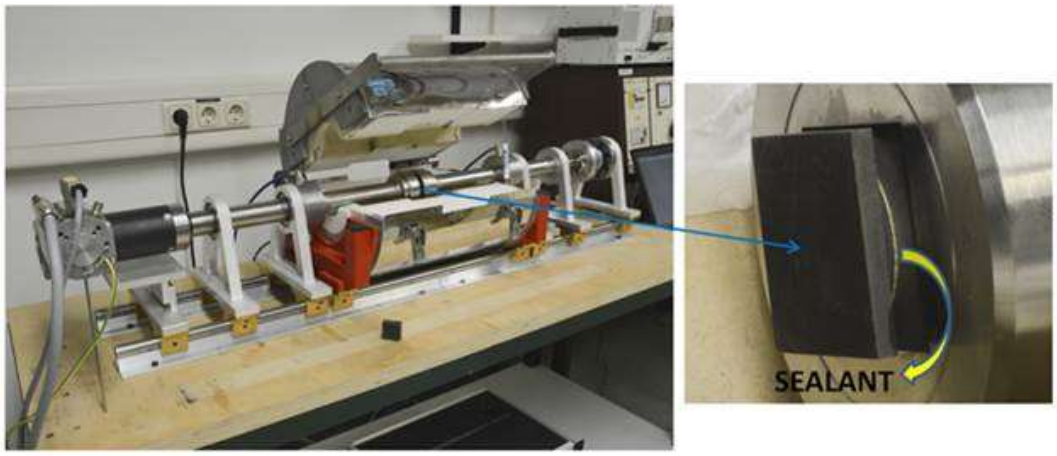

(a) (b)

Figure 8: Torsion test equipment at FZJ, suitable for RT and HT tests; particular of the hourglass shaped joined sample inside the fixture (b); a similar equipment is operative at Politecnico di Torino, Italy, for room temperature test only.

GC1 has been tested at 600°C since this composition due to its characteristic viscosity could be potentially used at T lower than 700 °C; being in fact a temperature envisaged recently for advanced intermediate temperature SOFC applications, specifically, torsion tests were carried out at 600°C in order to evaluate its joining performance around its parent glass transition temperature, but being still below its glass ceramic softening temperature.

GC2 has been tested at 800 °C, since this composition is specifically designed for an operating T of 800-850 °C for more standard applications; furthermore, at low T (i.e. 700°C) the steel was plastically deformed during the test with this joining material due to its appreciable torsional resistance.

The torsion tests at POLITO were performed in a universal testing machine (Zwick 100, Zwick/Roell, Hertfordshire, UK), where the load was applied until fracture occurred. The torsion load was applied using a rotating disc fixture with a chain equipped in the mechanical test frame. The crosshead speed was 0.5 mm/min with an estimated rotation speed of 0.010 rad/min [2]. In the torsion tests at FZJ the specimens were twisted with a speed of ~ 4° /min until fracture occurred [3].

A round-robin test with the two torsion machines has been done using epoxy adhesive bonded steel hourglasses (THG-5) prior to this work, to test the comparability of the obtained results.

The joined samples fracture surfaces and interfaces have been observed by FESEM (Merlin, ZEISS) and their composition measured by EDS.

2.2.2. Structural adhesives

2.2.2.1. Adhesive: DP490

An epoxy adhesive EPX DP490 (3M™ Scotch-Weld™) supplied as a paste was used as joining material for soda-lime glass slabs (50 x 50 x 10 mm3) and AISI304 steel samples of different size and shape (Figure 9).

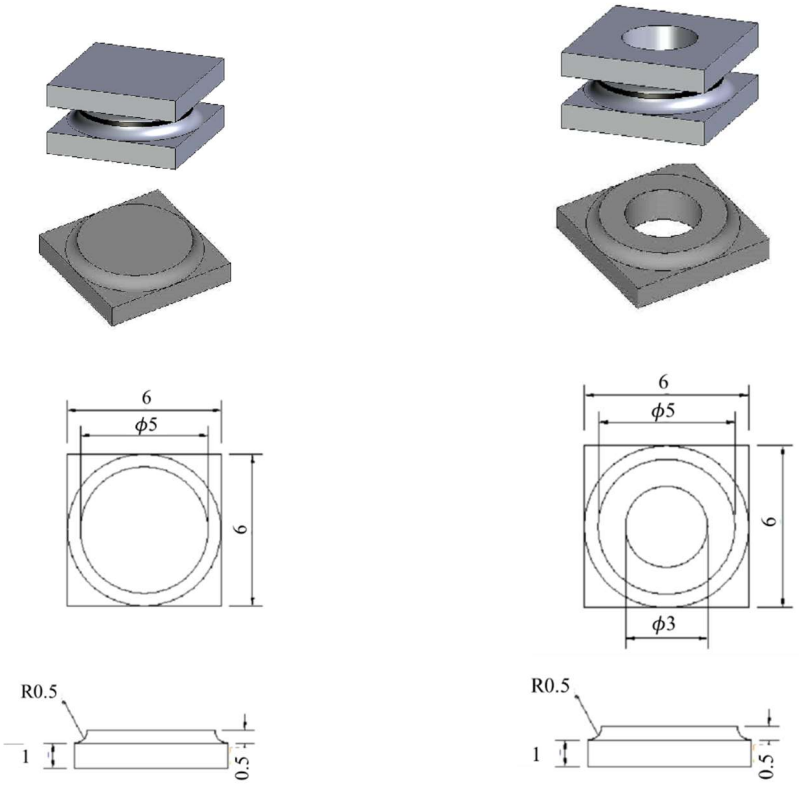

a) THG5 geometry b) TDHG geometry

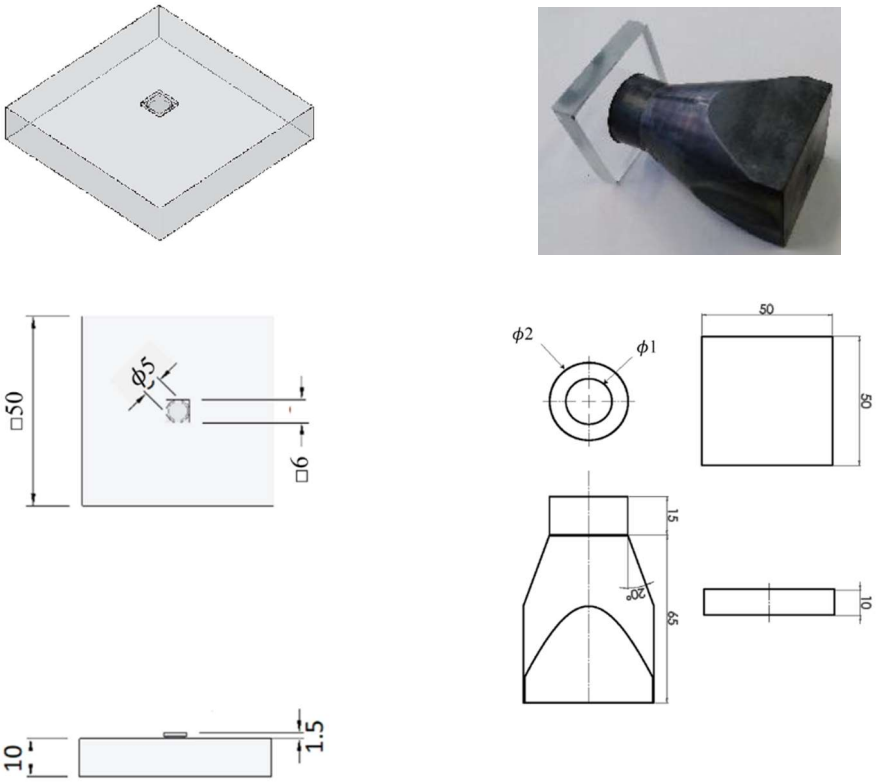

c) THG5-Glass geometry d) SGrFS geometry

Figure 9 – Size and shape of joined samples tested in torsion: a) full joined steel hourglass, 5 mm joined area diameter (THG5); b) ring-shaped steel hourglass (TDHG); c) steel half hourglass joined to a glass plate (THG5-Glass); d) full-scale (φ2 = 30 mm) ring-shaped steel fixture joined to a glass plate (Steel-Glass-ring-shaped-Full-Scale, SGrFS, with diameter ratios φ1/φ2 = 0.40, 0.53, 0.67, 0.80).

Steel surfaces to be joined were polished by SiC grit paper (P1000) then ultrasonic cleaned with acetone before joining. Both as received and etched glass slabs were joined to steel. Glass etching was done by hydrofluoric acid (HF, 40%, Sigma-Aldrich): HF droplets were dropped on the glass surface to be joined (5 to 15 minutes), then rinsed with distilled water and dried with compressed air [4].

To manufacture the joints, a thin layer of adhesive was manually placed between the two adherends: particular attention was paid to control and avoid the formation of adhesive spew fillets. Samples were placed in suitable sample holders and loaded with about 1 kPa during the whole curing time to keep them in the

correct position during curing, done at room temperature for seven days, according to the adhesive datasheet. The thickness of each joint, ranging between 100 μm and 150 μm, was calculated ex-post by measuring the difference of the sample height before and after joining [5].

With the aim of measuring the mechanical behaviour of the joints under shear stress, full joined steel hourglass (THG5, figure **Errore. L'origine riferimento non è stata trovata.**9a), ring-shaped steel hourglass (TDHG, figure 9b) and half hourglass joined to a glass slab (THG5-Glass, figure 9c) were prepared and tested (at least five samples per type) at room temperature. Size and shape of the joined hourglasses in figure 9a have been described and their behaviour in torsion has been modelled in [6].

Full-scale joint tests (similar to the real component in Figure 1) were performed on a 30 mm (outer diameter) ring-shaped steel component joined to a glass slab (SGrFS, figure 9d), with diameter ratios of 0.40, 0.53, 0.67, and 0.80, respectively.

Figure 10 shows the home-built apparatus used to perform torsional tests. In particular, it is possible to identify the load transmission chain (1), the sample grips (2), the chassis of the torsion apparatus (3) and a 2 kN load-cell (4). The torsion apparatus was coupled with a Universal Testing Machine Zwick-Roell Z100 (Germany) setting a constant crosshead speed to 0.5 mm/min corresponding to about 0.65 degree/min.

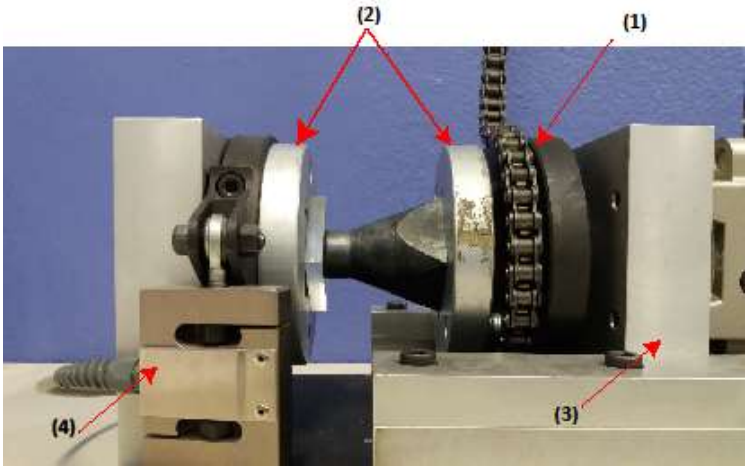

Figure 10 - Torsion test set up with the full-scale ring-shaped steel fixture joined to a glass plate and ready to be tested.

For torsion tests the shear strength was calculated as:

$$\tau = M\ max/J*R \qquad \text{(eq. 1)}$$

with,

$$J = \pi Re^4/2 \qquad J = \pi(Re^4 - Ri^4)/2 \qquad \text{(eq. 2 a, b)}$$

for full joined (THG5, THG5-Glass) and ring-shaped (TDHG, SGrFS) samples, respectively; where:

M max = maximum torque; J = polar moment of inertia; R = radius; Re = outer radius; Ri = inner radius

The shear strength of bars of the same steel joined by the same adhesive (joined sample size: 36 mm x 3 mm x 4 mm) was also measured at room temperature on five samples with A4PB tests (ASTM C1469 [7]), using a universal testing machine SINTEC D/10 with suitable fixtures and cross-head speed of 0.3 mm/min.

The peak load P_{max} was recorded for each test and the shear strength (τ_J) was calculated with Eq. (1), according to the ASTM C1469 [7]:

$$\tau_J = Shear\ Strength = \frac{P_{max}(S_o - S_i)}{A(S_o + S_i)} \qquad \text{(eq. 3)}$$

where A = 4 mm x 3 mm = 12 mm^2 is the cross section, S_o = 30 mm is the outer span, and S_i = 4 mm is the inner span.

All samples fractured in the joined region. After mechanical tests, the fracture surfaces were observed by optical microscopy to determine their adhesive or cohesive failure mode.

The elastic modulus of the adhesive inside the joined area and as bulk material was measured in triplicate by nano-indentation technique, using the Continuous Stiffness Measurement (CSM) method with a Berkovich indenter [8]. The elastic modulus was continuously measured up to the fixed maximum penetration depth of 1500 nm. The fixed distance of 50 μm was kept between the individual indents from all sides. The elastic modulus results measured by indentation were compared with the elastic modulus obtained by Impulse Excitation Technique (IET, ASTM E-1876 [9]) on the adhesive bulk samples (2 mm x 3 mm x 25 mm) cured with the same curing protocol of the joined samples (room temperature, seven days, in triplicate).

2.2.2.2. Adhesive: Hysol

The adhesive joining material was LOCTITE EA 9321 AERO (Henkel Corporation, USA), also known as Hysol® EA9321 (Hysol in the following, for brevity), a two-component thixotropic adhesive, cured according to supplier specifications (Henkel-adhesives, 2018).

The three joined substrates (adherends) were:

- Silicon nitride, produced by FCT Ingenieurkeramik GmbH (Germany), a polycrystalline β-Si3N4 obtained by gas pressure sintering using 3-10 wt% of sintering additives [10]. Chemical composition and properties of silicon nitride SN-GP can be found in [11].
- Silicon carbide Boostec® SiC (former SiC100®) produced by Mersen (France). It is a polycrystalline α-SiC (> 98.5 wt% SiC) obtained by pressure less sintering. Chemical composition and properties of Boostec® SiC can be found in [12].
- Crofer® 22 APU steel produced by ThyssenKrupp VDM GmbH (Essen, Germany). It is a high-temperature ferritic stainless steel especially developed for application in solid oxide fuel cells (SOFC). Chemical composition and properties can be found in [13].

All the materials were cut as in figure 11 (a-c) to obtain parts to be joined for SLO (a), A4PB (b) and torsion tests (c): the dimensions of the joined samples are reported in figure 11 (a-c). SiC and steel samples were grinded then polished to 1-µm diamond paste, then sonicated in acetone; Si_3N_4 samples were surface engineered as described in [14]; all of them were then bonded according to Henkel Hysol® EA9321 data sheet [15].

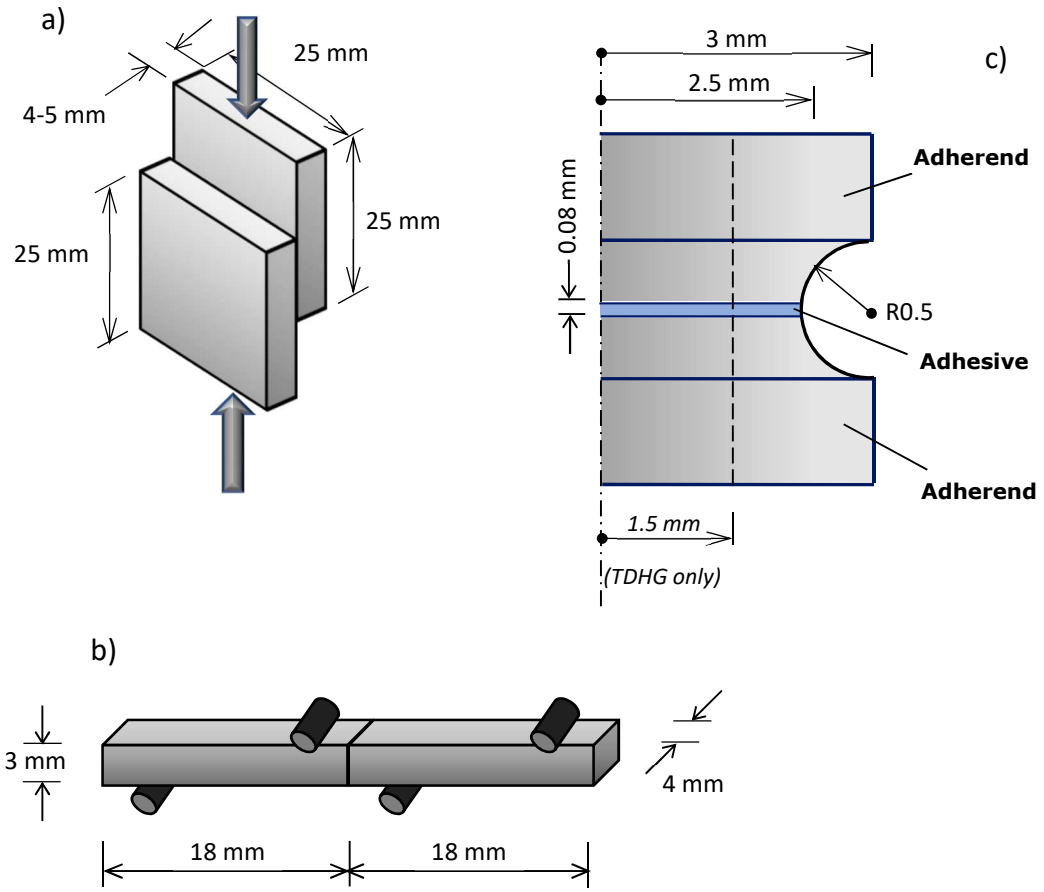

Figure 11: schematic representation of the three mechanical tests used for comparison of shear strength measurements on Hysol EA9321 joined samples: Single Lap Offset (SLO) (a), Asymmetric 4-point bending (A4PB) (ASTM C1469) (b); torsion on hourglass shaped samples with full joined (THG5) or annular joined area (TDHG) (c). (size in mm)

Four-point bending test (according to ASTM C1161-13, 2013) was used to test the bending strength of joined samples, before A4PB (figure 11a): all the values were lower than 25% flexural strength of the substrates (Si_3N_4, SiC and steel) and a specimen geometry without V-notches for the A4PB was then used. The A4PB samples were bonded one by one.

The torsion samples were fully joined hourglass shaped samples (THG5) obtained by joining two half hourglasses, or ring joined hourglass shaped samples (TDHG) obtained by drilling a 3 mm diameter hole along the vertical axis of an hourglass, cut it in two parts, then joined in the central section (figure 11c).

The shear strength of all the joined samples was measured at room temperature on at least 5 samples by a single lap offset (SLO) test in compression (figure 11c) (adapted from ASTM D905-08 and described in [16], asymmetrical 4-point bending test (A4PB, ASTM C1469-10, 5 2015) (figure 11a), torsion test on fully joined (THG5) and ring shaped samples (TDHG) (figure 11b) [17]. All the mechanical tests were done by using a universal testing machine SINTEC D/10 with suitable different fixtures and cross-head speed for the three tests. Torsion fixtures [18] have been applied to the universal testing machine for torsion tests. The maximum force was recorded for each test and the shear strength (τ) was calculated by dividing the maximum force by the joined area for SLO or by using the equation (3) for A4PB.

In the case of torsion tests the shear strength was calculated using equation 1 and 2a (for THG5) or 2b (for TDHG):

$$\tau = M\,max/J*R \qquad \text{(eq. 1)}$$

with,

$$J = \pi Re^4/2 \qquad J = \pi(Re^4 - Ri^4)/2 \qquad \text{(eq. 2 a,b)}$$

Where:

$M\,max$ = maximum torque; J = polar moment of inertia; R = radius; Re = outer radius; Ri = inner radius

2.2.2.3. Adhesive: Araldite

In this case, a structural two component epoxy paste adhesive, Araldite (Araldite 2015, Huntsman Advanced Materials) was used to join steel substrates. Crofer 22 APU steel was used, produced by ThyssenKrupp VDM GmbH (Essen, Germany). It is a high-temperature ferritic stainless steel especially developed for application in solid oxide fuel cells (SOFC) (Vdm-metals, 2018).

Steel was machined to obtain the hourglass shaped sample substrates (dimensions in figure 9a, 9b). For this part of the study, THG5 and TDHG specimens were used. Steel surfaces were cleaned with acetone and dried with compressed air, before the adhesive was applied manually on both substrate surfaces, particular attention was paid to control and avoid the formation of adhesive spew fillets. Then the hourglass samples were placed in a suitable sample holder for curing. The joined samples were cured at 85 °C for 1 hour according to the adhesive technical datasheet. The thickness of each joint, ranging between 100 μm and 150 μm, was calculated ex-post by measuring the difference of the sample height before and after joining.

The shear strength of the adhesive was evaluated with torsion test, that was performed at room temperature, for at least 5 samples of each type, using the torsion machine shown in figure 10, at a constant speed of 0,65 degree/min.

The shear strength of the adhesive was calculated using eq. 1, and the polar moment of inertia was calculated with eq. 2a for THG5 and eq. 2b for TDHG. The maximum torque was calculated from the maximum of the torque-angle of rotation curves.

All samples fractured in the joined region. After mechanical tests, the fracture surfaces were observed by optical microscopy to determine their adhesive or cohesive failure mode.

The elastic modulus of the adhesive inside the joined area and as bulk material was measured by nano-indentation technique, using the Continuous Stiffness

Measurement (CSM) method with a Berkovich indenter [8]. The elastic modulus was continuously measured up to the fixed maximum penetration depth of 1500 nm. The fixed distance of 50 µm was kept between the individual indents from all sides. The indentation elastic modulus average values were determined in the 900-1000 nm penetration depth range. The elastic modulus results measured by indentation were compared with the elastic modulus obtained by Impulse Excitation Technique (IET, ASTM E-1876 [9]) on the adhesive bulk samples (2 mm x 3 mm x 25 mm) cured with the same curing protocol of the joined samples (85 °C for 1 hour).

A summary of all sample geometries used for torsion testing is presented in Table 3; made of the different substrate materials and employed with the joining materials described previously.

Sample name	Joined area diameter	Description
THG-5	5 mm	full hourglass
THG-25	25 mm	full hourglass
TDHG	3-5 mm	ring-shaped hourglass
THG5-Glass	5 mm	full half hourglass + glass plate
SGrFS	30 mm	full-scale ring-shaped fixture + glass plate

Table 3: summary of samples used for torsion testing

References

(2.2. Torsion test)

1. F. Smeacetto, A. De Miranda, A. Ventrella, M. Salvo, M. Ferraris, Shear strength of glass ceramic sealant for SOFC, J. Am. Ceram. Soc., 97 (2014) 3835–3842.

2. Luca Goglio, Monica Ferraris, Bonding of ceramics: An analysis of the torsion hourglass specimen, Int. J. Adhesion and Adhesives, 70 (2016) 46-52.

3. M. Fakouri Hasanabadi, A. H. Kokabi, M. A. Faghihi-Sani, S. M. Groß-Barsnick, J. Malzbender, Room- and high-temperature torsional shear strength of solid oxide fuel/electrolysis cell sealing material, Ceram. Int. 45, (2019) 2219-2225.

4. Iliescu C, Jing J, Tay FEH, Miao J, Sun T. Characterization of masking layers for deep wet etching of glass in an improved HF/HCl solution. Surf Coat Tech 2005;198:314–8. doi:10.1016/j.surfcoat.2004.10.094.

5. Oliveira J.J.G, Campilho R.D.S.G, Silva F.J.G, Marques E.A.S, Machado J.J.M, da Silva L.F.M. Adhesive thickness effects on the mixed-modefracture toughness of bonded joints, J Adhesion 2020; 96:1-4, 300-320

6. Goglio L, Ferraris M. Bonding of ceramics: An analysis of the torsion hourglass specimen. Int J Adhes Adhes 2016;70:46–52.

7. ASTM. ASTM C1469-10(2015) - Standard Test Method for Shear Strength of Joints of Advanced Ceramics at Ambient Temperature 2015.

8. Li X., Bhushan B. A review of nanoindentation continuous stiffness measurement technique and its applications; Mater Charact, 2002; 48:11-36

9. ASTM. ASTM E1876 Standard Test Method for Dynamic Young's Modulus, Shear Modulus, and Poisson's Ratio by Impulse Excitation of Vibration.

10. Berroth K., 2010. Silicon Nitride ceramics for product and process innovations, Adv. Sci. Technol. 65, 70-77.

11. FCTI, 2018. www.fcti.de/de/download/FCT-SiN-Standard-Materials-2016_12-en.pdf.

12. Mersen, 2018. www.mersen.com/fileadmin/user_upload/pdf/ht/21-silicon-carbide-sic-boostecmersen.pdf.

13. Vdm-metals, 2018. www.vdmmetals.com/fileadmin/user_upload/Downloads/Data_Sheets/Data_Sheet_VDM_Crofer_22_APU.pdf

14. Salvo, M., Casalegno, V., Suess, M., Gozzelino, L., Wilhelmi, C., 2018. Laser surface nanostructuring for reliable Si_3N_4/Si_3N_4 and Si_3N_4/Invar joined components, submitted (2018).

15. Henkel-adhesives, 2018. http://na.henkel-adhesives.com/product-search-1554.htm?nodeid=8806185926657.

16. Amara, D., Levallois, F., Baziard Y., Petit, J.A., 1996. Study of a single-lap compression-shear test for brittle substrates bonded with a structural adhesive, J. Adhes. Sci. Tech. 10, 1153-1164.

17. Ferraris, M., Ventrella, A., Salvo, M., Gross, D., 2014. Shear strength measurements of AV119 epoxy-joined SiC by different torsion tests. Int. J. Appl. Ceram. Technol. 11, 394-401.

18. Ferraris, M., Salvo, M., Casalegno, V., Ventrella, A., Avalle, M., 2012. Torsion Tests on AV119 Epoxy-Joined SiC. Int. J. Appl. Ceram. Technol. 9, 795-807.

3. Results

3.1. Sandwich structures for aerospace applications

3.1.1. Joining of sandwich structures

3.1.1.1. Joining material selection

The relatively low maximum temperature (160°C) acceptable for the CFRP used in this work comes from the fact that a post-curing treatment was not used during their production to avoid detrimental effects in the coefficient of moisture expansion: as a consequence, the glass transition of these CFRP is lower than in case of post-cured ones.

Because of that, most high performance adhesives that have been developed for aeronautics and space applications, with typical curing temperature at about 250-260 °C, cannot be used.

Another constraint is the possibility to spread the adhesive in an easy way, suitable for a cleanroom environment, during the production of the Zerodur™ - CFRP - Zerodur™ sandwich structures (figure 12): the use of a cyanate ester adhesive such as CY, *even in case of a low temperature curing*, would be more difficult because the adhesive must be kept at least at 70 °C in order to have a suitably low viscosity for the joining process (..); this is not the case for the phenolic based adhesives, which can be used at room temperature.

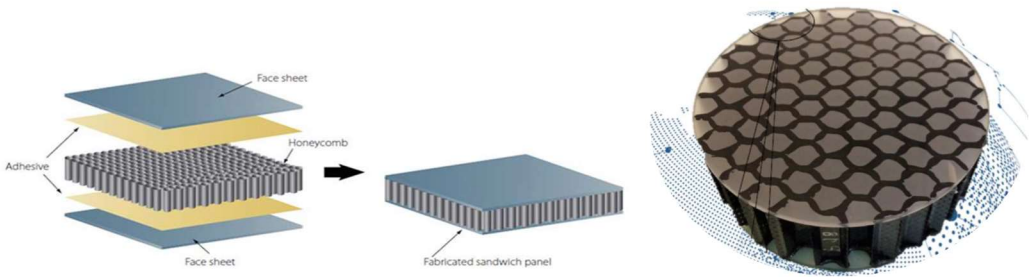

(a) (b)

Figure 12: Sketch of the sandwich structure (a) and final prototype (b) with face sheets made of Zerodur ™ and CFRP honeycomb in between. The adhesive joint between CFRP and Zerodur ™ is visible.

In consideration of what discussed above, attempts to reduce the curing temperature to 150 °C while increasing the curing time to 10 hours have been done on one of the phenolic adhesives used in this work, PH, since it was already fully characterized with the curing at 260°C in [1].

However, it is worth comparing the low temperature cured adhesive PH150 properties with those of the other adhesives cured at higher temperatures.

The commercial adhesive referred to as GB in this work was considered because it was previously used by some of the authors to join C/C composites and its properties were discussed in [2]. GB joined C/C have been tested in lap shear obtaining a sound value of 14 ± 3 MPa for SiC paper abraded C/C, while only 7 ± 4 MPa was obtained with as-received C/C. The elastic modulus inside the C/C joint was measured by a Nanoindenter XP (depth limit 2000 nm) and gave 18 ± 3 GPa [2], with a high standard deviation due to the porosity of the joint.

The GB adhesive required a curing at 260 °C, and the cyanate ester at 270 °C, both too high for the thermo-mechanical integrity of the CFRP to be joined: however, bulk samples of these adhesives were cured as slabs to be tested by dilatometry to measure their CTE for comparison purposed with PH260 and PH150.

3.1.1.2. Joining material characterization

As it can be seen in figure 13, the huge porosity of the bulk samples made it difficult to obtain suitable samples for dilatometry tests: smaller specimens were cut from these larger ones, trying to avoid large pores. It was possible to test the CTE of PH150, PH260 and GB. Every attempt to obtain suitable samples with CY failed.

Figure 14 shows the huge variation in CTE measurements on six bulk samples of PH150. The CTE measured between 25 and 100 °C ranges between 33 and 82 x 10^{-6} K^{-1} The porosity of each sample was most likely the source of this deviation. The CTE of PH260 was at about 50 x 10^{-6} K^{-1}, and in the range of 16-24 x 10^{-6} K^{-1} for GB (curves not reported here). There is a certain deviation from the GB CTE on the data sheet (7.4 10^{-6} K^{-1}) with respect to what measured in this work (16-24 x 10^{-6} K^{-1}): again, porosity can be a reason, however, there isn't any indication on the data sheet [3] about the way the GB CTE was measured.

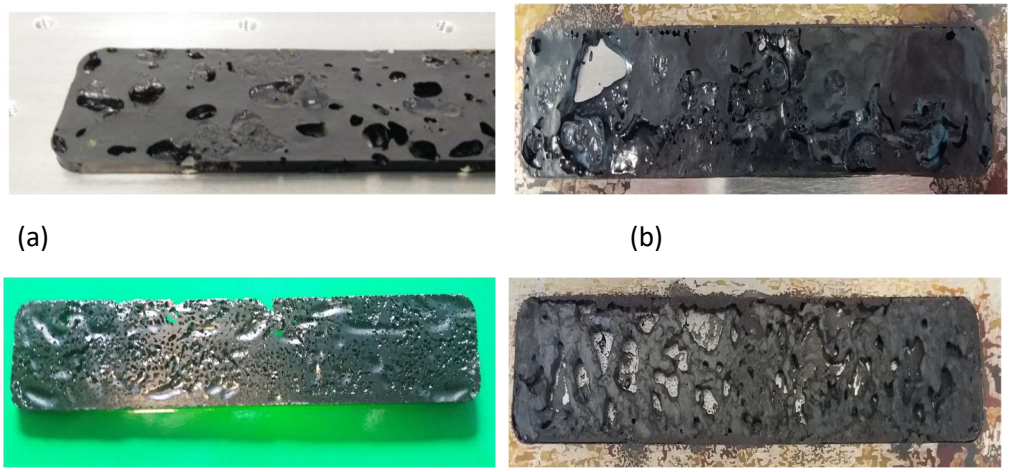

(a) (b)

(c) (d)

Figure 13: Bulk adhesives: phenolic adhesive cured at 150 °C (PH150) (a), at 260 °C (PH260) (b), cyanate resin cured at 270 °C (CY) (c), commercial adhesive cured at 260 °C (GB) (d).

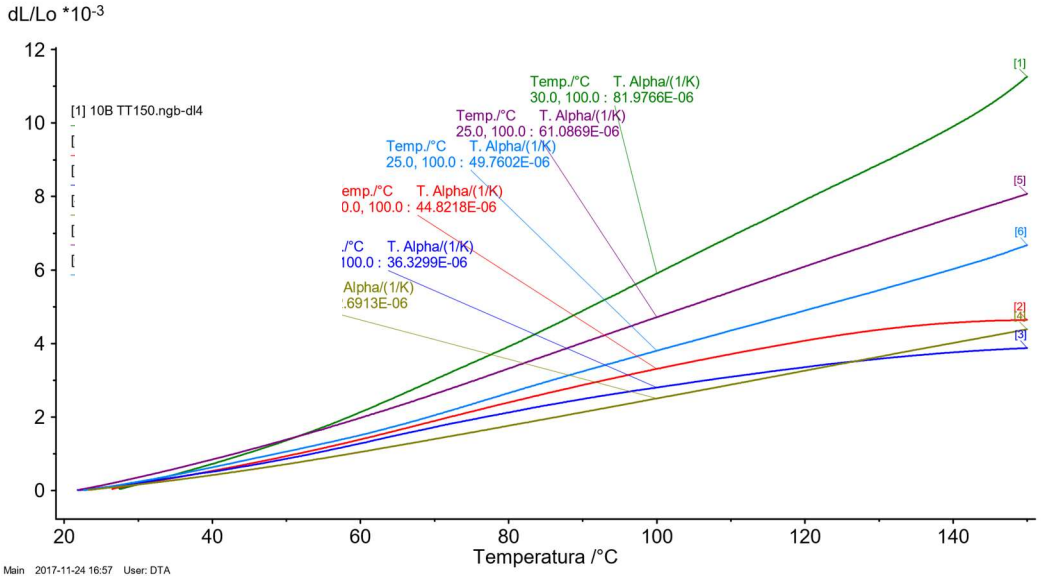

Figure 14 CTE of the phenolic adhesive cured at 150 °C (PH150) measured on 6 different bulk samples showing the huge variation of results

CFRP, the commercial adhesive (*GB*), the phenolic one with both curing cycles (*PH260 and PH150*) and the cyanate ester (*CY*) were analysed by TGA-EGA (figure 15, 16).

In order to fully characterize the thermal behavior of the selected phenolic resin with the modified curing process at 150 °C (PH150) necessary to preserve the CFRP mechanical properties, TGA-EGA was used to investigate the chemical nature of the gaseous species evolved during its heating by FTIR [4, 5] and compared with the typical curing at 260°C (PH260) (figure 15); the same analysis was done, as a comparison, on the cyanate ester resin cured at 270 °C (CY) , on the commercial carbon based adhesive cured at 260 °C (GB), and on the CFRP honeycomb used in this work.

The FTIR analysis on the phenolic cured adhesives (PH150, PH260 and GB) allowed identifying NH_3, phenol (Phe-OH), CH_4 and alkyl-lisocyanate (R-NCO). In figure 16a, the FTIR profiles of such species are reported as the absorbance at a characteristic wavenumber (namely 965 cm^{-1} for NH_3, 748 cm^{-1} for phenol, 3015 cm^{-1} for CH_4 and 2280 cm^{-1} for R-NCO) expressed as a function of the temperature. The decomposition started at ca. 200 °C with a first process during which the release

of NH_3 and R-NCO was observed. The higher temperature (ca. 500 °C) the release of CH_4 and Phe-OH was also observed at 800 °C.

The same experiment carried out on the cured cyanate ester (CY) evidenced the evolution of NH_3, R-NCO and CH_4 (figure 15). In this case, during the main degradative process, which started at ca. 400 °C, NH_3 and R-NCO were observed. A lower amount of such species was detected also at higher temperature (from ca. 550 up to 850 °C). Moreover, during this minor process, CH_4 was produced likely via the combination of residual carbon and hydrogen. The CFRP, analysed for comparison, showed a similar behaviour, being also made with a cyanate ester matrix.

For phenolic PH150 and PH260, and cyanate ester (CY) adhesive a residual 70% wt was measured after heating at 1000 °C (in nitrogen atmosphere), corresponding to the inorganic fillers content of these adhesives. While a higher filler content was found for GB, where the residual after heating was 77% wt of the initial weight. Finally for CFRP the residue after test was 83 %, showing the highest filler content for the composite honeycomb material.

In Figure 16 is highlighted the comparison between PH150 and PH260, to verify possible differences of the modified curing cycle on the adhesive properties. In general the whole TGA curves showed comparable behavior. Focusing on the main degradation mechanisms, up to 200°C no differences are detected. Between 200 and 300 °C PH150 showed a NH_3 release not detected for PH260. At higher temperatures the degradation mechanisms and species released are comparable as well as the final mass loss.

In order to univocally assess the gaseous species released during the main degradative process, the gas produced was sampled at the temperature where the main degradative process of the cured phenolic PH150 and PH260 adhesives reached the maximum speed (560 °C) and analysed with GC-MS. The gas chromatogram for both phenolic adhesives (fig. E b) evidenced that the main degradative process was a complex mixture of aromatic species (namely benzene; toluene; 1,3-dimethylbenzene; phenol, 2-methylphenol; 4-methylphenol; 2,6-dimethylphenol; 2,3-dimethylphenol or 2,4-dimethylphenol).

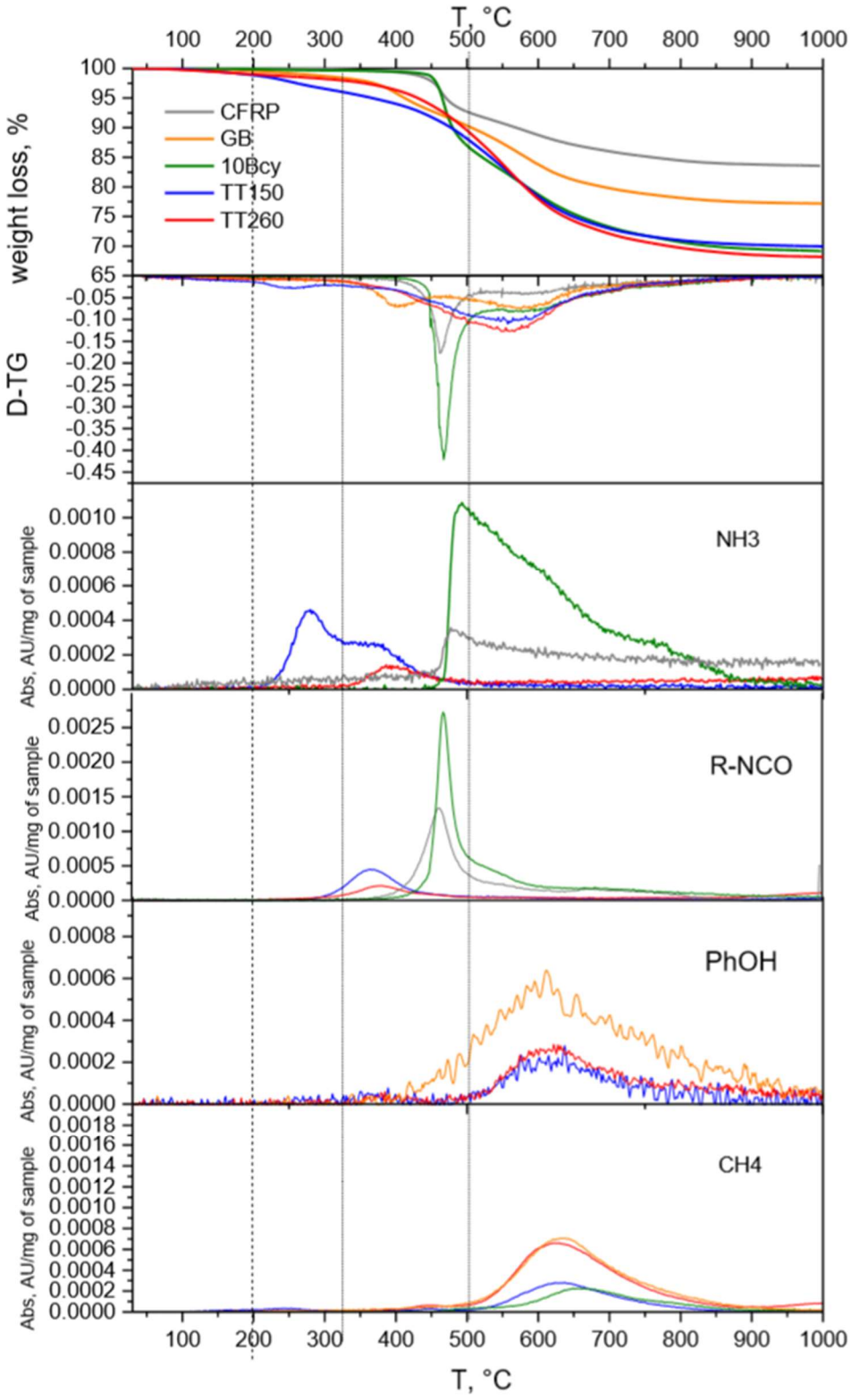

Figure 15: Weight loss %, derivative curves (D-TG) and gaseous products release by FTIR for CFRP, commercial adhesive GB, cyanate ester adhesive CY, phenolic adhesive cured at 150 °C (PH150), phenolic adhesive cured at 260 °C (PH260)

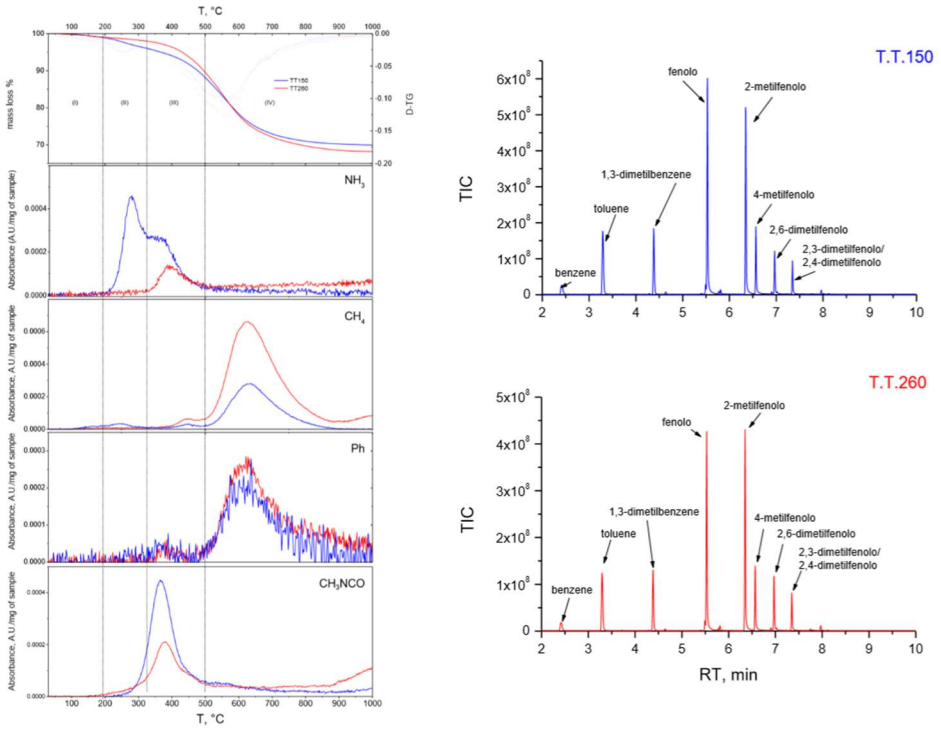

(a) (b)

Figure 16: Weight loss %, derivative curves (D-TG) and gaseous products release by FTIR (a) and gas chromatogram (b) for the phenolic adhesive cured at 150 °C (PH150) and at 260 °C (PH260)

The phenolic adhesive cured with both high (PH260) and low (PH150) temperature, and the commercial adhesive GB were used to join Zerodur™ slabs, to measure the indentation elastic modulus by nano-indentation inside the joints, figure 17: values of 8.1 ± 0.8 GPa was measured on PH150, 7.9 ± 1.3 GPa on PH260 and 12.0 ± 2.8 GPa for GB. The value measured here for GB is slightly lower than what reported in [2], always inside the joined region, but with another instrument, which gave 18 ± 3 GPa. In order to test the suitability of the nano-indentation method, the indentation elastic modulus was measured also on Zerodur ™ and it gave a consistent value of 89.9 ± 0.9 GPa. (Young's Modulus 90.3 GPa) [6]. The elastic modulus values are summarized in Table 4.

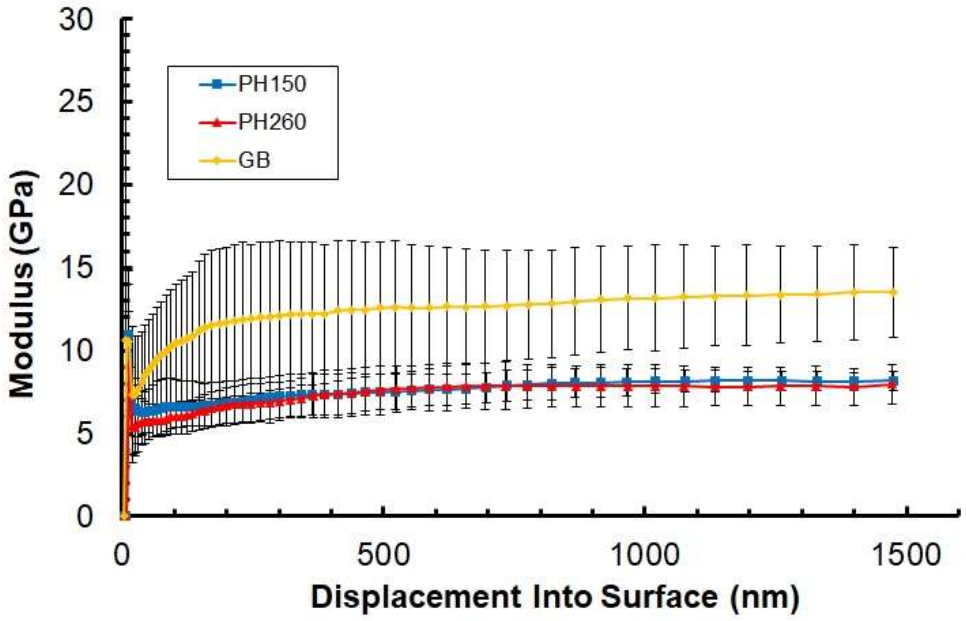

Figure 17: Indentation elastic modulus measurements by nano-indentation test: comparison between Zerodur™ joined by the phenolic adhesive cured at 150 °C (PH150) and at 260 °C (PH260)

Joining material	E (GPa)	St.Dev. (GPa)
10B (tt150)	**8,1**	0,8
10B (tt260)	**7,9**	1,3
Graphi-Bond 551-RN	**12,0**	2,8

Table 4. Elastic modulus values obtained from micro/nano-indentation

As specified by ThalesAleniaSpace requirements, the elastic modulus of the joint layer must be higher than 500 MPa and it must be measured inside the joined region. Lower values, cannot guarantee the rigidity of the final sandwich component: on this respect, PH150, PH260 and GB fulfilled the requested value. The value for CY is unavailable yet.

The phenolic adhesive PH*150* was used to join CFRP slabs: the polished cross section of a typical joint is shown in figure 18 (a-c). The interface with CFRP is

continuous and pore free and the inorganic charges are clearly visible, well dispersed in the adhesive. However, as shown in figure 18 (a) some large pores are still present, even if the curing has been done at a very slow heating rate (0.3 °C/min). The interface between the adhesive and the CFRP is barely distinguishable (figure 18 b,c), showing a perfect wettability of PH150 on CFRP.

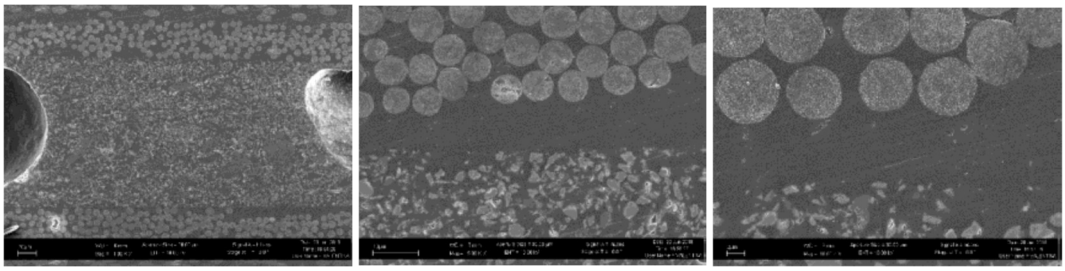

(a) (b) (c)

Figure 18: Phenolic adhesive (PH150) bonded CFRP: SEM polished cross sections at increased magnification showing the residual porosity in the phenolic adhesive (a) and the perfect wettability at the interface adhesive/CFRP (b,c); the inorganic charges in the phenolic adhesive are also visible in all pictures.

3.1.1.3. Mechanical tests

Figure 19 (a) shows the typical cohesive fracture obtained by joining CFRP slabs by PH150, after SLO testing; with an average lap shear strength of 16 ± 1 MPa both before (a) and after (b) thermal ageing of the joints (as shown in table 5).

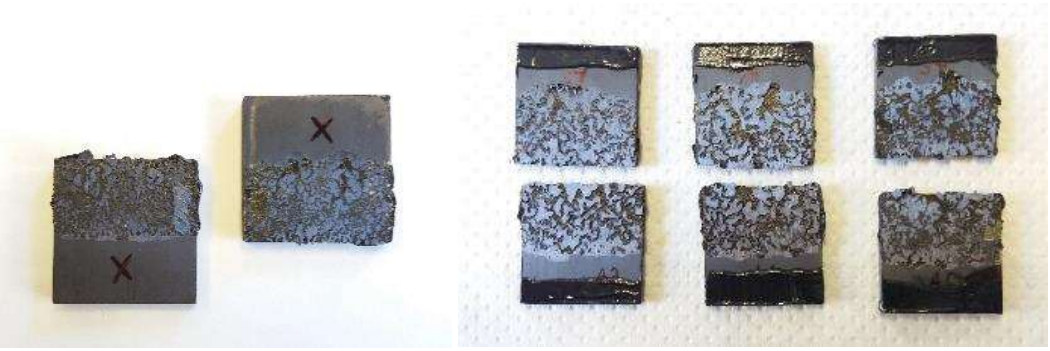

(a) (b)

Figure 19: Phenolic adhesive (PH150) bonded CFRP cohesive fracture surfaces after Single Lap Offset test, giving 16 ± 1 MPa both before (a) and after (b) thermal ageing

Test	Substrates	thermal history	Average Tensile Strength [MPa]	Type of failure
SLO	CFRP plates	No	**16 ± 1**	cohesive
SLO	CFRP plates	**Yes**	**16 ± 1**	cohesive

Table 5. SLO test and tensile glass-glass adhesion test results

As reported in [1] the lap shear strength of PH260 joined C/C was 16 MPa for joined C/C, thus showing that this phenolic based adhesive is effective as joining materials for C/C and CFRP, with both curing cycles, at least from a mechanical point of view. Also the cyanate ester adhesive joined C/C gave 13 MPa, but the main drawback for this cyanate ester resin was the temperature necessary to apply CY to large structures, as discussed above.

This drawback could be avoided by selecting a different CY having low viscosity at room temperature and some activities are ongoing on this respect.

Zerodur™ - CFRP - Zerodur™ sandwich structures (100 mm x 100 mm; 150 mm x 100 mm) joined by the low temperature cured phenolic adhesive (PH150) have been tested in triplicate in tensile (figure 20) and lap shear mode (figure 21).

The tensile test set-up built at Polito is shown in figure 20: sandwiches have been joined to metal fixtures with an epoxy glue spread on the whole fixture surface.

For tensile tests a cohesive/mixed fracture, i.e. some adhesive is visible on Zerodur™ and some on CFRP HC, and an average tensile strength of 0,78 ± 0,28 MPa was measured by dividing the maximum load at failure by the total joining area, i.e. the Zerodur™ area (100 mm x 100 mm).

If the joining area is calculated by considering the honeycomb walls area joined to Zerodur™, i.e. by multiplying the total number of honeycomb walls in each sandwich (79) by the area of a single wall, where the single wall area was derived from average thickness (0.22 mm) and length (11.55 mm) of a honeycomb wall. Then the average tensile strength was calculated dividing the maximum load at failure by the honeycomb walls area, thus giving 39 ± 14 MPa.

The shear tests set up built at Thales Alenia Space is shown in figure 21: again, the fracture is cohesive/mixed as before. An average lap shear of 0.66 ± 0.1 MPa was obtained by dividing the maximum load at failure by the total joining area, i.e. the Zerodur™ area ? (150 mm x 100 mm).

Then the apparent shear strength was calculated dividing the maximum load at failure by the honeycomb walls area (calculated as 201 mm^2), thus giving 33 ± 5 MPa.

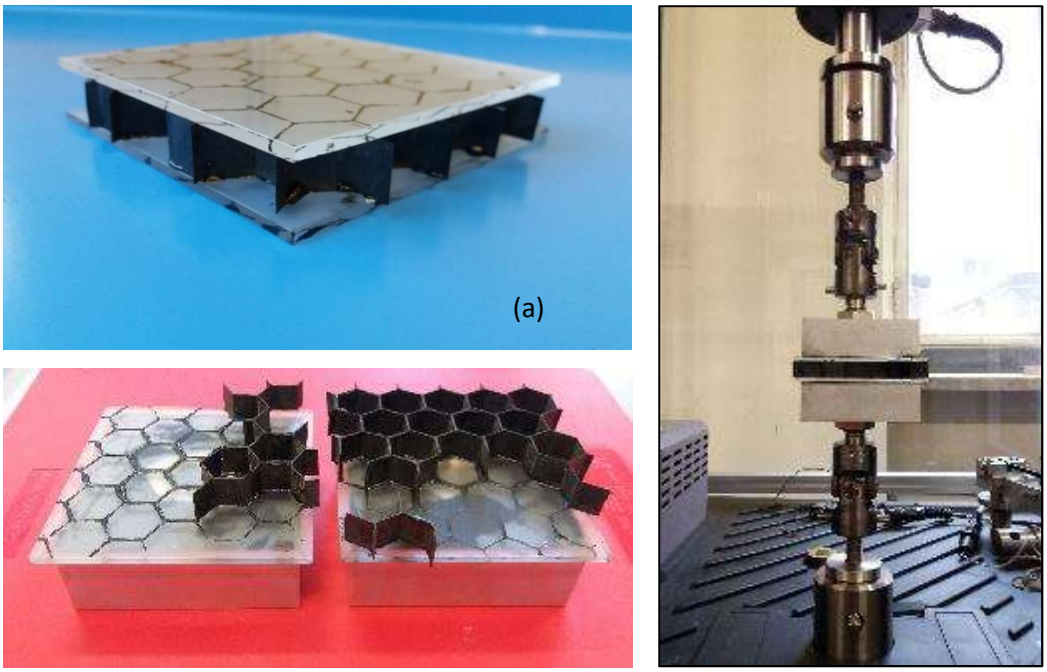

(c) (b)

Figure 20: Phenolic resin bonded (PH150) Zerodur™-CFRP honeycomb-Zerodur™ sandwich assembly (100 mm x100 mm) (a) for tensile test (b) and fracture surface of sandwiches after tensile test (c).

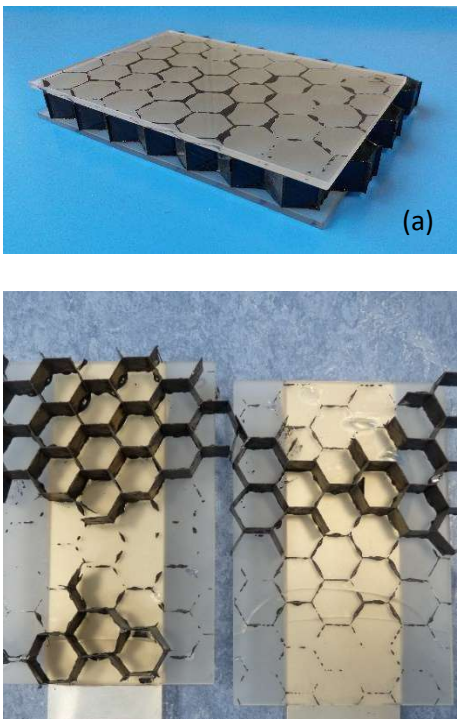

(c) (b)

Figure 21: Phenolic resin bonded (PH150) Zerodur ™-CFRP honeycomb-Zerodur™ sandwich assembly (150 mm x100 mm) (a) for shear test (b) and fracture surface of sandwiches after tensile test (c)

Table 6 summarizes the mechanical characterization carried on for aerospace structures on CFRP plates and sandwich structures joined components.

Test	Substrates	Joining material	Results [MPa]	Description
SLO	CFRP plates	PH150	16 ± 1	thermal history: NO
SLO	CFRP plates	PH150	16 ± 1	thermal history: YES
Tensile	Sandwich structure	PH150	39 ± 14	Size: 100 x 100 mm^2
Shear	Sandwich structure	PH150	33 ± 5	Size: 150 x 100 mm^2

Table 6: Summary of mechanical test results of joined structures for aerospace applications

3.1.2. CFRP surface modification

3.1.2.1. Etching

With the aim of chemically remove only a few microns of the matrix while keeping the carbon fibers unaffected H_2SO_4 was selected and tested to minimize temperature, time and acid concentration, in order to remove only a very thin layer of the CRFP matrix, while keeping the carbon fibers unaffected and thus exploiting their mechanical strength in the adhesive joints.

The experimental procedure sketched in figure 3 a was used to optimize the etching process for CFRP top surface (figure 3 b) or the CFRP side surface (figure 3 c).

Figure 22 shows the typical morphology obtained by SEM analysis of the CFRP surface after etching 10 minutes (two steps, 5 minutes each) with H_2SO_4, 96% at 100°C (a) and 125°C (b), (higher magnification pictures on the left): after etching at 100°C (Figure 22 a), the fibers are still partially embedded in the matrix and part of the matrix is still visible on the surface, making it unsuitable for a sound joint; on the contrary, etching at 125°C (Figure 22 b) gave much better results, fibers are completely clean and no matrix is visible on the etched surface. Etching at 115 °C gave similar results as at 100 °C, while etching at 150 °C resulted in an excessive removal of the matrix with loose fibers on the surface (SEM pictures not reported here), again, unsuitable for a sound joint.

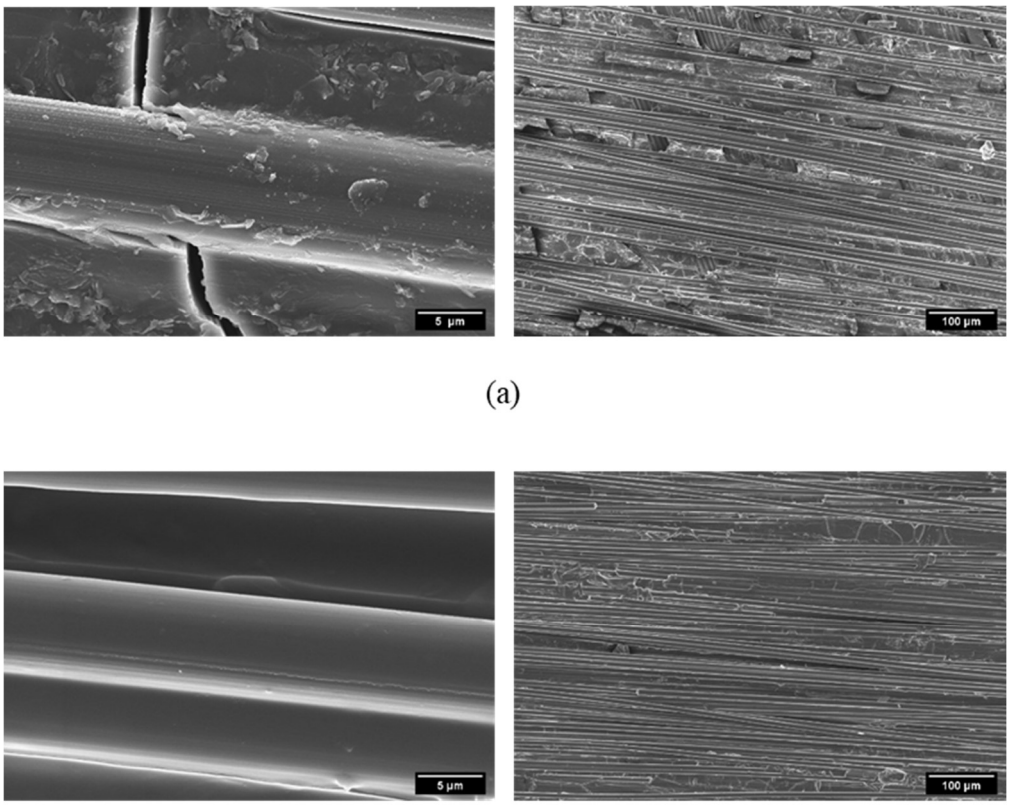

Figure 22: SEM of the CFRP surface after etching at 100°C (a) and 125°C (b), 10 minutes, higher magnification pictures on the left: after etching at 100°C (a), fibers are still partially embedded in the matrix, while with etching at 125°C (b), fibers are completely clean and no matrix is visible.

The CFRP mass loss after etching was measured (in triplicate) by weighting each sample before and after etching and was found to be 0,16 % ± 0,05 for samples etched at 125 °C, 10 minutes, and 0,13 % ± 0,01 for samples etched at 100 °C, 10 minutes.

Figure 23 shows the profilometry done on the surface of etched CFRP (125°C, 10 minutes) (a) and on as received CFRP surface, as comparison (b): as expected, the profile ranged from ±5 microns for the non-etched CFRP surface (R_a: 1,004 µm) to a ±10 microns for the etched one (R_a: 1,965 µm). The overall etched surface shows a uniform etching, with room between fibers for the adhesive to infiltrate and giving a composite joint.

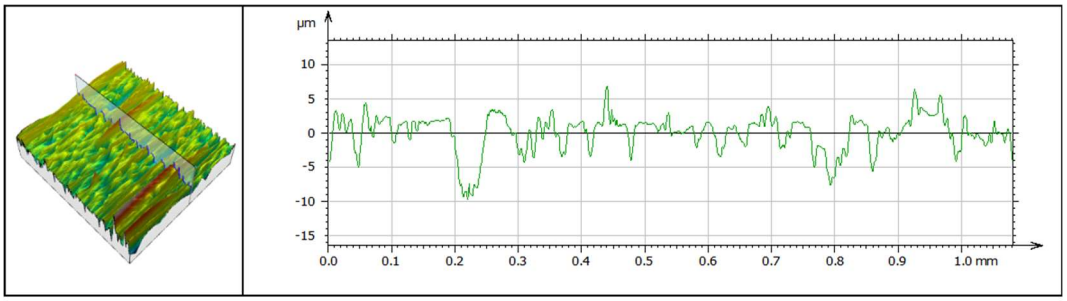

(a)

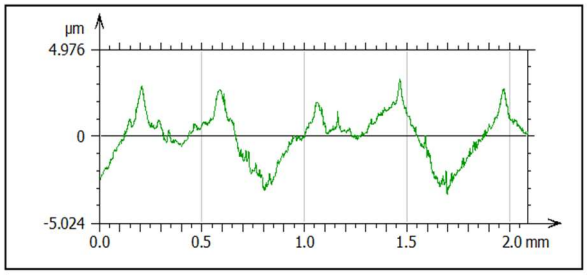

(b)

Figure 23: Profilometry of etched CFRP (125°C, 10 minutes) surface (a); as received CFRP surface profilometry, as comparison (b)

The same etching process was used and adapted to (HC)CFRP to be joined in a sandwich structure between two skins, as in Figure 4: in this case the etching was done with less aggressive conditions, such as 5 minutes at 125 °C, 96%. Even though their matrix is the same one (cyanate ester), etching at temperature higher than 125 °C and longer than 5 minutes resulted detrimental for the (HC)CFRP integrity.

Etching of the side face of CFRP was aimed to obtain a “brush” like composite to be butt-joined to another “brush” like one (figure 3 (c)): the adhesive joint should infiltrate fibers, giving a stronger, composite joint.

Actually, etching the CFRP side face was much more difficult than expected: Figure 5 (a) sketches the localized and excessive CFRP delamination occurred after

etching at 150 °C, 10 minutes; the reason for that is most likely due to excessive acid infiltration and matrix removal due to capillary forces originating inside the uncontrolled cracks in the matrix following the composite cutting process.

The etching process was then modified by adding alumina powders to the acid: the alumina-acid thick suspension was effective to reduce the acid infiltration inside the composite; in order to locally remove the suspension to keep the etching reaction going on, some hydrogen peroxide drops were added during the process: the “brush” structure was successfully obtained (Figure 5 b, c).

3.1.2.2. Joining, mechanical tests and etching optimization

All the etched composites (CFRP slabs surface or side etched, (HC)CFRP were then joined by the PH150 adhesive, cured and their cross section polished and observed by FE-SEM. Not etched composites were also joined and observed for comparison purposes.

Figure 24 shows the polished cross-sections of adhesive joined CFRP slabs, not etched (figure 24 a) and surface etched (sulfuric acid, 96%) at 125 °C, 10 minutes (figure 24 b): the adhesive infiltration inside the etched region is evident in Figure 24 (b) where the interface between adhesive and CFRP is not distinguishable. The not etched interface adhesive/composite is, as expected, a straight discontinuity between the two materials (Figure 24 (a)), while the adhesive perfectly infiltrates the etched CFRP surface replacing the removed matrix, as shown in figure 24 (b). The high wettability between fibers and adhesive, especially synthetized for this purpose, is evident in Figure 24 (c).

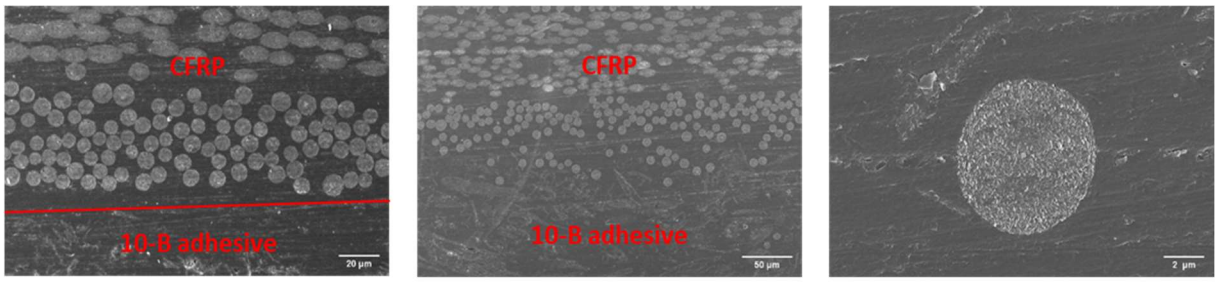

Figure 24: SEM cross-section of adhesive joined CFRP slabs: not etched (a) and etched at 125 °C, 10 minutes (b): the infiltration of the adhesive inside the etched region is evident. The interface between adhesive and CFRP is highlighted in red. The high wettability of the adhesive with carbon fibers is shown in (c)

Mechanical tests confirmed the influence of the adhesive infiltration inside the etched surfaces discussed above: a 100% increase in mechanical strength was measured by SLO test versus etching temperature, after etching at 125 and 140 °C, 10 minutes, with respect to the non-etched samples (Figure 25). A plateau in lap-shear strength was found for etching temperature higher than 125 °C. Notably, samples etched at temperature higher than 140 °C were not suitable for mechanical test, due to the excessive etching.

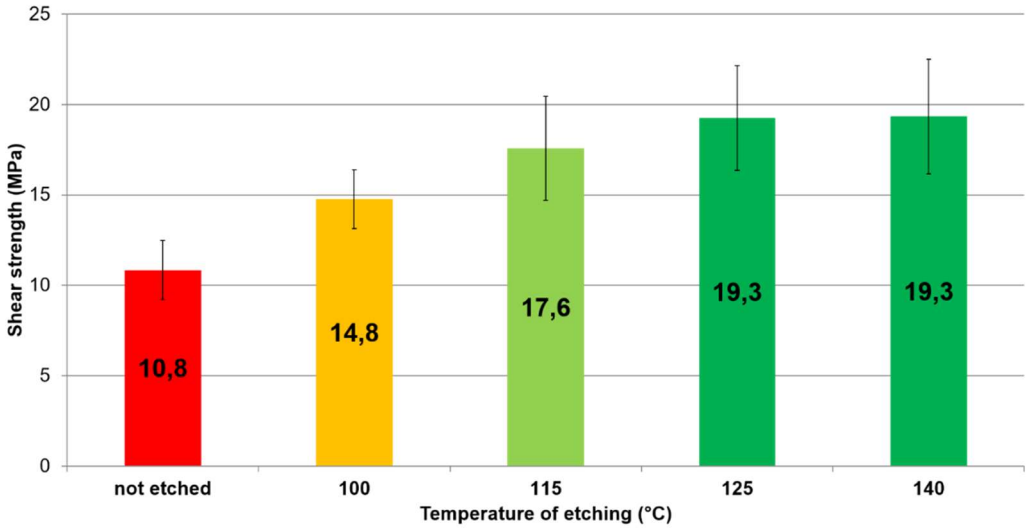

Figure 25: Results of SLO test for adhesive joined CFRP versus etching temperature (10 min, 96% H2SO4,) non-etched samples for comparison purposes.

Figure 26 shows the Load/Displacement curves of the joined CFRP after SLO test: non-etched, etched at 100 °C (10 minutes), etched at 125 °C (10 minutes); the deviation from linearity of samples etched at 125°C, 10 minutes, is due to the composite nature of the joining itself, obtained by etching and adhesive infiltration; this is in agreement with the fracture surface in figure 27 (c), where the fiber pull-out and composite delamination are evident. This is not the case for the other Load/Displacement curves in figure 26, where the adhesive does not infiltrate fibers (non-etched, figure 26) or the etching is not sufficient (etched at 100 °C, 10 minutes, figure 26).

The fracture surfaces (Figure 27) after SLO tests for joined CFRP (a) non-etched, (b) etched at 100 °C, (c) etched at 125 °C further confirm the differences discussed above due to etching and adhesive infiltration: while fractures in (a) and (b) are mixed adhesive/cohesive, with only part of the two fracture surfaces covered by adhesive, in (c) CFRP delamination and fiber pull-out is evident.

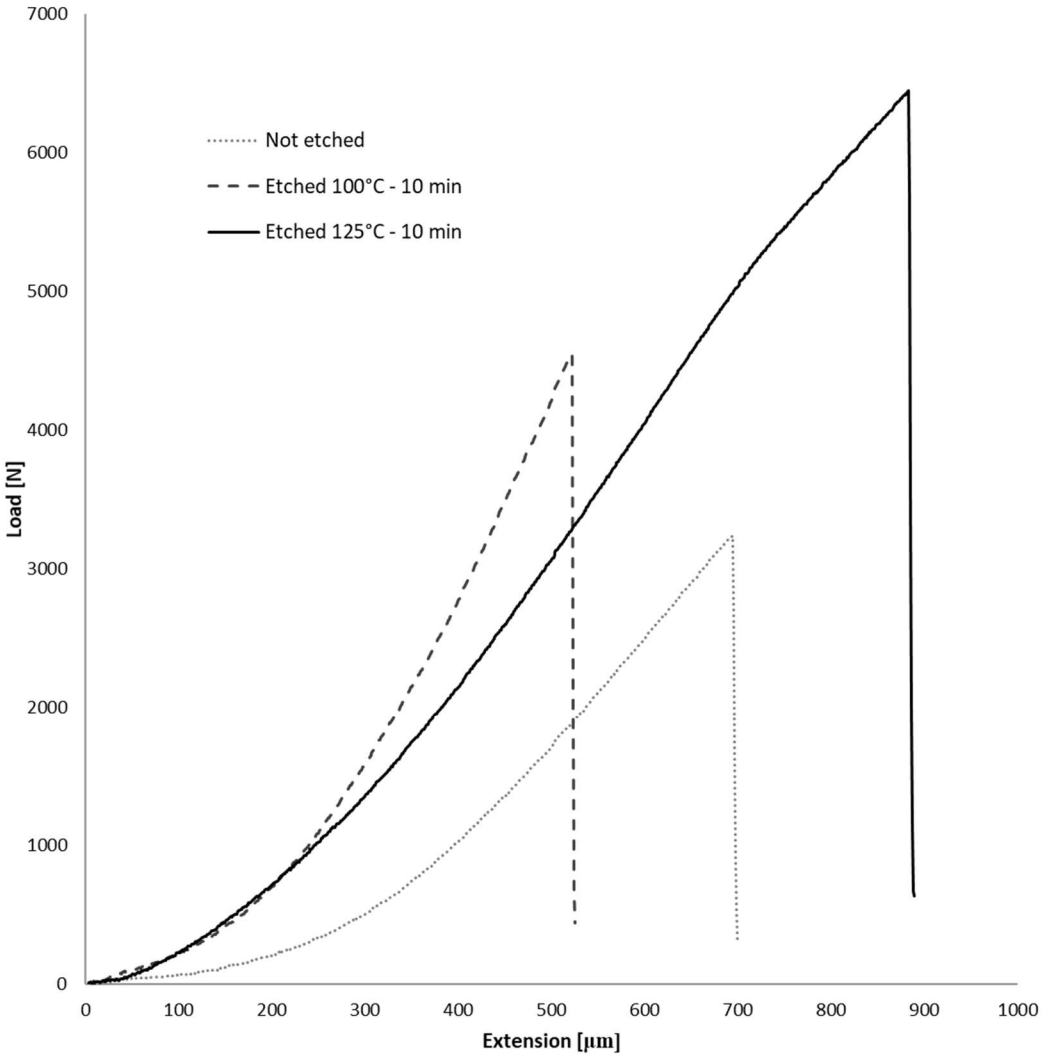

Figure 26: Typical load/displacement curves of joined CFRP after SLO test: non-etched, etched at 100 °C (10 minutes), etched at 125 °C (10 minutes); the deviation from linearity of samples etched at 125°C, 10 minutes showing the composite nature of this joint (c)

Figure 27: Fracture surfaces of joined CFRP after SLO test: (a) non-etched, (b) etched at 100 °C (10 minutes), (c) etched at 125 °C (10 minutes); fractures in (a) and (b) are mixed adhesive/cohesive, while in (c) CFRP delamination and fiber pull-out is evident.

Etching at 100 °C was found to provide a slight improvement in mechanical strength and the fracture is still mixed adhesive/cohesive; the same for samples etched at 115°C (fracture surfaces not reported here).

Remarkably, the adhesive infiltration and substitution of the removed CFRP matrix after etching 10 minutes at 125°C, showed in Figure 24 (b), corresponds to a 100% increase in lap-shear strength (Figure 25), with respect to the non-etched sample: in case of suitable CFRP etching (125 °C, 10 minutes) the joint is reinforced by unaffected carbon fibers and its strength is high enough to cause the composite delamination.

It must be considered that, even if the CFRP ILSS is about 33 MPa [7], the value of about 19 MPa measured by this lap-shear in compression is only an average one and it doesn't take into account the stress concentration peaks for this test: stresses higher than 33 MPa were probably reached at the two extremities of the lap joint, causing delamination and an average lap-shear of 19 MPa.

Different mechanical tests should be done to have a more reliable information about the effectiveness of this etching process: tensile tests, for instance, on etched and non-etched joined CFRP are under consideration.

In order to make the etching process more industrial-friendly, we tried to reduce acid concentration (96%, 76 %, 33%), etching time (ranging between 5 and 20 minutes) and temperature (ranging between 80 and 150 °C). Several surface etched CFRP were tested by the same SLO tests: Figure 28 (a) and (b) summarize the etching conditions optimized to have a 100% increase of the mechanical strength for the etched CFRP:

- the etching temperature can be lowered from 125 °C to 80 °C, but it requires a longer etching time (20 minutes) to give the same lap-shear strength (Figure 28 (a)).
- the acid can be diluted from 96 to 76%, but it requires a longer etching time (20 minutes) at 125 °C.

The attempt to further reduce the acid concentration to 33% gave a non-effective etching and lower mechanical strength.

It can be concluded that this H_2SO_4 etching is effective when done between 80-125 °C, 10-20 minutes, with 96 or 76 % H_2SO_4.

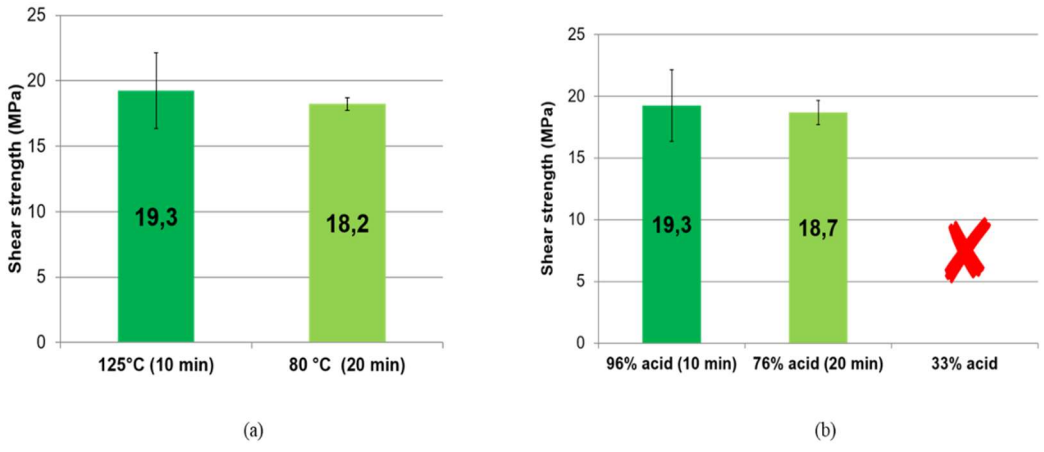

Figure 28: Influence of etching time (a) and acid concentration (b) on lap shear strength of the joined CFRP

The etching process for (HC)CFRP gave interesting results when done for 5 minutes, at 125 °C: longer time and higher temperatures had detrimental effects on the (HC)CFRP (results not reported here).

(HC)CFRP joined in sandwich structures with CPRP skins as in Figure 6 were tested in tensile mode (figure 6 a): Figure 6 (b) and 6 (c) show the sandwiches fracture surfaces after tensile tests: an adhesive failure with most of the adhesive attached to the (HC)CFRP was found for non-etched (HC)CFRP (figure 6 b); a completely different fracture surface showing cohesive failure with the adhesive on both sides and with partial (HC)CFRP detachment was found for the etched (HC)CFRP.

The tensile strength of sandwiches with not etched HC(CFRP) gave 21,4 MPa (maximum load at failure = 1708.5 N divided by the overall HC wall area = 80,02 mm^2), while for HC(CFRP) etched 5 min at 125°C it was 29,1 MPa (maximum load at failure = 2289.0 N divided by overall HC wall area = 78,75 mm^2).

Sandwich panels made of CFRP honeycomb joined to two soda-lime glass skins (figure 4, inset) gave fracture in the glass and results are not reported here. These results can only give preliminary information, but they demonstrate that this etching process can be also effective on (HC)CFRP: the effectiveness in term of mechanical strength and overall properties of the sandwich structures is still to be assessed.

Finally, the “brush” CFRP, successfully obtained by the alumina/hydrogen peroxide modified etching process (figure 5 b,c) were butt-joined by the PH150 adhesive and tested in four point bending according to ASTM D7264: up to now, no substantial improvement in the bending strength was measured, compared to the joined non-etched CFRP.

Four point bending strength of 28,8 ± 6,1 MPa were obtained for the non-etched joined “brush” CFRP and 14,3 ± 2,6 MPa, 27,0 ± 1,9 MPa, and 24,4 ± 2,5 MPa for those etched 10, 15 and 20 minutes, respectively, all of them at 150 °C. These results might be due to a still to be improved infiltration of the adhesive in the “brush” joint. Research is ongoing to optimize also this modified etching protocol

and made it suitable to etch CFRP side surfaces. Also in this case, tensile tests on etched and non-etched joined CFRP are under consideration.

All the described etching processes and the corresponding mechanical test results are summarized in table 7

Etched substrate	Etching process name	Temperature [°C]	time [min]	H_2SO_4 concentration	Test	Results [MPa]
CFRP slabs	not etched	/	/	/	SLO	10,8
CFRP slabs	100°C (10 min)	100	10	96%	SLO	14,8
CFRP slabs	115°C (10 min)	115	10	96%	SLO	17,6
CFRP slabs	125°C (10 min)	125	10	96%	SLO	19,3
CFRP slabs	140°C (10 min)	140	10	96%	SLO	19,3
CFRP slabs	80°C (20 min)	80	20	96%	SLO	18,2
CFRP slabs	76% acid (20 min)	125	20	76%	SLO	18,7
CFRP honeycomb	not etched	/	/	/	Tensile	21,4
CFRP honeycomb	125°C (5 min)	125	5	96%	Tensile	29,1
"brush" CFRP	not etched	/	/	/	4 point bending	28,8
"brush" CFRP	150°C (10 min)	150	10	96%	4 point bending	14,3
"brush" CFRP	150°C (15 min)	150	15	96%	4 point bending	27,0
"brush" CFRP	150°C (20 min)	150	20	96%	4 point bending	24,4

Table 7: summary of etching processes and their mechanical test results

References

(3.1. Sandwich structures for aerospace applications)

1. V. Casalegno, S. De la Pierre, I. Corazzari, F. Turci, P. Tatarko, O. Damiano , L. Cornillon, A. Terenzi , M. Natali, D. Puglia, L. Torre, M. Ferraris. Design, realization and characterization of advanced adhesives for joining ultra-stable C/C based components. 2020. Submitted to Macromolecular Materials and Engineering.

2. M. Salvo, V. Casalegno, Y. Vitupier, L. Cornillon, L. Pambaguian, M. Ferraris. Study of joining of carbon/carbon composites for ultra stable structures. Journal of the European Ceramic Society 30 (2010) 1751–1759

3. Graphi-Bond™ 551-RN (Aremco, USA) data sheet. http://www.aremco.com/a2.html

4. I. Corazzari, R. Nisticò, F. Turci et al. Advanced physico-chemical characterization of chitosan by means of TGA coupled on-line with FTIR and GCMS: Thermal degradation and water adsorption capacity. Polymer Degradation and Stability. 2015; 112: 1-9

5. F. Franzoso, R. Nisticò, F. Cesano et al. Biowaste-derived substances as a tool for obtaining magnet-sensitive materials for environmental applications in wastewater treatments. Chemical Engineering Journal. 2017; vol. 310: 307–316

6. Zerodur™ (Schott, Germany) datasheet. www.schott.com/advanced_optics

7. CFRP data sheet, NTPT ThinPreg™ 380CE. North Thin Ply Technology (NTPT, Switzerland) www.thinplytechnology.com

3.2. Torsion test

3.2.1. Glass-ceramic sealants for SOFC/SOEC applications

Both glass compositions were formulated so that the resulting glass-ceramics should have crystalline phases with suitable CTE (10 - 14 × 10^{-6} K^{-1}). Besides that, the glass compositions were further tuned using the SciGlass® database (Science Serve GmbH, Sciglass 6.6 software, Newton, MA, USA) in order to obtain glass transition temperatures between 600-700°C as main criteria for suitable sealants.

GC1 is a silica based glass containing Na, Mg and K oxides to adjust glass viscosity, decrease characteristic temperatures and increase the wettability on the metallic interconnect. This particular composition was also chosen for its good sintering behaviour at a joining temperature, as reported in [1].

Concerning a CTE evolution as a function of time, properties of GC1 have been published previously in [1]. XRD analysis of this glass-ceramic and associated Rietveld refinement revealed diopside as main crystalline phase and a substantial amount of a residual amorphous phase (58%wt) remaining after the joining process. Interfacial compatibility with Crofer22APU and YSZ was verified found to be very good, also after 500 h of thermal cycling (RT – 800 °C) in air (no crack formation, interactions, or failures were observed) thus, consequently, demonstrating an excellent compatibility and stability of the GC1 system in terms of thermomechanical properties.

The GC2 is a silica based glass with BaO as main modifier and without alkali metal oxides. BaO is most commonly used modifier, as it improves the wettability and CTE of the glass [2]. Moreover, in the silica based glasses, BaO tends to form $BaSi_2O_5$ phase, having CTE in the range of 11 - 14 × 10^{-6} K^{-1}, which is necessary to obtain a glass-ceramic with suitable CTE for SOFC applications for anode supported designs. However, BaO based glass systems are usually affected by the formation of a high CTE $BaCrO_4$ phase [3, 4]. The formation of $BaCrO_4$ takes place due to chemical reaction between Ba from glass and Cr from steel. The presence of this high CTE $BaCrO_4$ phase usually results in crack formation or delamination at steel/glass-ceramic interface, thus adversely affecting the mechanical stability of the joining area. In this context, in GC2, the SiO_2/SiO_2+BaO ratio has been adjusted to 0.68 to ensure the formation of a high CTE $BaSi_2O_5$ phase and to avoid/minimize the formation of the high CTE $BaCrO_4$ and cristobalite phase (SiO_2) with its different polymorphs. In addition to BaO, 7 mol% of CaO has been also added to fix the CTE and viscosity of the residual glassy phase. The Al_2O_3 concentration was kept at 4 mol% to avoid the formation of the low CTE celsian phase [5].

This particular hour-glass geometry, Figure 7 (a), labelled as THG-5, has been modelled and experimentally verified in several laboratories as one of the very few suitable methods being able to provide shear strength under torsional loading for a wide range of joined samples [1].

Results obtained by this test must be carefully analysed with the aid of advanced finite element simulation before using the derived values as shear strength values. However, in this current particularly favorable case, i.e. when the joining material is purely brittle and the fracture due to torsion load originates and propagates in the joined region only, the maximum of the torsion curves can be used to calculate the shear strength of the joint, according to the analytical formula for the shear strength of the joint, as in eq. 1 and 2 [6]:

$$\tau_{max} = Shear\ Strenght = \frac{M_{max}}{J \cdot R_e} \qquad Eq.\ 1$$

with:

$$J = \frac{\pi R_e^4}{2} \qquad Eq.\ 2$$

where τ_{max} is the shear strength, M_{max} the maximum torque, J the polar moment of inertia and R_e the outer radius of the joined area.

The area of the hourglass THG-5 geometry was multiplied by five in order to obtain larger samples (referred to as THG-25) for easier handling and in order to check if there is any size effect as typically observed in the fracture strength of brittle ceramic materials; it has to be emphasised that the THG-5 hourglass was designed a decade ago within an activity that focused on joining materials for nuclear applications and miniaturized samples were needed to test several samples in the same nuclear irradiation capsule of limited size [7, 8]. In fact, joining such small samples as here in the case of THG-5 can be an issue, in particularly when they are joined one by one: hence, this study aimed towards checking if larger samples of the same geometry (THG-25) still give the same shear strength of smaller ones (THG-5). If this is the case, the measured value is size independent and can be correctly defined and used as shear strength.

Figure 8 illustrates the torsion test equipment available at FZJ [9, 10], which is suitable for RT and HT tests; a larger magnification of a THG-25 joined sample inside the fixture is visible in Figure 8 (b); a similar equipment is operative at POLITO for room temperature test only [8].

It has been verified that the two torsion machines give statistically identical results on the basis of tests performed on more than twenty epoxy adhesive bonded steel hour-glasses (THG-5) within an internal round-robin test between the two laboratories, that was performed prior to this work as preliminary activity; since it is out of the scope of the current work, it is not reported here. Similar statistically identical results were obtained with the POLITO torsion machine within a previous

round-robin test done with two similar torsion equipment, one being at Kyoto University (Japan) and another one at ORNL (USA) [8].

In order to fully understand the torsion test results both at room and high temperature, it is important to consider potential reactions and transformations which might occur during the joining processes. Since the joining process with GC1 slurry has been done in Ar atmosphere to avoid unwanted oxidation of the graphite sample holder, a pre-oxidation process of steel counterparts was necessary prior to the joining, also with the aim to increase adhesion and compatibility between steel and GC1 sealant. Associated with this oxidation an oxide scale with a thickness of about one micron was verified to form on the steel during this pre-oxidation process, at 950 °C for two hours in air [1, 11].

Contrary to this, the joining process with the GC2 slurry could be done in a muffle furnace in air, and the oxidation process of steel took place hence directly during the joining procedure, at 950 °C for one hour.

Moreover, both sealants partially crystallized to glass-ceramics (GC1 and GC2) during the joining process; their main crystalline phases and characteristics temperatures are presented in Table 2. The GC1 has diopside (CaMgSi2O6), while GC2 has sanbornite ($BaSi_2O_5$) as main crystalline phase. As shown in Table 2, the as-joined GC1 and GC2 have CTEs of 10.9 and 11.4 × 10^{-6} K^{-1}, respectively, thus closely matching with that of Crofer22APU and assuring that they are suitable for SOFC/SOEC application. For both glass-ceramics, an oxide scale of > 1 µm thickness has been observed at the Crofer22APU surface by SEM, see for example Figure 29 (a), which is composed mainly of Cr_2O_3, as also observed in previous studies carried out on the same steel after being exposed to similar joining treatments [12].

3.2.1.1. Glass-ceramic 1 (GC1)

Figure 29 summarizes the post-test observations for GC1 joined THG-5 after torsion tests at room temperature: Figure 29 (a) is a cross-section and Figure 29 (b) presents the visual appearance of a typical fracture surface after torsion for a GC1 joint specimen. Figure 29 (c) sketches the typical fracture propagation for these samples, showing the adhesive failure behavior of these joints, i.e. with GC1 on one fracture surface only, as it can be observed in Figure 29 (d) by complementary SEM-EDS information. The measured average shear strength for these THG-5 joints corresponded to 35 ± 9 MPa.

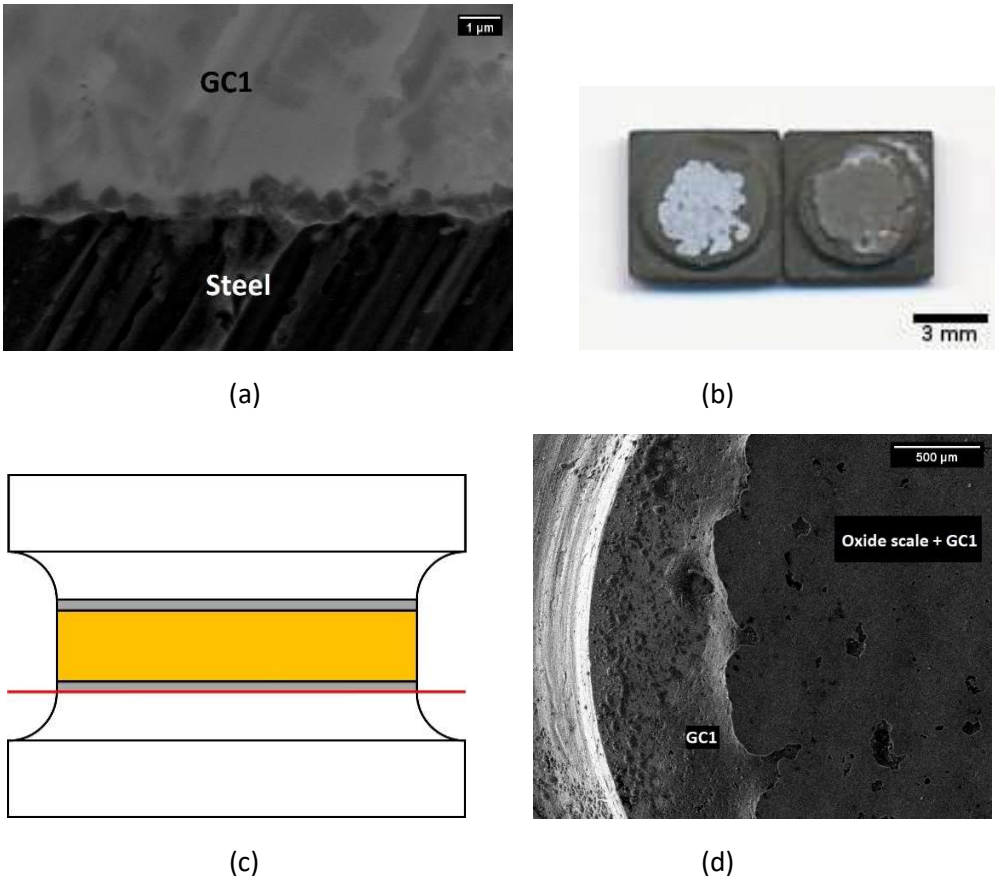

Figure 29: THG-5 joined sample tested at room temperature by glass-ceramic 1 (GC1): (a) polished cross-section; (b) typical fracture surfaces after torsion; (c) fracture propagation sketch (orange=glass-ceramic; grey=oxide scale; red=fracture propagation) showing the adhesive behavior, with glass-ceramic 1 (GC1) present on one fracture surface only, as observed in (d) by SEM-EDS, with each region identified.

The same behavior and failure morphology were also observed for the larger THG-25 tested in torsion at room temperature and the associated measured average shear strength was in this case 28 ± 6 MPa (pictures showing THG-25 specimens after testing are not reported for brevity, since they are identical to what is reported in Figure 29).

It has to be emphasized that GC1 joined TGH-5 specimens have already been the focus of a previous work and results for specimens tested at RT were reported and discussed in [11]; however, in that test series they yielded a much higher average shear strength (71 ± 10 MPa). In order to understand this unexpected difference, a comparison of fracture surfaces for the current GC1 joined samples and the previous ones was carefully performed in order to get insight into the reasons of the lower mechanical strength obtained here.

In fact, completely different fracture surfaces were observed and reported in [11]: all THG-5 joined by GC1 and tested at room temperature revealed mixed (adhesive/cohesive) mode fracture surfaces, i.e. with the glass-ceramic present on both sides. On the contrary, all the GC1 joined THG-5 that were tested in the current work showed a purely adhesive behavior as presented in Figure 29, with the fracture propagating between steel and oxide scale.

Despite careful SEM-EDS characterizations of cross-sections and fracture surfaces of several joined samples from both batches (i.e. CG1 joined samples from [11] and from this work), no evidence of different reactions at the interface between GC1 and steel was found. One may suppose that the different adhesion at the interface between steel and GC1 in [11] and in this work is most likely due to different furnaces used to prepare these samples or gas purity used to obtain the previous GC1 joints, resulting in different measured shear strengths.

To confirm this assumption, i.e. that the interface plays a strong role in the shear strength measured by torsion, it is worth noting an interesting behavior regarding torsion tests at room temperature and 600 °C for GC1 joined THG-5, (Figure 30): as expected for a brittle glass-ceramic joining material the typical torque (T, Nm)

versus time at room temperature is linear. In this case, the maximum of the four curves was used to calculate the average shear strength of these joints, according to eq.1 and 2, yielding 35 ± 9 MPa.

However, completely different torsion tests curves can be observed in Figure 30 at 600 °C (two curves) for GC1 joined THG-5, with an apparent increase in "torsional strength", which can be explained as follows: when the GC1 joined THG-5 samples were tested at 600 °C, the typical fracture surfaces, (Figure 31) has no clear adhesive failure anymore, but rather a mixed failure mode, i.e. with GC1 being present on both fracture surfaces. A certain interface strengthening might have occurred, as illustrated in Figure 31a, which shows the fracture surfaces after torsion testing of a GC1 joined THG-5 at 600 °C; the apparent mixed (i.e. adhesive/cohesive) fracture propagation is sketched in Figure 31b, with GC1 being present on both fracture surfaces, as verified by SEM-EDS , Figure 31c, which also gives evidence of some oxidation (purple zones) on the steel side.

Moreover, due to the viscoelastic behavior of GC1, which is tested in this case at a temperature close to its parent glass transition temperature, but still below its glass ceramic softening temperature (Table 2), the curves of the GC1 joined THG-5 tested in torsion at 600 °C (Figure 30) are not linear anymore and their maximum cannot be used to calculate a shear strength of the joints according to eq.1 and 2; however, it can be clearly seen that the "torsional resistance" for these samples increased when shifting from a purely adhesive-and-brittle to a mixed-and-partially viscoelastic failure mode.

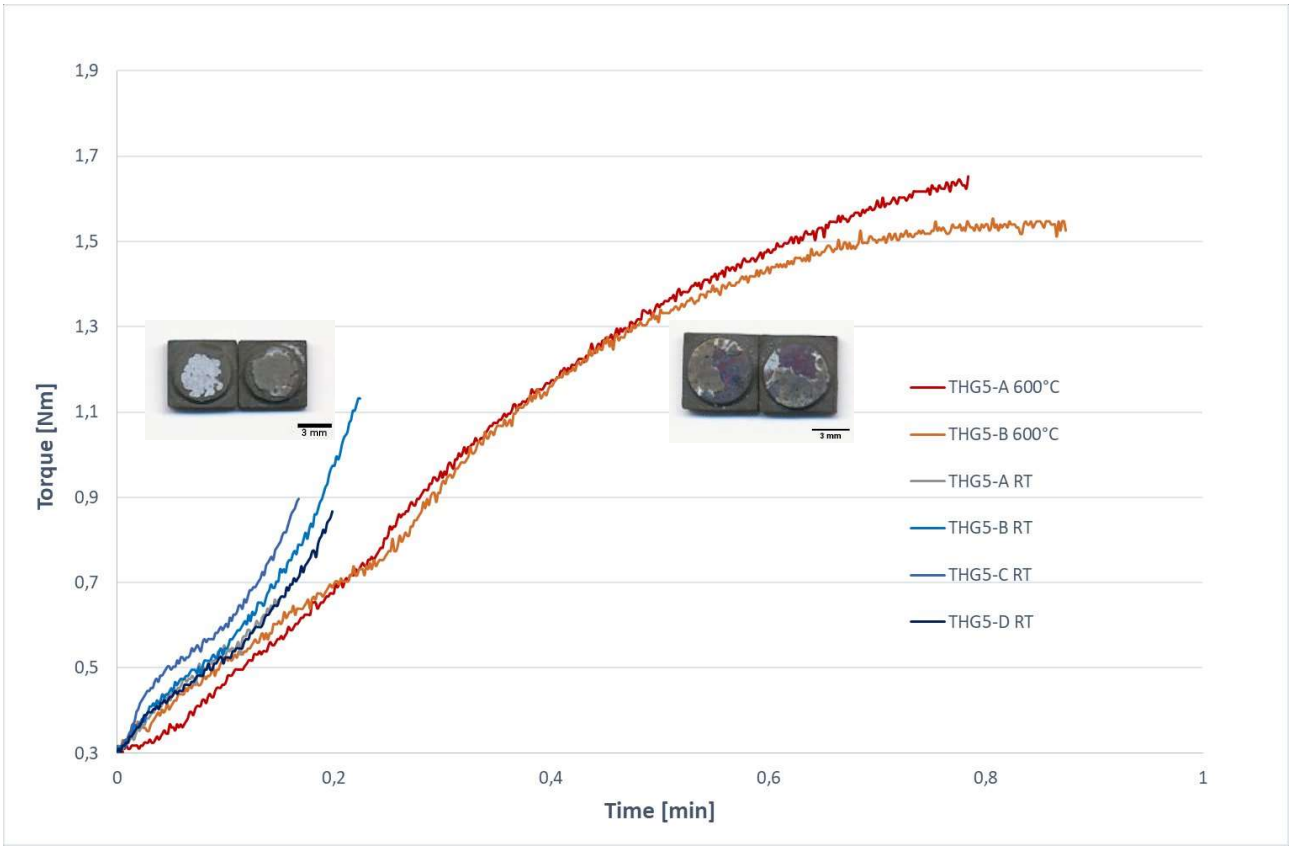

Figure 30: Typical torque (T, N/m) versus time (minutes, 4°/min) of THG-5 samples joined by GC1, showing the brittle behavior of the glass-ceramic joining material at room temperature (curves A-D, RT), with the typical fracture surfaces after torsion, (inset). Curves A-B 600°C refer to THG-5 joined samples tested at 600 °C: the elasto-plastic behavior is evident, with the typical fracture surfaces after torsion, (inset)

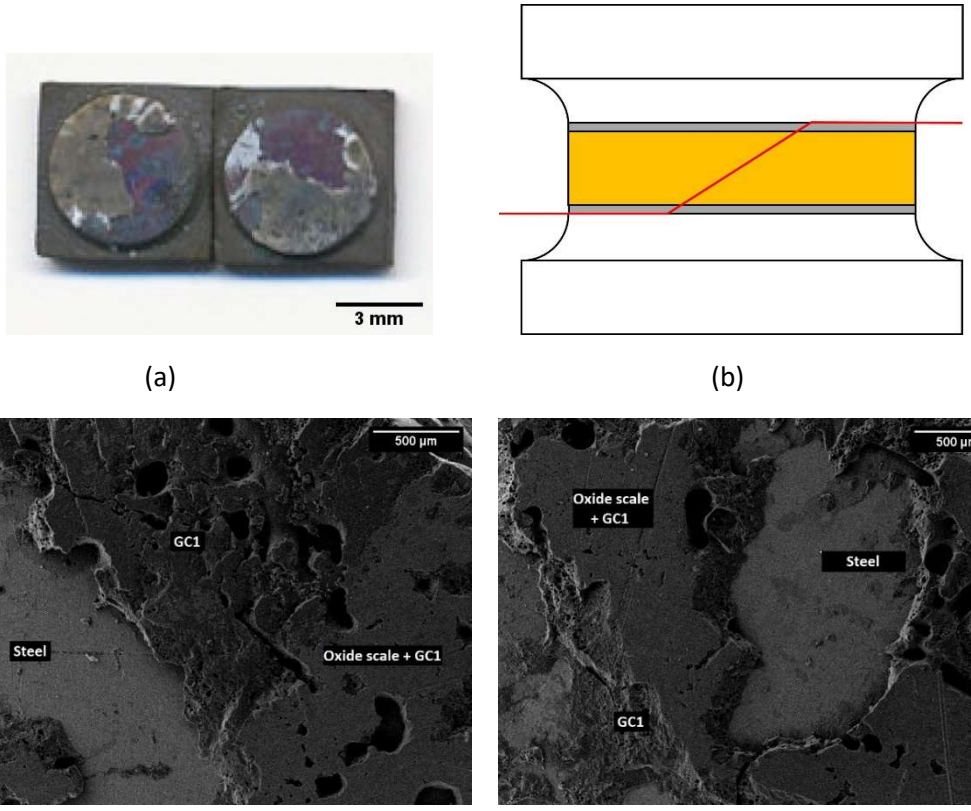

Figure 31: (a) fracture surfaces after torsion for a THG-5 sample joined by GC 1 and tested at 600 °C, showing mixed (i.e. adhesive/cohesive) behavior as sketched in (b), with GC1 being present on both fracture surfaces, as observed by SEM-EDS (c), with each region identified.

In some cases linear/brittle or non-linear/ductile behavior have been reported and discussed for epoxy adhesives tested in torsion with this kind of hour-glass geometry [13]: also for epoxy adhesives, when the torsion curves are not perfectly linear, their maximum cannot be used to calculate the shear strength of the joints according to eq.1 and 2; however, also for epoxy adhesives it can be clearly seen that the "torsional resistance" increases when the adhesive has a mixed and partially viscoelastic failure mode.

An increase in "torsional resistance" has been also reported for adhesively joined samples, when their interface strength was increased by pre-etching of substrate [14].

Table 8 summarizes all torsion results obtained with GC1 at room temperature along with information regarding the fracture mode: when GC1 is strongly bonded to steel it shows a mixed adhesive/cohesive fracture mode and gives a shear strength of 71±5 MPa at room temperature.

When the adhesion of GC1 is not optimal and its interface with steel is weak, then the fracture mode is adhesive (Figure 29) and the shear strength at room temperature (between 28 and 35 MPa) is a measure of the interface shear strength, which is about a half of what measured for the same GC1 sealant bonded by a stronger interface (71 ± 5 MPa), which fails in a mixed failure mode. It is worth emphasing that the shear strength for this (weak) interface is size independent, i.e. approximately the same values ranging between 28 and 35 MPa were obtained with both THG-5 and THG-25 geometries at room temperature.

Torsion tests on CG1 joined samples at 600°C evidenced two important features with respect to samples tested at room temperature: an interface strengthening might have occurred during heating the samples at 600°C, thus the fracture mode changed from adhesive (Figure 29) to mixed (Figure 31); moreover, curves in Figure 30 changed from elastic to elasto-plastic, due to the viscoelastic behavior of the glass-ceramic sealant at 600°C. Both features concurred in increasing the "torsional resistance" of the joined samples.

3.2.1.2. Glass-ceramic 2 (GC2)

In order to verify what has been discussed above, the results obtained with the second glass-ceramic sealant (GC2) are of some interest: GC2 was used to join hour-glass specimens made of the same steel, with the same geometry (THG-5 and THG-25), but it has higher characteristic temperatures than GC1 (Table 2). With GC2 the pre-oxidation treatment was not necessary and steel hour-glasses have been joined in air atmosphere, in alumina sample holders to keep samples in place.

Figure 32 (a,b) shows the polished cross-sections of the as-joined GC2, confirming a homogenous microstructure and a strong bonding with the Crofer22APU. Figure 32c represents fracture surfaces after torsional testing obtained for both THG-5 and THG-25 GC2 joined samples at room temperature, which yielded in the tests $\tau = 49 \pm 10$ MPa and $\tau = 45 \pm 17$ MPa, respectively; Figure 32d sketches the mixed fracture propagation behavior, with GC2 partially present on both fracture surface, as verified via SEM-EDS, in Figure 32e (pictures refer to THG-25).

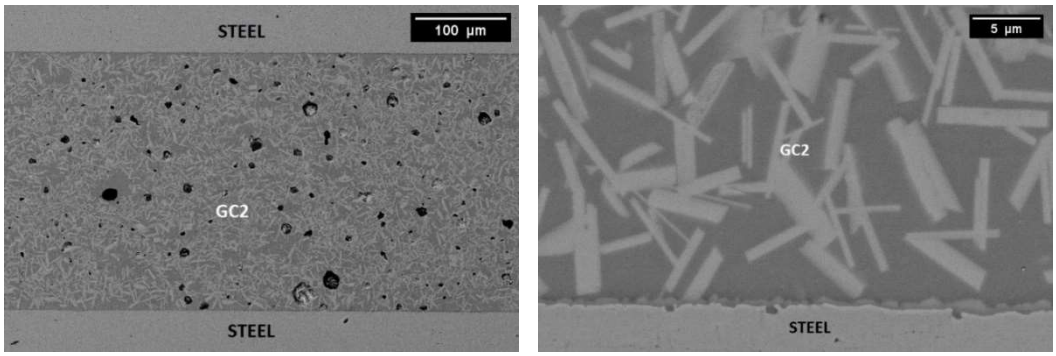

(a) (b)

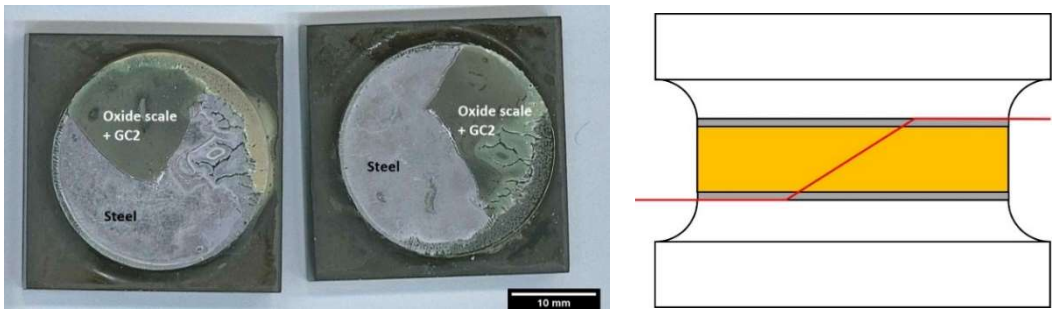

(c) (d)

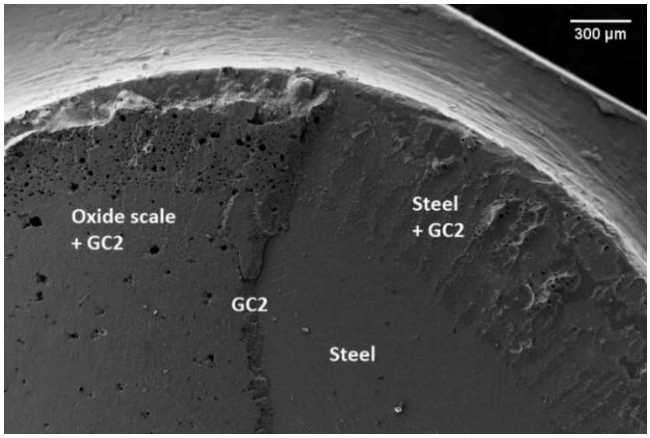

(e)

Figure 32: (a,b) typical polished cross-sections and (c) typical fracture surface after torsion for both THG-5 and THG-25 glass-ceramic 2 (GC2) joined samples after test at room temperature ($\tau = 49 \pm 10$ MPa and $\tau = 51 \pm 17$ MPa, respectively) (pictures refer to THG-25); (d) fracture propagation sketch (orange=glass-ceramic; grey=oxide scale; red=fracture propagation): mixed behavior, with GC2 partially present on both fracture surface, as verified in (e) by SEM-EDS, with each region identified.

It is evident in this case that the interface was strong enough to avoid a complete adhesive behavior: on the contrary, a mixed fracture mode was always found: consequently, the shear strength for GC2 joined hourglasses correspond to values ranging between 45-49 MPa for both THG-5 and THG-25 (Table 8). Similar post mortem results have been reported by Javed et al [15], where mixed mode fracture was observed when Crofer22APU/glass-ceramic/Crofer22APU joints were investigated under shear load, and this behavior was attributed to the strong bonding of the glass-ceramic with the Crofer22APU substrate.

It is worth noting in this context that statistically identical shear strength values were obtained for GC2 joined hourglasses of both sizes (THG-5 and THG-25), thus confirming the size independence of the measured value, which can hence be defined as shear strength of GC2 joined Crofer22APU at room temperature.

Figure 33 is an additional confirmation of the interesting peculiarity of the torsion test discussed in this work: this torsion test seems to be useful in detecting if there is something wrong in the interface strength in a joint: Figure 33a shows anomalous fracture surfaces that occurred after torsion tests of some GC2 joined THG-5 specimens tested at room temperature, with the fracture propagation mode sketched in Figure 33b. The GC2 material after the test was mostly located on one fracture surface only, as also verified by SEM-EDS in Figure 33c with each region identified. Sample fractured in this mode had an average shear strength lower than 30 MPa and have been discarded in further analysis, due to possible issues during GC2 joined samples preparation.

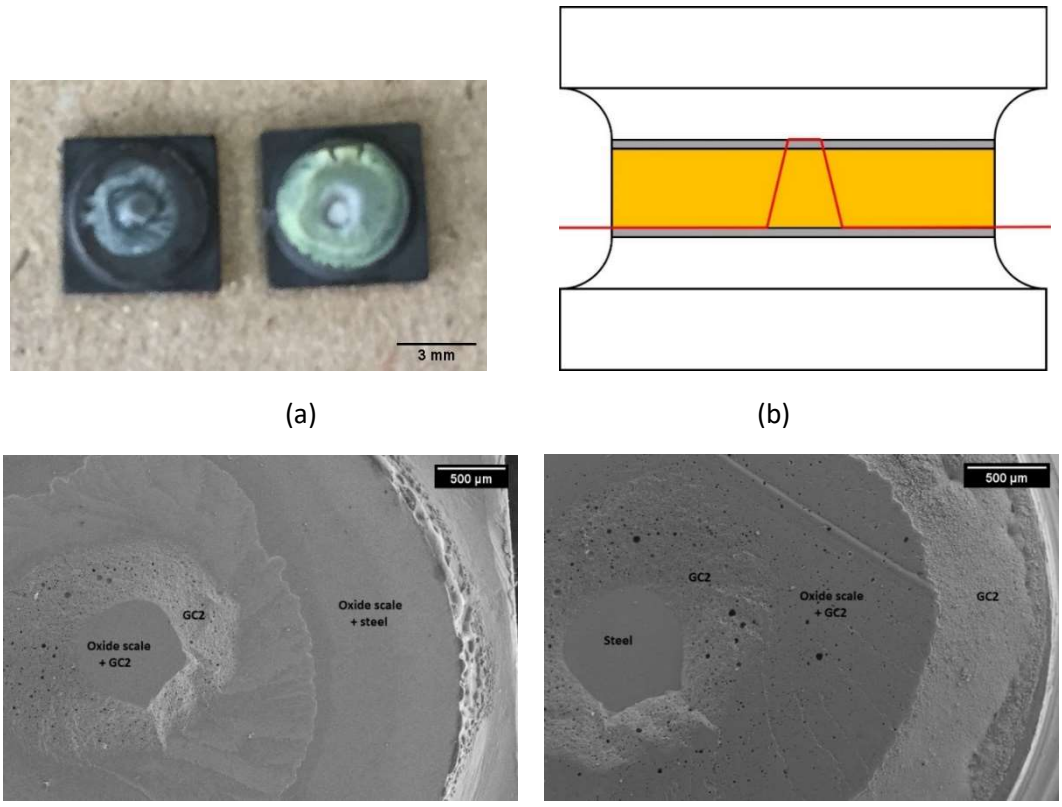

Figure 33: (a) anomalous fracture surfaces after torsion for some THG-5 GC2 joined sample tested at room temperature: (b) fracture propagation sketch (orange=glass-ceramic; grey=oxide scale; red=fracture propagation) with GC2 present mostly on one fracture surface, as observed by SEM-EDS in (c) with each region identified.

Both THG-5 and THG-25 joined by GC2 were also tested in torsion at a temperature higher than expected for these sealants, given their characteristic temperatures: their typical fracture surfaces are shown after testing temperatures of 700 °C, Figure 34a and 800 °C, Figure 34b. (pictures refer to THG-25). Their fracture mode can be defined as mixed mode for both temperatures, with the GC2 sealant material being present on both surfaces. In fact, GC2 possesses still a remarkable "torsional resistance" at 700°C, which is lower than its softening point (810°C) (Table 2); however, the steel is plastically deformed at 700°C, due to entering the plastic field under torsion, Figure 34a.

On the contrary, at 800 °C (Figure 34b) GC2 was close to its softening point (Table 2), therefore its negligible mechanical strength as joining material caused failure

of the THG-25 joined samples without plastic deformation of the steel (Figure 34b). (The same behavior was observed for GC2 joined THG-5 specimens tested at the same temperatures, which is not reported here for brevity).

A typical torque (T, N/mm) versus time curve of a THG-25 joined sample tested at 800 °C is shown in Figure 34c, from which the elasto-plastic behavior is evident. Also in this case, the maximum of the curve cannot be used to calculate the shear strength of the joint, but only to give an idea about a “torsional resistance”, as discussed above.

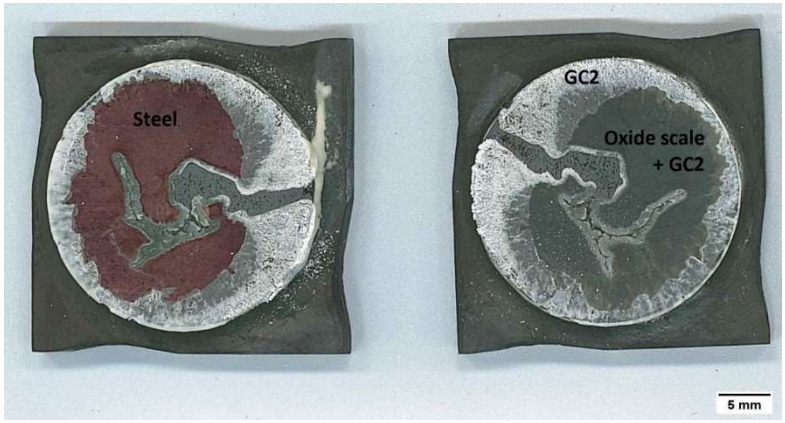

(a)

(b)

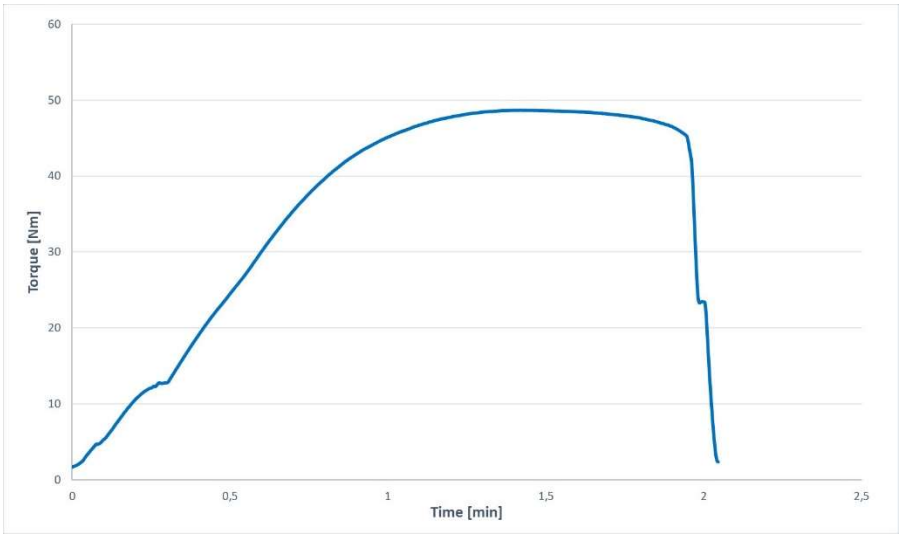

(c)

Figure 34: Typical fracture surfaces of both THG-5 and THG-25 joined by GC2 and tested in torsion (FZJ) at 700 °C (a) and 800 °C (b) (pictures refer to THG-25). Typical torque (T, Nmm) versus time (minutes, 4°/min) of a THG-25 joined sample tested at 800 °C (c).

Table 8 summarizes the results obtained with both glass-ceramics as joining materials: accordingly to what has been discussed above, it can be safely stated that the shear strength of these glass ceramic joined steel hour-glasses at room temperature ranges between 50 and 70 MPa, and it is size independent.

Both glass-ceramics retain a remarkable "torsional resistance" up to 700 °C, however, due to the non-linear behavior of these curves, a shear strength cannot be calculated by using the maximum of these curves.

		Test Temperature (°C)	N° of samples	Type of fracture	Shear strength (MPa)
GC1	THG-5	RT	11	**mixed**	**71 ± 5**
	THG-5	RT	9	adhesive	35 ± 9
	THG-25	RT	5	adhesive	28 ± 6
GC2	**THG-5**	RT	11	**mixed**	**49 ± 10**
	THG-25	RT	3	**mixed**	**45 ± 17**

Table 8 Summary of shear strength results obtained by torsion with both glass-ceramics as joining materials

3.2.2. Structural adhesives

3.2.2.1. Adhesive: DP490

The EPX DP490 adhesive (3M™ Scotch-Weld™) lap-shear strength reported on the datasheet and obtained according to BS 5350-C5 [16] on etched aluminium joined samples at room temperature is about 30 MPa. No data are provided for steel-to-steel or steel-to-glass joints.

According to the datasheet, this bi-component epoxy adhesive is a "black, thixotropic, gap filling adhesive, designed for use where toughness and high strength are required".

However, a brittle behaviour of this adhesive has been reported in [17], after lap-shear test on joined glass slabs: all joints failed with a brittle failure starting inside the adhesive and propagating inside the glass. No plastic deformation was measured in [17] for this adhesive and its average lap-shear strength was about 19 MPa, but as the authors correctly pointed out, this value is referred to the "adhesive shear strength governed by glass failure".

This is a typical problem arising with lap-shear tests where singularities due to the sample geometry (i.e., sharp edge of the adherend) and the presence of interfaces (i.e., adhesive/glass and adhesive/steel) induce stress concentration thus causing premature failure of the adherend [18].

Torsion tests on full joined hourglass samples (THG5 in Figure 9a) were modelled and demonstrated to be appropriate to measure the pure shear strength in case of brittle adhesives [19, 20]: in this case, the last (maximum) point of the torsion curve can be used to calculate the shear strength of the joint, providing that the fracture starts and propagates inside the joined area. If this is the case, the result obtained is the pure shear strength of the joined sample, without other spurious stresses (e.g. bending, tensile, peeling) involved.

However, if the adhesive is not purely brittle, full joined hourglass torsion curves show a certain nonlinear behaviour due to the adhesive plasticity and the maximum value of the torsion curve cannot be used to calculate the joint shear strength. In this work, we propose an experimental way to obtain a pure linear behaviour, by using ring-shaped joined samples. The diameter ratio of the ring-shaped sample must be increased until a linear behaviour is obtained.

Several configurations of steel-to-steel and steel-to-glass joints were tested in torsion. Since it was impossible to obtain hourglass-shaped glass samples, it was decided to start testing steel-to-steel hourglasses.

Torsion curves, together with representative fracture surfaces are shown in Figure 35-37. Curves are plotted from the onset of a steep increment of the torsional moment, immediately after an initial phase where the backlash inside the load transmission chain is fully compensated. Figure 35 is referred to full joined (Figure 35a) and 1 mm width ring-shaped (Figure 35c) steel hourglass samples, their size reported in Figure 9a and Figure 9b. All fracture surfaces showed a mixed adhesive/cohesive fracture mode with adhesive on both surfaces after fracture and their typical morphology is reported in Figures 35b and 35d. It is worth noting that a nonlinear behaviour before fracture ("plateau") is more evident for full joined samples than for ring-shaped ones, as expected for a ring-shaped geometry. This is due to a certain plasticity of the adhesive, even though it is defined as brittle in [17] after lap-shear test. A higher reproducibility of results is evident for the ring-shaped configuration: three out of four curves are almost overlapped, but they still show a certain plastic behaviour before fracture, and they are thus unsuitable to calculate the shear strength by using their maximum value.

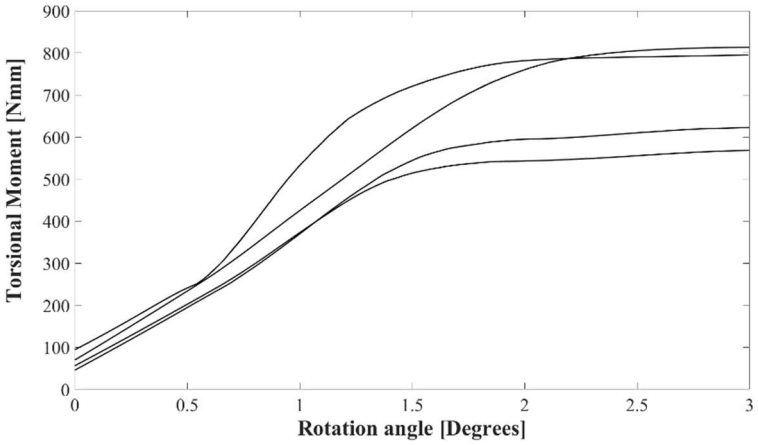

a) THG5 curves

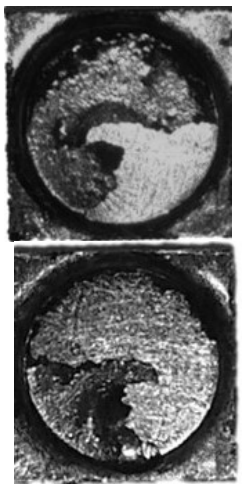

b) THG5 fracture surfaces

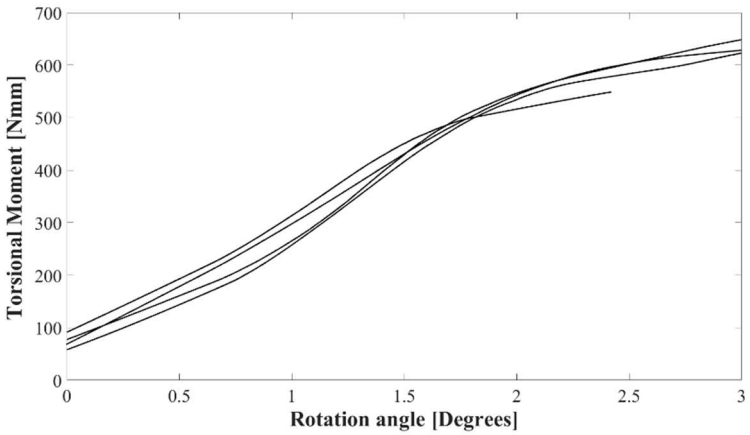

c) TDHG curves

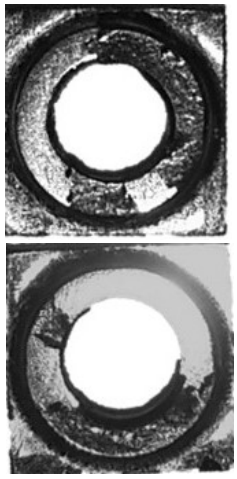

d) TDHG fracture surfaces

Figure 35 - Torsion versus angle curves (a and c) and representative fracture surfaces (b and d) of full joined (a and b), and ring-shaped (c and d) steel hourglasses after torsion test surfaces (adhesive is black).

Since it is practically impossible to join and test lower than 1 mm width ring-shaped hourglasses of this size, a different configuration was tested, with size shown in Figure 9c, and results in Figures 36a. This was also a way to test steel-to-glass joints with hourglass geometry: only one half of the steel hourglass was joined to glass slabs (Figure 9c). We selected the full joined hourglass and not the ring-shaped one, because it is experimentally very difficult to have the adhesive on the ring-shaped surface only, when such a tiny specimen is pushed on the glass slab for joining. Mechanical removal of spew fillets in this case was considered detrimental to the quality of the joint itself.

The torsion curves, together with their representative fracture surfaces, are shown in Figure 36.

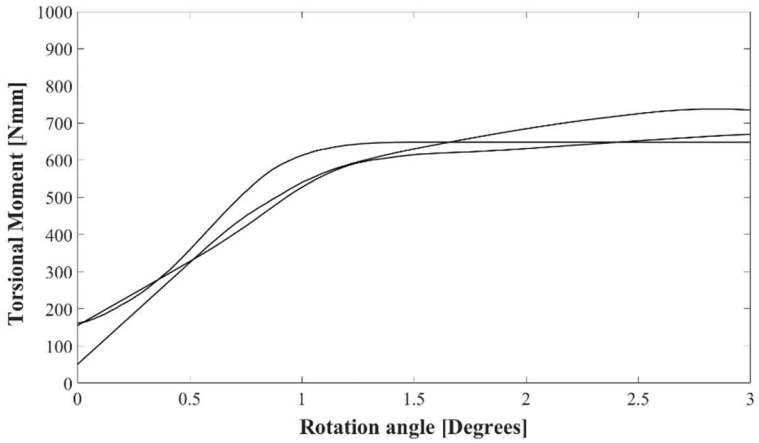

a) THG5-Glass curves

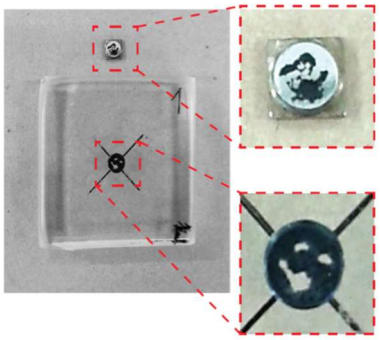

b) THG5-Glass fracture surfaces

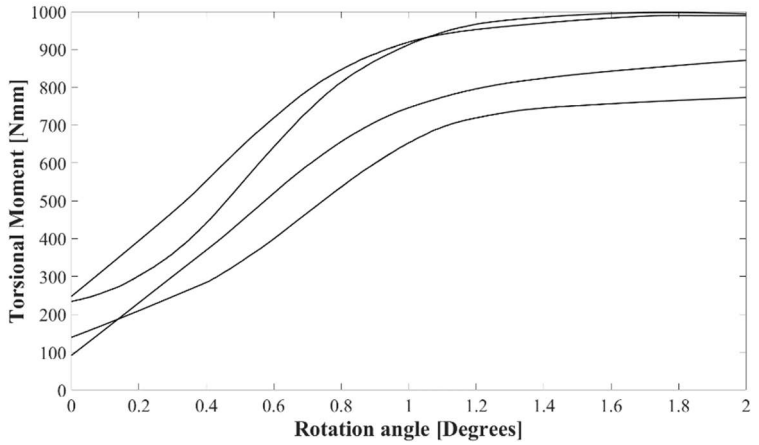

c) Etched THG5-Glass curves

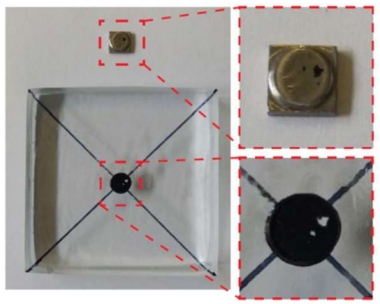

d) Etched THG5-Glass fracture surfaces

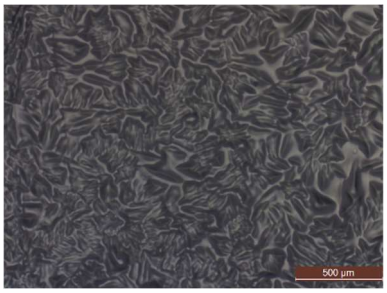

e)

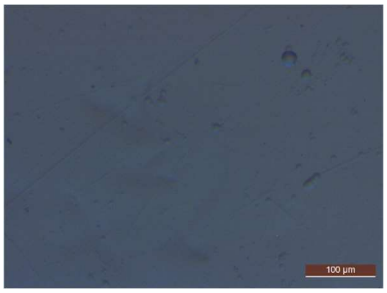

f)

Figure 36 - Torsion versus angle curves (a and c) and representative fracture surfaces (b and d) of glass plates joined to steel half hourglasses after torsion test: as received glass (a and b) and HF etched glass (c and d). Optical microscopy of HF etched glass, 15 minutes (e) and 5 minutes (f).

Mixed adhesive/cohesive failures were again obtained, with most of the black adhesive visible on the glass surface, thus suggesting a stronger adhesive/glass interface than the adhesive/steel one. As in the previous cases (Figure 35), a nonlinear-plastic behaviour before fracture is evident in Figure 36a.

A remarkably increased strength was measured when the steel half hourglasses were joined to etched glass slabs (Figures 36c and 36d), with the majority of the adhesive on the glass side. Even though in this case it was also not possible to measure the joint shear strength due to a certain plastic behaviour of the curve, it is worth noticing that this torsion test is able to detect an increased torsional resistance of the joint when the glass surface is properly etched (Figure 36e): the plateau ranges between 800-1000 Nmm with etched glass (Figure 36c), while for non-etched ones is 650-750 Nmm only (Figure 36a).

Even though etching seems to be effective to increase the shear strength of these joints, it must be considered that glass etching, like any other type of glass surface roughening, results in a reduction of the glass strength, which is disadvantageous in the design of structural glass components and must be properly tested.

A negligible increase in torsional strength was measured in case of a 5 minutes etching (Figure 36 f), compared to the non-etched ones and curves are not reported here.

In order to obtain a linear only torsion curve and to measure the shear strength for full-scale glass-to-steel joints, some ring-shaped steel samples close to the real geometry (30 mm outer diameter), with a ring-shaped joined area having ring width of 9, 7, 5 and 3 mm (Figure 9d) were joined with the same adhesive to the same glass slabs and tested in torsion. Resulting torsion curves, together with representative fracture surfaces, are shown in Figure 37.

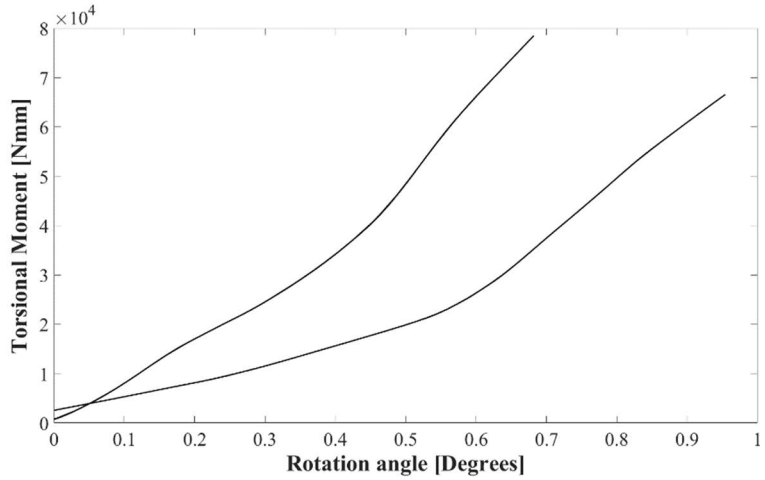

a) SGrFS curves (ϕ_1/ϕ_2 = 0.80, with ring width 3 mm)

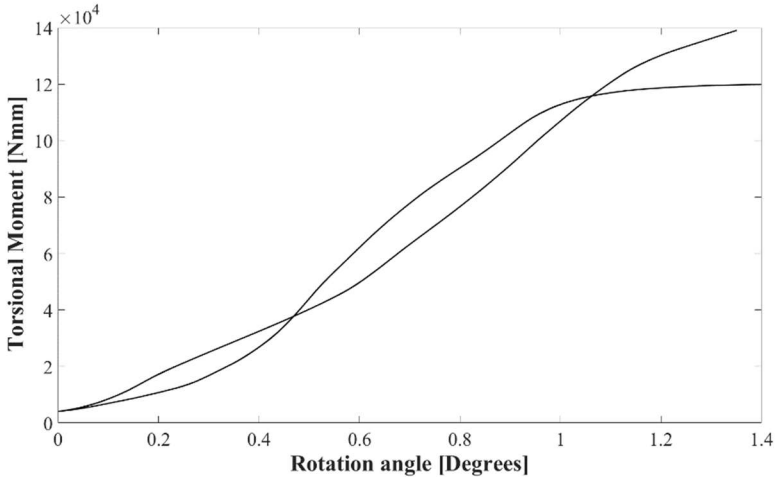

b) SGrFS curves (ϕ_1/ϕ_2 = 0.67, with ring width 5 mm)

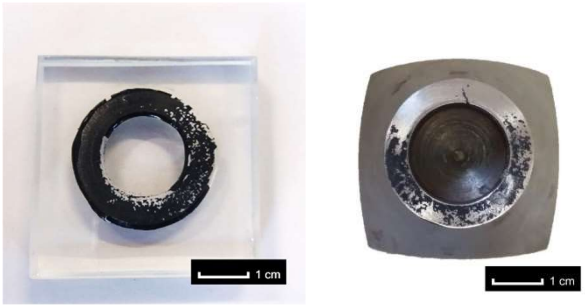

c) SGrFS fracture surfaces

Figure 37 - Torsion versus angle curves (a and b) and representative fracture surfaces (c) of full-scale (φ2 = 30 mm) ring-shaped steel fixture joined to a glass plate.

The option of testing a full joined steel fixture of 30 mm diameter to glass plates was discarded, due to the too high torque necessary to break it, unsuitable for this torsion equipment.

Torsion tests on steel fixtures with ring width of 9 and 7 mm caused indeed the fracture inside the glass on most of samples and curves are not reported here. Similar undesired failures were observed in other three tests on fixtures with ring width of 3 and 5 mm and are not reported in Figures 37a and 37b. For both ring widths, the fracture was mostly a mixed type adhesive-cohesive as observed before.

A nonlinear behavior is still visible in the curves related to the fixture with ring width of 5 mm (Figure 37b), whereas nonlinearity disappears in the curves related to the fixture with ring width of 3 mm (Figure 37a).

In figure 38a the asymmetrical four-point bending test (A4PB) setup is shown, where S_i is the inner span pin distance (4 mm), S_o is the outer span pin distance (30 mm), and the black arrows show the forces applied.

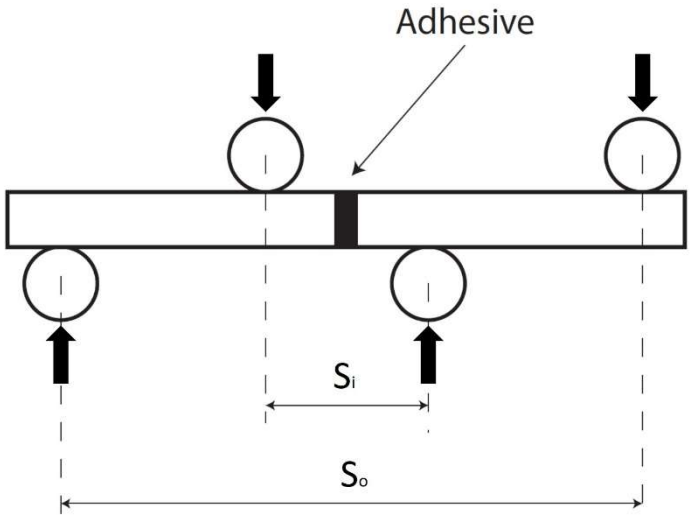

a)

b)

Figure 38 - Asymmetrical four-point bending test (A4PB) setup (a), and fracture surfaces after test on adhesive joined steel bars (b).

A4PB tests were performed on steel bars (same steel) joined by the same adhesive, with the same curing: due to the difficulty of obtaining glass bars of this size, it was decided to use A4PB on steel-to-steel joints. An average shear strength of 23 ± 2 MPa was obtained. As reported in Figure 38b, all fracture surfaces showed a mixed adhesive/cohesive fracture mode, as already observed in the torsion specimens.

In order to provide a complete range of data for modelling of these adhesively bonded glass-to-steel components, the elastic modulus of the adhesive was measured by nano-indentation technique both in the joined area and in the adhesive as a bulk specimen.

An Impulse Excitation Technique (IET) was also used to measure the elastic modulus of the adhesive as a bulk, for comparison purposes: all results are summarized in Table 9.

A value of 1100 ± 100 MPa was measured when the adhesive is in the joined region (EJ in Table 9), while 1900 ± 100 MPa was measured on bulk samples of the same adhesive (EB in Table 9), comparable to what measured by IET (2100 ± 100 MPa, E_B, IET in Table 9). A possible explanation can be in the different arrangement of the polymeric chains during curing when they are between two surfaces or in a free, un-constrained volume.

	Nanoindentation		**IET**
Poisson's Ratio ν	**E_J**	**E_B**	**$E_{B,IET}$**
	[MPa]	[MPa]	[MPa]
0.40	1100±100	1900±100	2100±100

Table 9 - Elastic properties of the adhesive measured on bulk adhesive and inside the joint by nano-indentation and Impulse Excitation Technique (IET) as indicated

The modelling activity was carried out by prof. Luca Goglio and prof. Davide Paolino.

The experimental results showed that a nonlinear-plastic behaviour is present in most of the joint types. In some cases, e.g. the THG5 and the THG5-Glass joints, an evident plateau revealed an extended plastic region in the torsion curve when the maximum of the torsional moment was reached. In some other cases, e.g. the TDHG and the SGrFS with ring width 5 mm, the plateau was less evident, and in only one case, the SGrFS with ring width 3 mm, the behaviour was completely elastic, with no plastic plateau. These different responses, for the same ductile adhesive, are directly related to the joint geometry. The effect of the joint geometry on the torsion curve was approximately described by taking into account a simplified model of joint geometry and material behaviour. In particular, the different geometries were simplified into an equivalent torsion bar, with hollow cross-section and length L (Figure 39a and Table 10), made of the investigated adhesive. The inner and outer radii of the hollow cross-section were directly taken from the joint geometries in Figure 9. The length L was instead estimated to have a torsional stiffness of the equivalent bar that matched the stiffness of the tested joints (Figures 35-37).

The material behaviour of the adhesive was approximately assumed elastic-perfectly plastic (Figure 39b), with shear modulus G equal to 393 ± 36 MPa (G = EJ / (2(1+ν)), being EJ = 1100 ± 100 MPa and ν = 0.4 the material parameters in Table 9) and elastic limit τ_{el} equal to 23 ± 2 MPa (from A4PB tests) in case of non-etched joints (Table 10).

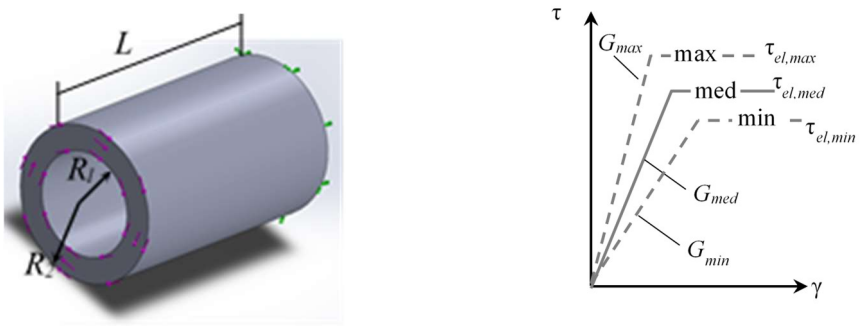

a) b)

Figure 39 – Equivalent torsion bar: a) geometric model; b) material model.

For the etched joints, the median elastic limit $\tau_{el,med}$ (equal to 29 MPa, Table 10) was estimated in order to have the modelled plastic plateau that matched the mean experimental plateau of the etched THG5-Glass joints (Figure 36c).

Joint type	R_2[1] [mm]	R_1[1] [mm]	L[2] [mm]	τ_{el} [MPa]	G[5] [MPa]
THG5	2.5	0	1.10	23±2[3]	393±36
TDHG	2.5	1.5	1.35	23±2[3]	393±36
Non-etched THG5-Glass	2.5	0	0.65	23±2[3]	393±36
Etched THG5-Glass	2.5	0	0.65	29[4]	393±36
SGrFS 3 mm	15	12	4.00	23±2[3]	393±36
SGrFS 5 mm	15	10	4.00	23±2[3]	393±36

Table 10 – Numeric data used for the equivalent torsion bar.

Figure 40 compares the experimental curves with those obtained with the simplified model of the equivalent torsion bar (Figure 39).

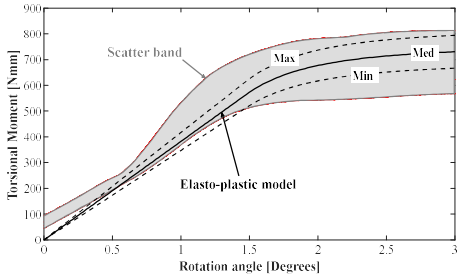

a) THG5

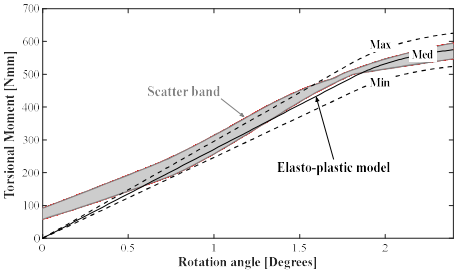

b) TDHG

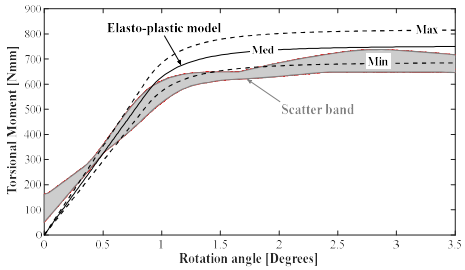

c) Non-etched THG5-Glass

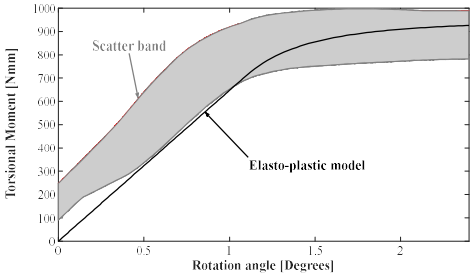

d) Etched THG5-Glass

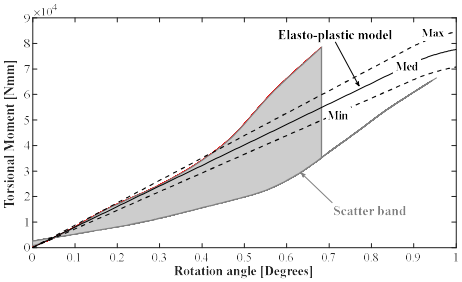

e) SGrFS, with ring width 3 mm

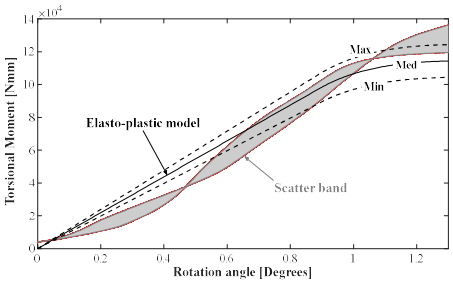

f) SGrFS, with ring width 5 mm

Figure 40 – Comparison between experimental torsion curves (grey band) and analytically modelled torsion curves (minimum and maximum curves with dashed lines and median curve with solid line): a) THG5 joint; b) TDHG joint; c) Non-etched THG5-Glass joint; d) Etched THG5-Glass joint (the solid line refers to the predicted median curve); e) SGrFS joint with ring width 3 mm; f) SGrFS joint with ring width 5 mm.

As shown in Figure 40, the modelled curves overlap the scatter bands associated to the experimental curves, in all cases. Even though strong simplifications were behind the equivalent torsion bar, Figure 40 shows that it can be usefully exploited to explain the different torsion responses for the tested joint geometries. Moreover, the simplified model also permitted an approximate estimation of the enhancement induced by the etching process (Figure 40d), which increased the median elastic limit $\tau_{el,med}$ from 23 MPa to approximately 29 MPa.

The effect of the ring width in SGrFS joints was also estimated from the simplified model of the equivalent torsion bar. Figure 41 depicts the modelled torsion curves for different ring widths in SGrFS joints.

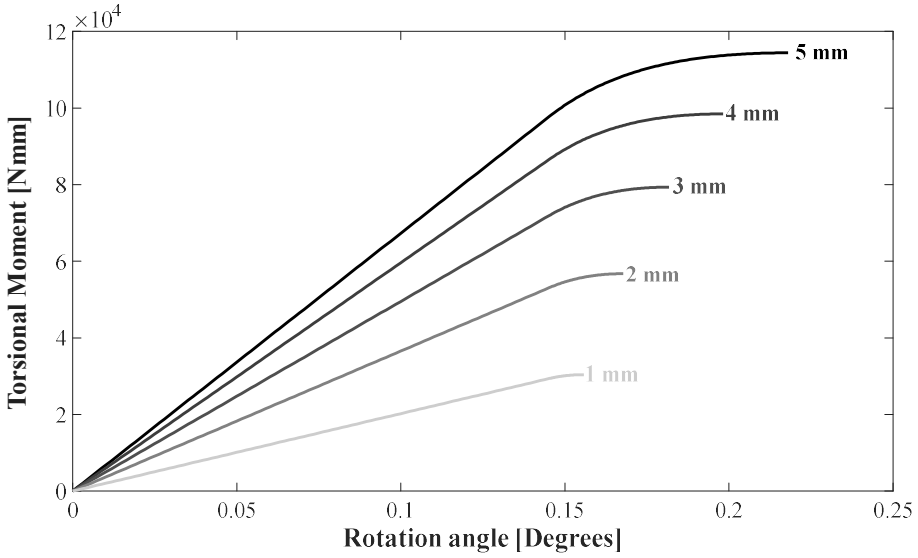

Figure 41 – Modelled torsion curves for different ring widths in SGrFS joints.

According to Figure 41, the smaller the ring width, the more brittle the behaviour. Furthermore, both the stiffness and the maximum torsional moment significantly decrease with the ring width. These considerations can be helpful when designing the SGrFS joint: for a given outer diameter, the ring width must be properly chosen in order to avoid unexpected failures in the glass slab and to have an immediate estimation of the torsional shear strength of the ductile adhesive. Table 11 reports, for different ring widths of the SGrFS joint, the errors made when estimating the torsional shear strength from the simple linear elastic torsion formula:

$$\tau_{MAX} = \frac{16 M_{t,MAX}}{\pi \phi_2^3 (1 - (\phi_1/\phi_2)^4)}$$

where $M_{t,MAX}$ is the maximum torsional moment, ϕ_1 and ϕ_2 are the inner and outer diameters.

Ring width [mm]	$M_{t,MAX}$ [Nmm]	τ_{MAX} [MPa]	***Error***
5	114×10^3	26.9	16.9%
4	98.5×10^3	26.1	13.6%
3	79.3×10^3	25.3	10.2%
2	57.7×10^3	24.6	6.8%
1	30.4×10^3	23.8	3.4%

Table 11 – Effect of ring width on the estimation of the torsional shear strength from SGrFS joints

Table 11 shows that the error decreases with the ring width and it becomes acceptable only if the ring width is below 2 mm (i.e., the estimated torsional shear strength is within the scatter band observed with A4PB tests). Nonetheless, the experimental scatter of these kinds of torsion tests should be carefully controlled through an accurate joint preparation, to avoid too much scattered results as those shown in Figure 40e. In this respect, it is expected that, thanks to a more limited extension of the adhesive region and to a smaller maximum torsional moment (which means less probability of having unexpected failures in the glass slab), the experimental scatter should significantly reduce in case of SGrFS joints with 1 mm ring width.

3.2.2.2. Adhesive: Hysol

All samples failed in the joined region, in cohesive or interfacial mode, as reported in Table 12.

Hysol EA9321 joined:	SLO (MPa)	A4PB (MPa)	THG5 (MPa)
Si_3N_4 (*)	42.2 ± 1.3	41.6 ± 8.0	44.5 ± 4.4 (62.6 ± 5.0)
SiC	41.6 ± 0.9	41.5 ± 5.0	46.5 ± 3.7 (62.0 ± 4.0)
Steel	40.8 ± 4.6	39.0 ± 3.0	52.2 ± 4.6 (67.0 ± 6.0)

(*) engineered surface, cohesive failures; all other failures are interfacial.

Table 12: Results after mechanical tests on Hysol EA9321 joined samples. Torsional (THG5) shear strength results obtained by modelling; in grey, in parenthesis, results obtained by using the maximum of the torsion curve, for discussion purposes only.

Producer reports a tensile lap shear strength (measured according to ASTM D1002-10 (2010) of 27 MPa on Hysol joined Al samples tested at room temperature (25 °C) after curing. Reported bulk properties for casted and cured Hysol samples are: tensile strength of 49 MPa with elongation at break of 6% and ultimate compressive strength of 116 MPa, with yield in compression of 64 MPa (measured according to ASTM D695), thus indicating a certain elasto-plastic behavior [21].

Table 12 summarizes results obtained by SLO, A4PB and torsion (THG5 only) on Hysol joined samples: all the failures are interfacial, except those for surface engineered Si_3N_4, which are cohesive, as discussed in [22].

The results in Table 12 have been calculated considering the maximum of each test curve for SLO and A4PB; in the case of torsion (THG5), the reported shear strength results have been obtained by modelling and, in parenthesis for discussion purposes only, those incorrectly calculated with Eq. 1 using the maximum torque value of the THG5 test curves. Results obtained on TDHG have

not been reported, due to the difficulty of obtaining reproducible results on such a small size specimen.

The purpose of this work is to propose a correct use of results obtained by torsion tests on joined components. In the case of elasto-plastic behavior of the joining material, the shear strength measured by torsion cannot be calculated by using Eq. 1 (based on elastic behavior) and the maximum torque of the experimental curve: calculating an elasto-plastic behavior with the elastic equation is obviously wrong, misleading, and cause an overestimation of shear strength results, as it is evident from the THG5 values in parenthesis in Table 12. Moreover, the strength (incorrectly) obtained in this way is size dependent, as the result is influenced by the diameter of the specimen.

These features have been observed and reported in [23, 24] for a different adhesive (AV119) and briefly discussed there as the effect of a plastic behavior for that adhesive.

Reaching elastic limit does not imply immediate failure of the elasto-plastic joining material: failure occurs when its whole section has yielded.

Figure 42 shows the modelling (this activity was done by prof. Luca Goglio) of torsion tests results (torque versus rotation per unit axial length, i.e. twist gradient) in case of a 5 mm diameter circular section joined by an ideal elasto-plastic joining material for full (THG5, R_i = 0) and annular shapes, (TDHG, R_i = 1.5, 2 mm): after yield limit is reached in the periphery and under increasing torque, zone R_i to R* has an elastic linearly varying shear stress, while zone R* to R_e a plastic (ideally constant) shear stress τ_{el} (see inset). In the analytical model used to obtain the curves in figure 42, the total torque (M_{tot}) was evaluated as the sum of the elastic (M_{el}) and plastic terms (M_{pl}):

$$M_{tot} = M_{el} + M_{pl}$$

where:

$$M_{el} = \tau_{el}\frac{J^*}{R^*}, \quad J^* = \frac{\pi}{4}\left(R^{*4} - R_i^4\right)$$

$$M_{pl} = \int_{R^*}^{R_e} \tau_{el} 2\pi r^2 dr = \tau_{el} \frac{2\pi}{3} (R_e^3 - R^{*3})$$

Thus the twist gradient is governed by the elastic zone as follows:

$$\theta' = \frac{M_{el}}{GJ^*} = \frac{\tau_{el}}{GR^*}$$

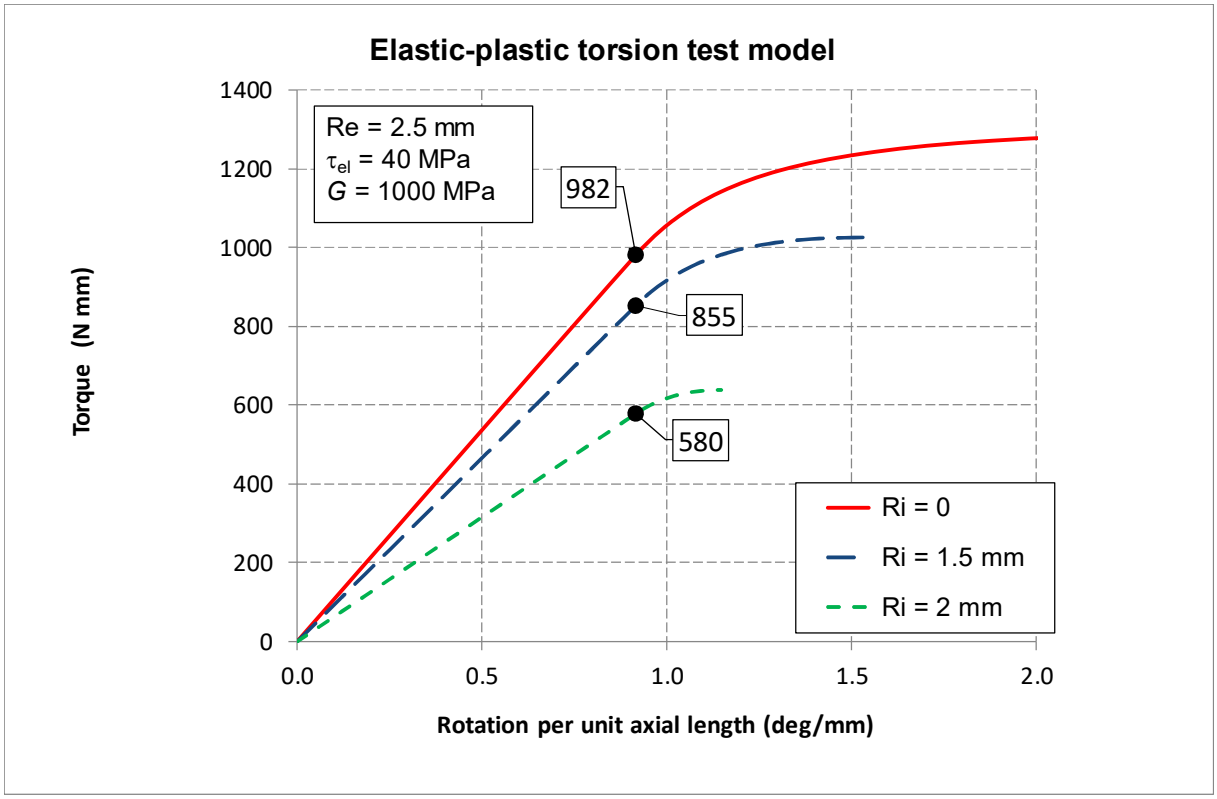

Figure 42: Modelling of torsion tests results (torque versus rotation per unit length) in case of a 5 mm diameter hourglass joined by an elasto-plastic joining material: Ri = 0 for THG and Ri = 1.5 or 2 mm for TDHG; black dots show torque values corresponding to the modelled elastic limit. When the elastic limit is reached in the periphery and under increasing torque, zone Ri to R* has an elastic linear shear stress, while zone R* to Re a plastic (ideally constant) shear stress (inset).

Curves in figure 42 (Torque, Nmm, versus rotation per axial unit length, deg/mm), are obtained for a hypothetical adhesive with τ_{el} = 40 MPa, G = 1000 MPa where R* increases from Ri = 0 mm (for fully joined sample, i.e. THG5) to Ri = 2 mm (TDHG used in this work has Ri = 1.5 mm).

It is clearly shown that in the case of a very thin joined annulus (Ri → Re) τ_{el} can be obtained as under elastic behavior, i.e. the plastic contribution is minimal and the obtained result is correctly approaching the shear strength of the joined samples. Thus, as the result is practically the true shear strength of the adhesive, it is not influenced by the size of the specimen.

Experimentally, this means that when dealing with a non-purely brittle joining material, such as an elasto-plastic one, the full joined hourglass samples give overestimated results when the maximum torque of the experimental curve is used to calculate the shear strength, because it does not take into account correctly the plastic contribution, as reported in [23].

The size independent pure shear strength with torsion test for an elasto-plastic joining material can be obtained by joining ring shaped TDHG and gradually reducing the thickness of the joined annulus, to reduce the plastic contribution.

Once the size independence in the torsion test is achieved, the obtained shear stress must converge to the A4PB result calculated as force to area ratio, considering that, due to the elasto-plastic behavior of the adhesive, the shear stress becomes uniform also in the A4PB joined section.

Experimental results on TDHG samples with a drilled hole of 3 mm gave values higher than those expected by modelling, thus confirming the residual and non-negligible contribution of a plastic deformation for Hysol also with these TDHG: due to the impossibility of joining TDHG samples with a drilled hole of 4 mm (Ri=2, figure 42), i.e. an annulus of 0.5 mm, the expected size independence has not been obtained yet with this hourglass geometry and results are not reported here. Further experimental activity is ongoing.

Model and experimental curves for Hysol joined THG5 samples, Si_3N_4 (a), SiC (b), steel (c), respectively are reported in figure 43. Torque values corresponding to the modelled elastic limit are indicated by black dots, with shear strength obtained from these torque values also indicated in each graph.

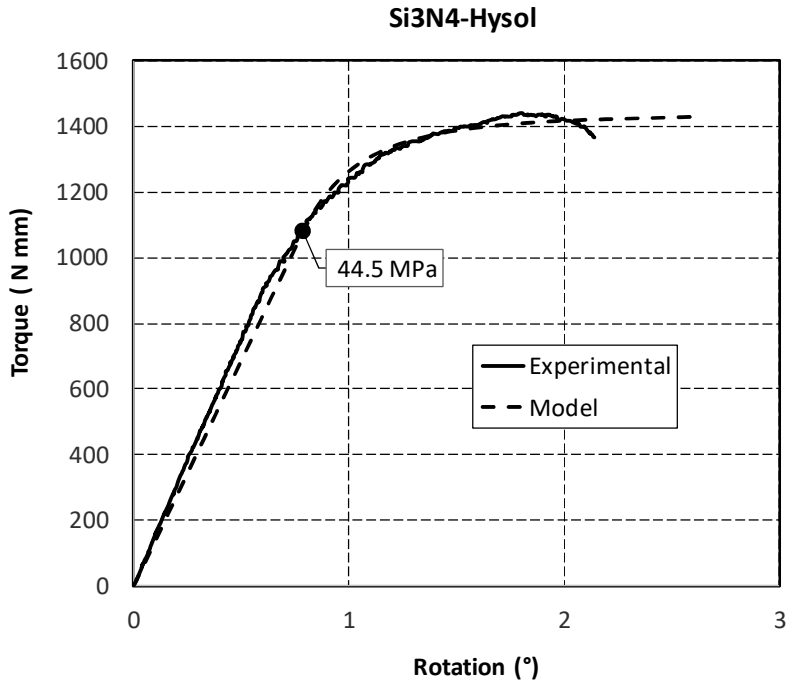
Si3N4-Hysol
Torque (N mm)
Rotation (°)
44.5 MPa
Experimental
Model
0
200
400
600
800
1000
1200
1400
1600
0
1
2
3

(a)

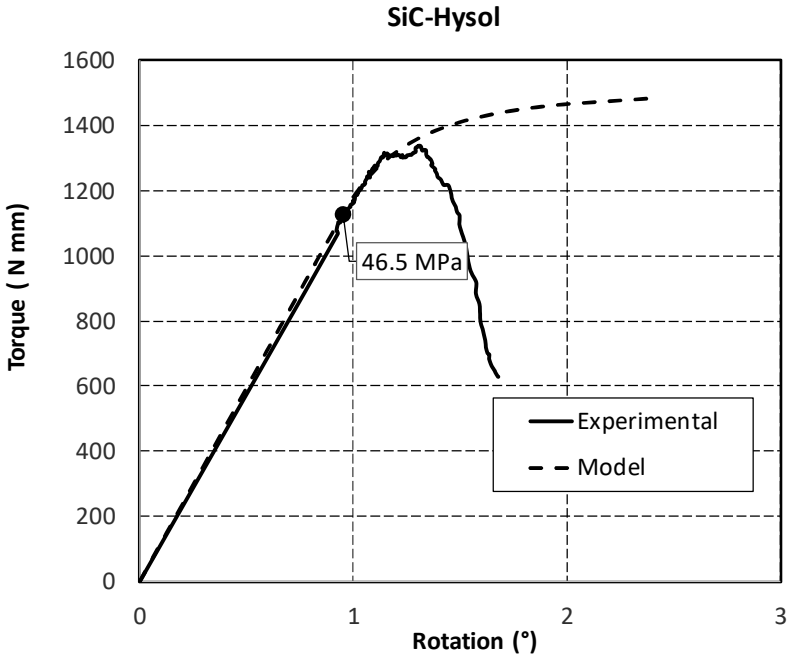
SiC-Hysol
Torque (N mm)
Rotation (°)
46.5 MPa
Experimental
Model
0
200
400
600
800
1000
1200
1400
1600
0
1
2
3

(b)

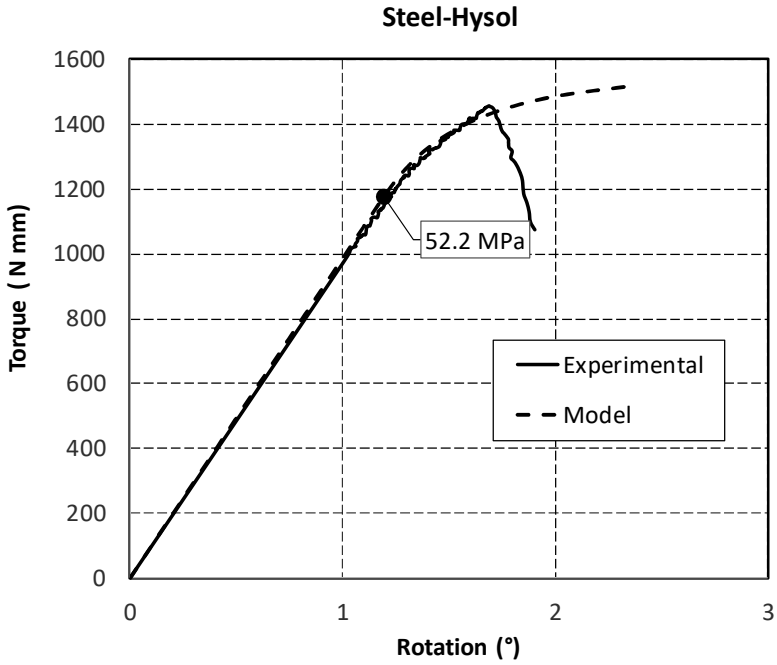

(c)

Figure 43 (a-c): Model and experimental curves for Hysol joined THG samples after torsion tests: samples are Hysol joined Si3N4 (a), SiC (b) and steel (c). Torque values corresponding to the modelled elastic limit are indicated by black dots, with shear strength calculated from torque indicated in each graph. Cohesive failure of the surface structured Si3N4 (a) shows an evident plastic behavior in the experimental torsion curve, while interfacial failure of SiC (b) and steel (c) evidences a limited plastic region.

In order to avoid the time consuming (and sometimes experimentally impossible) activity of gradually reducing the thickness of the joined annulus, the model discussed before shows that the elastic limit can be obtained in fair agreement with the experimental torque/rotation curves (figure 43 a-c) and with A4PB results, which provide the correct shear strength for all the joined samples (Table 12).

It is worth noting that the cohesive failure of the surface structured Si3N4 shows an evident plastic behavior in the experimental torsion curve, while interfacial failures of SiC and steel joined samples evidence a limited plastic region in the experimental curve. This strikingly different shape of the experimental torsion curve in case of interfacial or cohesive failure of the same adhesive can be explained as follows: in the case of cohesive failure, the plastic deformation acts

from the outer diameter to the center of the hourglass; instead, in case of interfacial failure, this progressive extension of the plastic zone cannot take place and the experimental torsion curve drops earlier.

This also leads to an overestimated value of the shear strength, as can be noticed from Table 12, especially in case of steel: the value 52.2 MPa obtained from THG5 is out of the range in respect with the other results. Actually, the elasto-plastic behavior assumed by the model implies a rounded upper part of the curve, which does not match with the sudden drop experimentally observed in case of interfacial failures. Thus, trying to reproduce with the model at least the early part of the experimental post yield curves (i.e. immediately after yield and before the drop), leads to adopt a yield stress value higher than the actual one, to "lift" enough the model curve.

It is also remarkable to see that the SLO in compression used in this work (figure 44) [25] gives similar results as those obtained by both A4PB and correctly used torsion. This similarity can be explained as follows:

-the elastic shear stress-strain distribution in lap joints under compression is far from being constant, as it exhibits peaks in the ends of their overlap. The longer the overlap, the higher are the peaks with respect to the mean shear stress. In case of a brittle adhesive, stress concentration due to these peaks triggers the fracture that causes failure of the whole joint. In case of an elasto-plastic adhesive, the plastic behavior starts from these peaks and progressively extends towards the center of the joint under increasing load [26]. Ideally, the load can increase until the adhesive has yielded also in the center, but if the behavior is not ductile enough the limit strain giving fracture is reached before, thus the ultimate load is lower than the value corresponding to complete adhesive yielding.

-moreover, also peel stress is present in most lap joints under compression; this is due both to the non-alignment of the adherends (unavoidable in a single lap joint) and to their flexibility, which induce relative displacement of the bonded surfaces also in normal direction.

- however, in the present work, a peculiar version of SLO under compression (figure 44) [25], derived from ASTM D905-08, which applies primarily to bonded timber, has been used. The two joined adherends are relatively thick and short, thus their flexibility is minimized.

Moreover, the specimen is kept in a fixture which supports also the backface of each adherend by means of rollers to allow its sliding; therefore, a nearly uniform relative sliding of the adherends is obtained during this test. This condition is similar, and even more favorable, to the case of the thick adherend shear test ASTM D5656 in tensile, which aims at a condition of nearly pure shear. Thus, by testing an elasto-plastic adhesive able to “smooth” stresses, and by using a carefully designed SLO, as the one described in this work, the ultimate load is obtained under a nearly uniform shear stress distribution equal to the elastic limit of the adhesive, i.e. its shear strength.

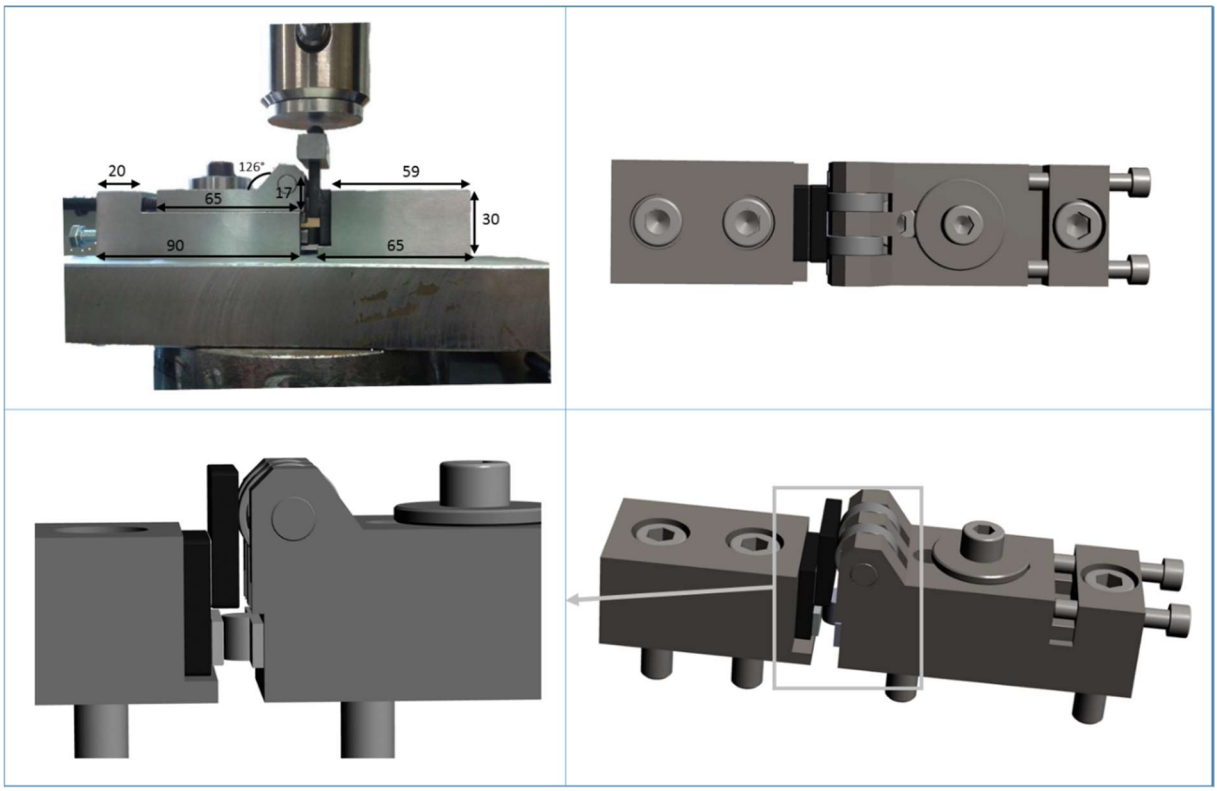

Figure 44: Single Lap Offset fixtures used in this work, (size in mm)

In the case of the asymmetric 4-point bending (A4PB), the elastic shear stress distribution in the joint section is parabolic, exhibiting at mid-height the peak value equal to 1.5 of its mean value. With an elasto-plastic adhesive, plasticity progressively extends under increasing load from midheight to the joined section edges and the ultimate load is, again, attained under a uniform shear stress distribution, equal to the elastic limit of the adhesive, i.e. the shear strength.

Thus, the final situation being similar for both tests (this SLO and A4PB), it is not surprising that the results are nearly equal.

In general terms, it is usually found that interfacial failures lead to lower strength values than cohesive ones, as the potential of the adhesive is not completely exploited. However, in this case the strength of the interface was most likely close to the intrinsic strength of the adhesive, leading to nearly equivalent results in terms of ultimate torque.

However, as already discussed above, it is remarkable that the experimental torsion curves in case of interfacial or cohesive failure of the adhesive show a very different behavior, which can be explained in term of partial or fully exploitation of the adhesive plasticity, respectively.

Finally, to summarize how to correctly use torsion tests results on joined samples, figure 45 shows with a flowchart the procedure to follow in case of brittle (purely elastic) or ductile (elasto-plastic) joining materials.

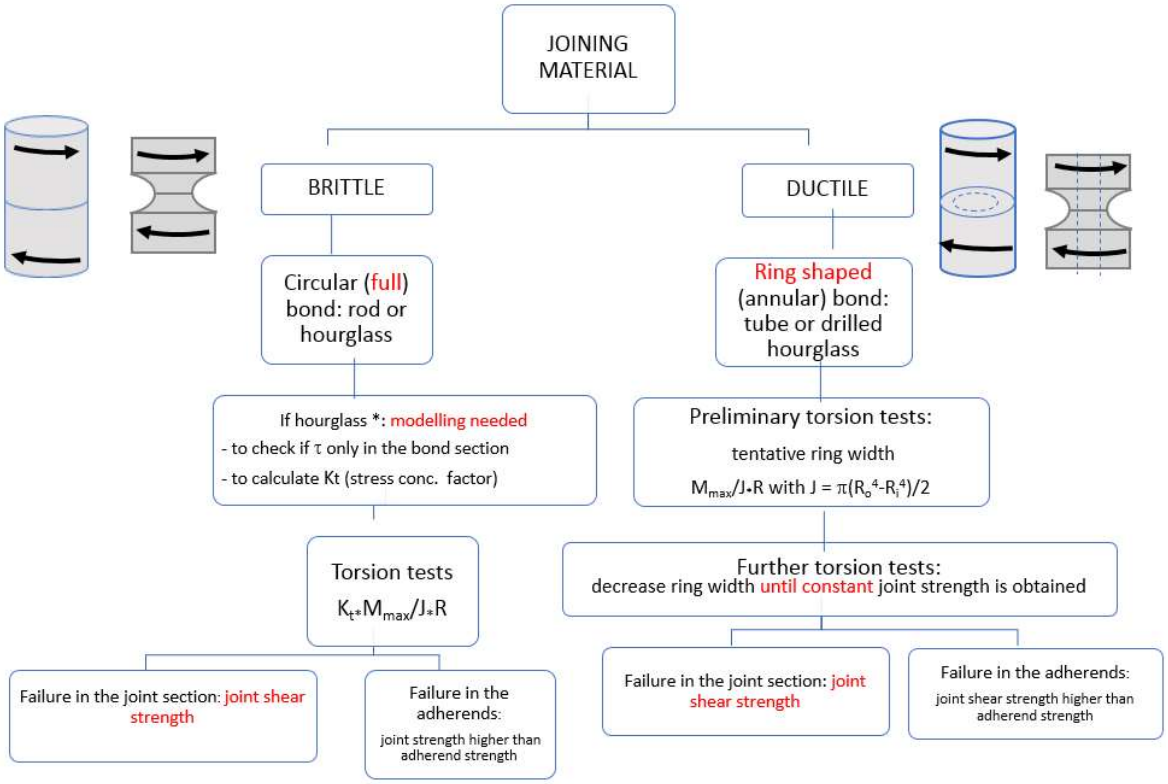

Figure 45: Flowchart for a correct use of torsion tests in case of brittle or ductile (elasto-plastic) joining materials. The ductile protocol is to be used also in the case of brittle joining materials tested at high temperature (e.g. glasses or glass ceramics or polymers as joining materials, when tested above their glass transition temperature)

First of all, the failure must start and propagate in the joined region, in a cohesive mode. Results from failures occurred in interfacial (or mixed cohesive-interfacial as well) are suspicious, as in such a case the stress distribution is not homogenized by plasticity. Samples with failure starting and/or propagating in the substrates must not be considered to calculate the shear strength; in these cases, results might be defined “torsion resistance” of this joined sample, and the joint strength might be higher than the substrate strength [27].

If the adhesive is brittle (purely elastic) [28], once reached the elastic limit the immediate (catastrophic) failure occurs and the joint failure is due to the maximum principal stress in the 45° skew plane: if the brittle joining material is weaker than the adherends, the failure is "confined" in the bond region; however,

if the adhesive is as strong as, or stronger than the adherends, a cone-shaped failure occurs in the joined substrate [28]. A circular full joined sample can be used (hourglass, rod, tube, …). In the case of an hourglass shape, a proper finite element modelling is needed to check if shear stresses are in the bond section only and to

calculate its stress concentration factor (in the case of the THG5, Kt = 1.21-1.29) [27]. It is worth of note that with this geometry no singular behavior at the interface substrate/joining material occurs under torsion [29, 30].

The shear strength of the joined sample can be calculated by:

$\tau = Kt*M/J*R$ (eq. 3)

where *Kt* is the stress concentration factor, the other terms defined as in eq. 1.

A ring-shaped bond in this case does not offer any advantage, on the contrary, it adds possible manufacturing defects that can cause premature failure.

If the adhesive is ductile (elasto-plastic), a ring (annular) shaped joined sample must be used, (tube or drilled hourglass) [31]. Tentative ring width must be tested and gradually decreased in annular section until a constant joint strength is obtained. The shear strength of the joined sample can be then calculated as in eq. 2. The model discussed in this work can be of help in predicting the correct shear strength in case of elasto-plastic joining material. In any case, results should be comparable to A4PB tests results, when available.

It must be underlined that the ductile protocol must be used also in the case of brittle joining materials tested at high temperature (e.g. glasses or glass ceramics or polymers as joining materials, when tested above their glass transition) [32], as their behavior can be regarded as ductile.

In both cases, cohesive failure after torsion in the joint section means joint shear strength, due to maximum shear stress in the joined cross section. It must be remarked that in case of elasto-plastic joining material, the failure occurs in the plane orthogonal to the specimen axis, i.e. the plane of max shear stress. Again, failure in the adherends means a joint shear strength higher than substrate strength.

In case of non-cohesive failures, measured values give nonetheless indication on joint strength for that particular pair adherend-adhesive. However, the obtained values could be lower than those obtained from cohesive failure, typically achievable when the optimal surface treatment is applied.

3.2.2.3. Adhesive: Araldite

The torsion test results for the steel-steel samples joined by Araldite adhesive were:

- THG5 samples: 38 ± 1 MPa (torque-rotation angle curves in figure 46a)
- TDHG samples: 38 ± 4 MPa (torque-rotation angle curves in figure 46b)

So constant shear strength was obtained by decreasing the joined area. To evaluate the contribution of plasticity especially for THG5 samples with larger joined area, it is interesting the comparison between one representative curve for THG5 and one representative curve for TDHG in figure 47. In this case MPa instead of torque is displayed on Y axis to be able to compare the 2 samples on the same level. For TDHG no effect of plasticity can be detected, with linear elastic deformation up to failure. For THG5 some plasticity can be detected, but only after reaching the maximum torque with linear behaviour. And in the end the same shear strength results are obtained for both type of samples.

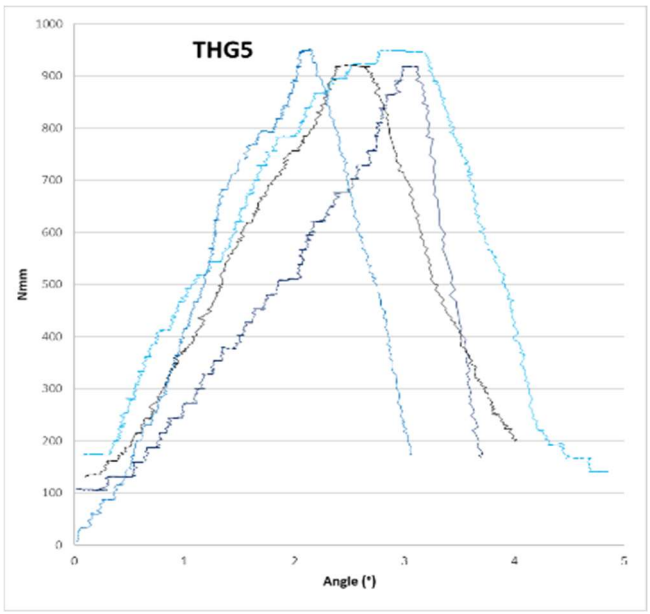

a)

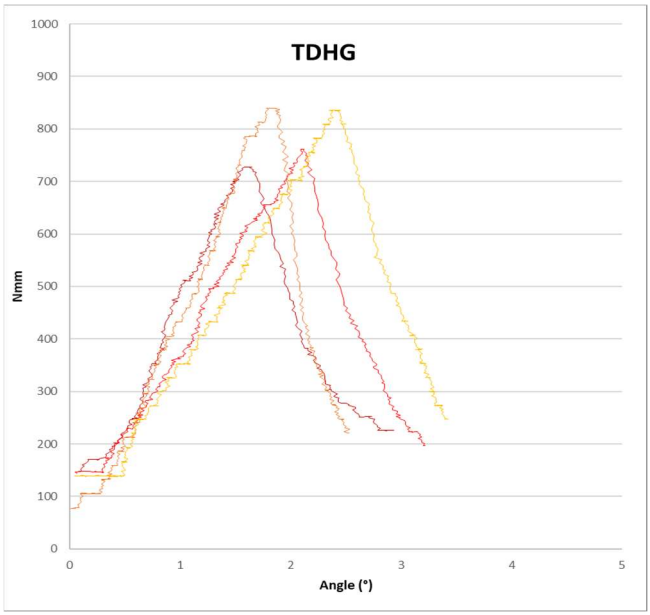

b)

Figure 46: torsion test curves (torque vs angle of rotation) for joined THG5 samples (a); and TDHG samples (b)

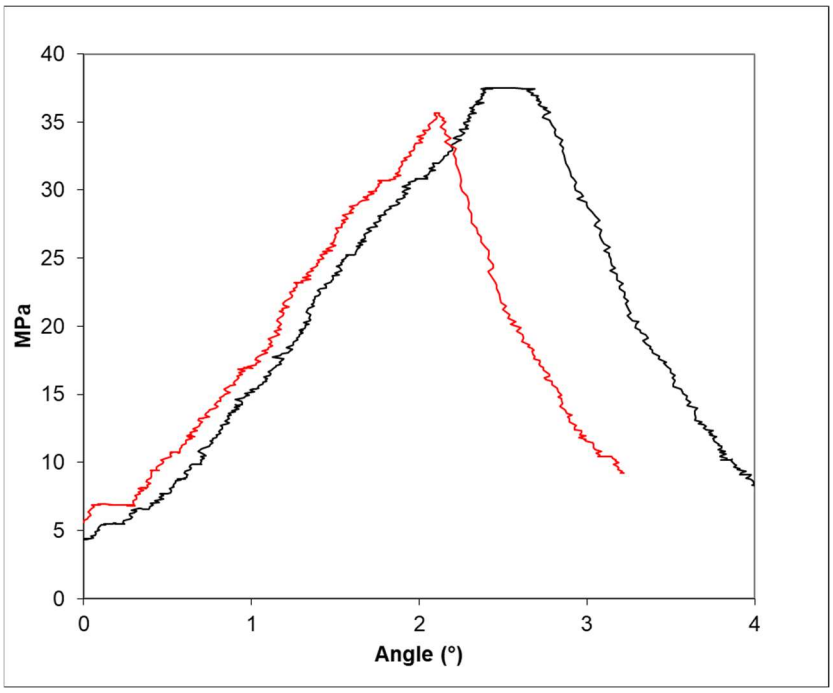

Figure 47: comparison between THG5 (black line) and TDHG (red line) torsion test curves (MPa vs angle of rotation)

This linear elastic behaviour of araldite joined samples is different from what has been shown previously for DP490 and Hysol adhesives, where some plasticity was always detected before reaching the maximum of the torque-angle curve for full joined area samples (THG5).

This behaviour is related to 2 factors; the different type of adhesive itself but also the different type of failure mechanism observed. Figure 48 shows the fracture surfaces after torsion test (figure 48a for THG5 and 48b for TDHG). As can be seen the failure is completely cohesive, with adhesive present on both substrates and covering the full area. Which means the failure proceeded only through the adhesive layer with no effect from the adhesive-steel interface. Also for these torsion test results modelling could give a deeper explanation of the elastic-plastic behaviour of the adhesive, in fact this activity is ongoing.

a)

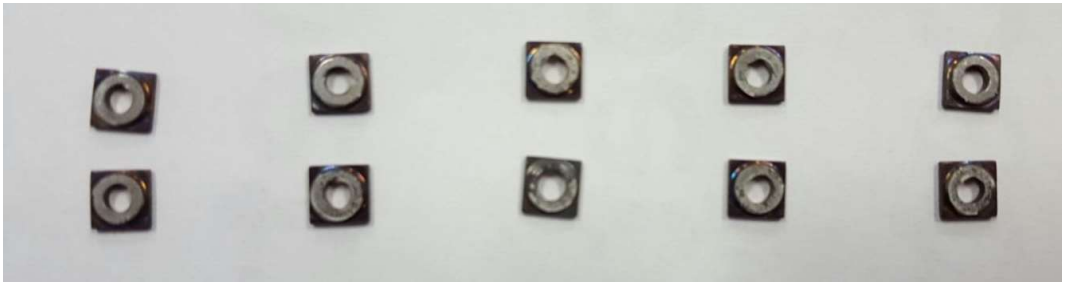

b)

Figure 48: fracture surfaces after torsion test for THG5 samples (a); and TDHG samples (b)

The elastic modulus results are shown in table 13.

When the elastic modulus is measured on the bulk adhesive, a slightly higher result (2,5 ± 0,2 GPa) was obtained by nano-indentation with respect to the impulse excitation technique (IET 2,2 ± 0,2 GPa). On the other hand, the elastic modulus measurement made by nano-indentation of the adhesive directly inside the joint gave a slightly lower value than on bulk specimen with the same technique. This difference might be due to the different curing conditions of the adhesive when it is pressed between two substrates and/or the effect given by the interfaces with steel. In any case the difference is quite small.

For comparison purpose, the elastic modulus of the steel substrates was also measured with nano-indentation and a value of 222,7 ± 4,8 GPa was obtained, in good agreement with the steel producer datasheet.

	nano-indentation		IET
	In the joint	bulk	bulk
Poisson's ratio v	**E_J (GPa)**	**EB (GPa)**	**E_{IET} (GPa)**
0,25	2,2 ± 0,1	2,5 ± 0,2	2,2 ± 0,2

Table 13: Elastic modulus results for Araldite adhesive, measured with nano-indentation directly in the joint and on a bulk sample and with impulse excitation technique (IET) on a bulk sample

A summary of all torsion and shear test results presented in chapter 3.2 (torsion test) is shown in table 14.

Joining material	Substrates	Sample geometry	Test	Shear strength [MPa]
GC1	Steel	THG-5	Torsion	35 ± 9
GC1	Steel	THG-25	Torsion	28 ± 6
GC1	Steel	THG-5	Torsion (600°C)	plastic deformation
GC2	Steel	THG-5	Torsion	49 ± 10
GC2	Steel	THG-25	Torsion	45 ± 17
GC2	Steel	THG-5	Torsion (800°C)	plastic deformation
GC2	Steel	THG-25	Torsion (800°C)	plastic deformation
DP490	Steel	THG-5	Torsion	plastic deformation
DP490	Steel	TDHG	Torsion	plastic deformation
DP490	Steel	THG5-Glass	Torsion	plastic deformation
DP490	Steel	Etched THG5-Glass	Torsion	plastic deformation
DP490	Steel	SGrFS (3 mm)	Torsion	plastic deformation
DP490	Steel	SGrFS (5 mm)	Torsion	plastic deformation
DP490	Steel		A4PB	23 ± 2
Hysol	Steel	THG-5	Torsion	63 ± 5
Hysol	Steel	THG-5	Torsion+modelling	45 ± 4
Hysol	Steel		SLO	42 ± 1
Hysol	Steel		A4PB	42 ± 8
Hysol	SiC	THG-5	Torsion	62 ± 4
Hysol	SiC	THG-5	Torsion+modelling	47 ± 4
Hysol	SiC		SLO	42 ± 1
Hysol	SiC		A4PB	42 ± 5
Hysol	Si_3N_4	THG-5	Torsion	67 ± 6
Hysol	Si_3N_4	THG-5	Torsion+modelling	52 ± 5
Hysol	Si_3N_4		SLO	41 ± 5
Hysol	Si_3N_4		A4PB	39 ± 3
Araldite	Steel	THG-5	Torsion	38 ± 1
Araldite	Steel	TDHG	Torsion	38 ± 4

Table 14: summary of torsion and shear test results (chapter: 3.2 torsion test)

References

(3.2. Torsion test)

1. F. Smeacetto, A. De Miranda, A. Ventrella, M. Salvo, M. Ferraris, Shear strength of glass ceramic sealant for SOFC, J. Am. Ceram. Soc., 97 (2014) 3835–3842.

2. M. Kerstan, C. Rüssel, Barium silicates as high thermal expansion seals for solid oxide fuel cells studied by high-temperature X-ray diffraction (HT-XRD), J. Power Sources 196 (2011) 7578–7584

3. M.J. Pascual, A. Guillet, A. Durán, Optimization of glass-ceramic sealant compositions in the system MgO-BaO-SiO2for solid oxide fuel cells (SOFC), Journal of Power Sources. 169 (2007) 40–46.

4. L. Peng, Q. Zhu, Thermal cycle stability of BaO-B2O3-SiO2 sealing glass, Journal of Power Sources. 194 (2009) 880–885.

5. H. Javed, A.G. Sabato, K. Herbrig, D. Ferrero, C. Walter, M. Salvo, Federico Smeacetto. Design and characterization of novel glass-ceramic sealants for solid oxide electrolysis cell (SOEC) applications, Int. J. Appl. Ceram. Technol. 15 (2018) 999–1010

6. Luca Goglio, Monica Ferraris, Bonding of ceramics: An analysis of the torsion hourglass specimen, Int. J. Adhesion and Adhesives, 70 (2016) 46-52.

7. M. Ferraris, M. Salvo, S. Rizzo, V. Casalegno, S. Han, A. Ventrella, T. Hinoki, Y. Katoh, Torsional shear strength of silicon carbide components pressurelessly joined by a glass-ceramic, Int. J. Appl. Ceram. Technol. 9 (2012) 786-794.

8. M. Ferraris, M. Salvo, V. Casalegno, S. Han, Y. Katoh, H.C. Jung, T. Hinoki, A. Kohyama, Joining of SiC-based materials for nuclear energy applications, J. Nuclear Mater. 417 (2011) 379-382.

9. T. Osipova, J. Wei, G. Pećanac, J. Malzbender, Room and elevated temperature shear strength of sealants for solid oxide fuel cells, Ceram. Int. 42 (2016) 12932-12936.

10. J. Wei, G. Pećanac, J. Malzbender, Review of mechanical characterization methods for ceramics used in energy technologies, Ceram. Int. 40 (2014) 15371-15380.

11. F. Smeacetto, A. De Miranda, A. Ventrella, M. Salvo, M. Ferraris, Shear strength tests of glass ceramic sealant for solid oxide fuel cells applications, Adv. Appl. Ceram. 114 (2015) S70-S75.

12. H. Javed, A.G. Sabato, K. Herbrig, D. Ferrero, C. Walter, M. Salvo, Federico Smeacetto Design and characterization of novel glass-ceramic sealants for solid oxide electrolysis cell (SOEC) applications, Int. J. Appl. Ceram. Technol. 15 (2018) 999–1010

13. M. Ferraris, A. Ventrella, M. Salvo, D. Gross, Shear strength measurement of AV119 epoxy-joined SiC by different torsion tests, Int. J. Appl. Ceram. Technol. 11 (2014) 394-401.

14. S. De La Pierre, T. Scalici, P. Tatarko, A. Valenza, L. Goglio, D. Paolino, M. Ferraris, Torsional shear strength and elastic properties of adhesive bonded glass-to-steel components, Materials and Design, paper under revision.

15. H. Javed, A.G. Sabato, I. Dlouhy, M. Halasova, E. Bernardo, M. Salvo, K. Herbrig, C. Walter, F. Smeacetto, Shear Performance at Room and High Temperatures of Glass–Ceramic Sealants for Solid Oxide Electrolysis Cell Technology, Materials 12 (2019) 298.

16. BSI. BS 5350-C5:2002 Methods of test for adhesives. Determination of bond strength in longitudinal shear for rigid adherends.

17. Nhamoinesu S, Overend M. The mechanical performance of adhesives for a steel-glass composite façade system. Challenging Glas. 3 Conf. Archit. Struct. Appl. Glas. CGC 2012, 2012, p. 293–306.

18. Gleich DM, Van Tooren MJL, Beukers A. Analysis and evaluation of bondline thickness effects on failure load in adhesively bonded structures. J Adhes Sci Technol 2001;15:1091–101.

19. Goglio L, Ferraris M. Bonding of ceramics: An analysis of the torsion hourglass specimen. Int J Adhes Adhes 2016;70:46–52.

20. Ferraris M, Ventrella A, Salvo M, Gross D. Shear strength measurement of AV119 epoxy-joined SiC by different torsion tests. Int J Appl Ceram Technol 2014;11:394–401.

21. Henkel-adhesives, 2018. http://na.henkel-adhesives.com/product-search-1554.htm?nodeid=8806185926657

22. Salvo, M., Casalegno, V., Suess, M., Gozzelino, L., Wilhelmi, C., 2018. Laser surface nanostructuring for reliable Si3N4/ Si3N4 and Si3N4/Invar joined components, submitted (2018).

23. Ferraris, M., Ventrella, A., Salvo, M., Gross, D., 2014. Shear strength measurements of AV119 epoxy-joined SiC by different torsion tests. Int. J. Appl. Ceram. Technol. 11, 394-401.

24. Ferraris, M., Ventrella, A., Salvo, M., Katoh, Y. Gross, D., 2015. Torsional Shear Strength Tests for Glass-Ceramic Joined Silicon Carbide. Int. J. Appl. Ceram. Technol. 12:693-699.

25. Amara, D., Levallois, F., Baziard Y., Petit, J.A., 1996. Study of a single-lap compression-shear test for brittle substrates bonded with a structural adhesive, J. Adhes. Sci. Tech. 10, 1153-1164.

26. Crocombe, A., 1989. Global yielding as a failure criterion for bonded joints. Int. J. Adhes. Adhes. 9,145-153.

27. Goglio L., Ferraris, M., 2016. Bonding of ceramics: An analysis of the torsion hourglass specimen. Int. J. Adh. Adh. 70, 46-52.

28. Ferraris, M., Salvo, M., Rizzo, S., Casalegno, V., Han, S., Ventrella, A., 2012. Torsional Shear Strength of Silicon Carbide, Components Pressurelessly Joined by a Glass-Ceramic. Int. J. Appl. Ceram. Technol. 9, 786–794.

29. Ma, C.-C., Hour, B.-L., 1989. Analysis of dissimilar anisotropic wedges subjected to antiplane shear deformation. Int. J. Solids Structures. 25, 1295-1309.

30. Qian, J., Hasebe, N., 1997. Property of eigenvalues and eigenfunctions for an interface V-notch in antiplane elasticity. Eng. Fract. Mech. 56, 729-734.

31. Ferraris, M., Salvo, M., Casalegno, V., Ventrella, A., Avalle, M., 2012. Torsion Tests on AV119 Epoxy-Joined SiC. Int. J. Appl. Ceram. Technol. 9, 795-807.

32. Fakouri Hasanabadi, M., Faghihi-Sani, M.A., Kokabi, A.H., Malzbender, J., 2017. The analysis of torsional shear strength test of sealants for solid oxide fuel cells. Ceram. Inter. 43, 12546-12550.

4. Conclusions

4.1. Sandwich structures for aerospace applications

4.1.1. Joining of sandwich structures

The aim of this work was to develop and test a high performance adhesive able to join Zerodur™ to Carbon Fiber Reinforced Polymer (CFRP) honeycomb (HC) in a sandwich structure for aerospace applications. The main problem was to find an adhesive having suitable thermomechanical stability such as sound mechanical strength, low coefficient of thermal expansion and ease of application on large components *together with a* curing temperature lower than 160 °C, to avoid detrimental effects on the CFRP matrix itself.

Two phenolic- and one cyanate ester- based adhesives have been tested. One phenolic based adhesive already proven effective for joining of carbon/carbon composites (C/C) has been used in this work to join CFRP slabs and Zerodur™ - CFRP - Zerodur™ sandwich structures with a longer curing time, but lower temperature (150 °C) than the one used to join C/C (260 °C). To verify the properties of the phenolic adhesive cured at 150°C, it was characterized by dilatometry, thermogravimetric analysis (TGA) with differential thermo-gravimetry (DTG) and Thermo-Gravimetric-Evolved Gas analysis (TGA-EGA). And compared with the other adhesives.

The phenolic adhesive cured at 150 °C was considered the most suitable choice to join CFRP to Zerodur™ for aerospace applications, and was mechanically tested by measuring the lap shear strength of joined CFRP slabs as joined and after thermal cycling. The joints kept the same strength before and after ageing demonstrating the ability of the adhesive to resist in the aerospace environment.

Zerodur™ - CFRP - Zerodur™ sandwich structures joined by the phenolic adhesive cured at 150 °C have been also tested in tensile and lap shear mode, and the resulted measured strength fulfilled the aerospace requirement specifications.

In figure 49 is shown the 600 mm diameter sandwich breadboard structure manufactured at TAS Cannes, with Zerodur skins and CFRP honeycomb joined by the phenolic adhesive cured at 150 °C.

This activity was developed in the frame of the EU 2020 project SMS (Sandwich Materials and Structure).

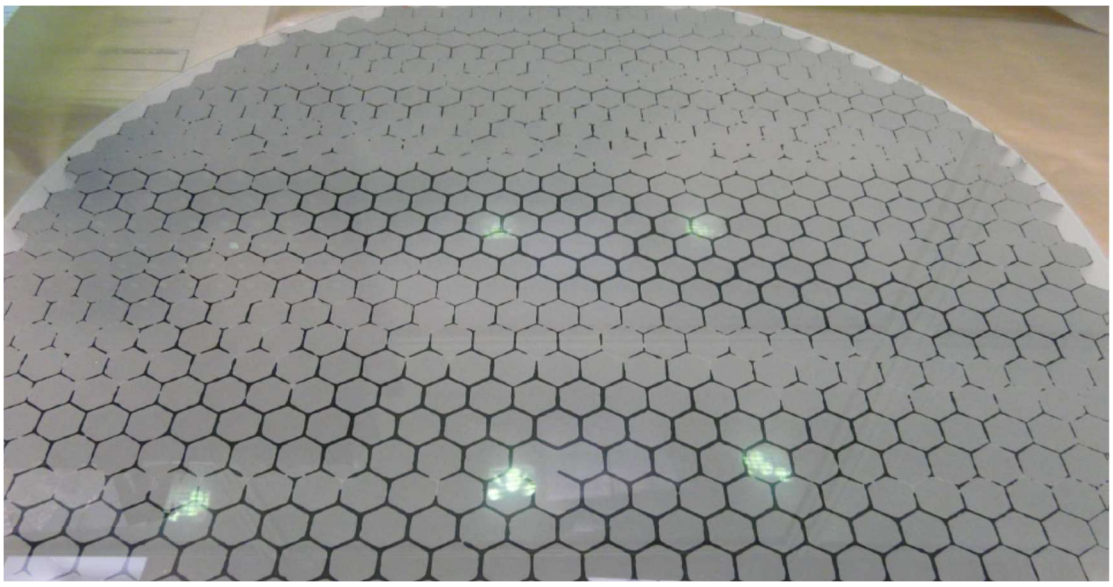

Figure 49: The final breadboard (600 mm diameter manufactured at TAS Cannes, France)

4.1.2. CFRP surface modification

The original etching procedure described in this thesis (figure 50), based on controlled sulfuric acid etching on the CFRP surface, was found effective in increasing up to 100% the mechanical strength (lap shear) of adhesive joined etched CFRP slabs.

Also the etched Honeycomb CFRP based sandwich structures showed an increased tensile strength compared to the non-etched ones.

The "brush" CFRP, successfully obtained by the alumina/hydrogen peroxide modified etching process is still to be optimized in term of adhesive infiltration in the brush structure.

Tests are ongoing to test these etching protocols at the industrial scale: even though the use of acids is more complex to manage than mechanical abrasion commonly used to increase adhesive joint strength, this method has the advantage of leaving fibers unaffected. Furthermore, the proposed etching can be useful to join CFRP with other adhesives such as, for instance epoxy-based ones.

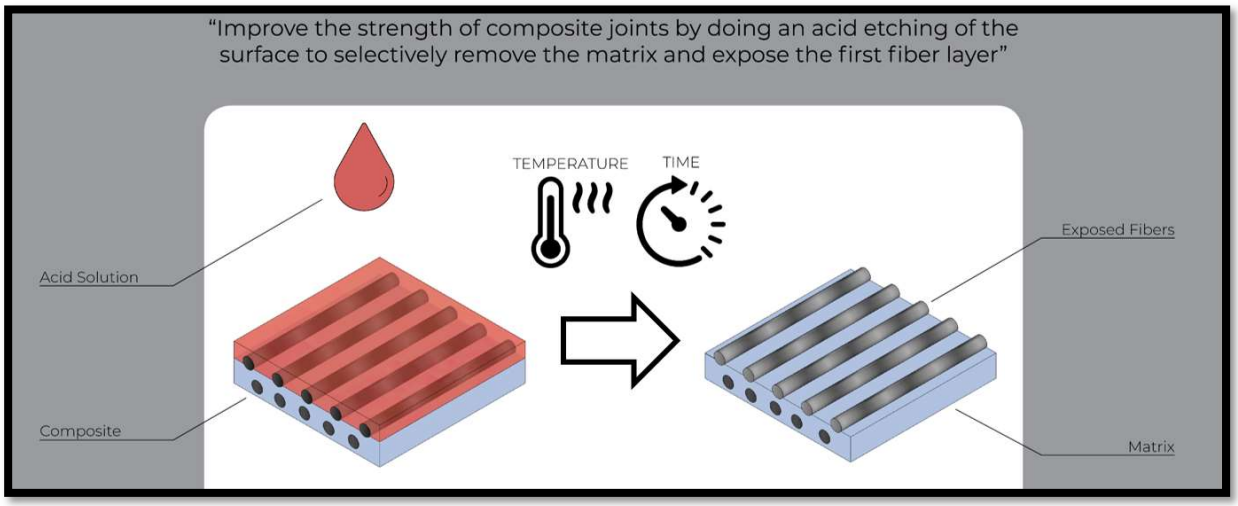

Figure 50: Scheme of the CFRP Etching process to increase joint strength [7].

4.2. Torsion test

The aim of this work was to provide designers with reliable shear strength and elastic properties for almost any kind of joined component. For this reason different types of joining materials have been studied; ranging from brittle glass-ceramic sealants for SOFC/SOEC applications to elasto-plastic adhesives for structural applications. Furthermore, Torsion test proved to be a valuable method to asses the shear strength of joints. When the correct conditions and samples are employed, it is possible to obtain size independent shear strength results, that can be used to design larger and more complex components and structures.

4.2.1. Glass-ceramic sealants for SOFC/SOEC applications

This work focused on the shear strength measured by torsion test on two different glass-ceramic sealants used to join Crofer22APU substrates for SOFC/SOEC stacks.

The shear stresses are measured by torsion test for two different sealants by measuring their behavior at room temperature and at application relevant temperatures. The results are supported by extensive post-operation characterizations by using electron microscopy and compositional analysis on the fracture surfaces.
Statistically identical shear stress values were measured by torsion at room temperature for joined hourglass shaped samples of different size, thus confirming the size independence of the measured shear strength values. Experimental post-test examinations confirmed that interfaces play a strong role regarding the measured shear strength and provide important insights with respect to integration of metallic and glass-ceramic components in SOFC/SOEC stacks.

In addition to this, the high temperature (600-850°C) torsion tests were fundamental to understand the behavior of the sealants at operation temperatures. However in this case the shear strength could not be calculated directly from torsion test, due to the effect of plasticity that has to be taken into account. Since both sealants were tested at temperatures above their Tg and close to the softening point.

4.2.2. Structural adhesives

4.2.2.1. Adhesive: DP490

The aim of this part was to measure the pure shear strength and elastic modulus for design and modelling of adhesive joined glass-to-steel structures

An epoxy resin adhesive EPX DP490 (3M™ Scotch-Weld™ Epoxy Adhesive) was used as joining material for AISI304 steel and soda-lime glass. Several steel-to-steel and steel-to-glass joined samples were tested in torsion and asymmetrical four-point bending. Torsion curves showed an evident nonlinear plastic behaviour in almost all cases. Finally, the full-scale steel component joined to a glass slab provided a quasi-linear behaviour, when the width of the ring-shaped steel component was reduced to 3 mm.

The elastic modulus of the adhesive was measured by nano-indentation technique both in the joined area and in the adhesive as a bulk specimen, together with an impulse excitation technique, for comparison purposes; suggesting a lower elastic modulus for the adhesive when constrained in a joint.

A simplified equivalent torsion bar made of an elastic-perfectly plastic material was also considered to model the ductile-brittle behaviour of the adhesive joints. The simplified model was in good agreement with the experimental data and permitted to estimate the positive effect of the etching process made on glass slabs before joining to steel.

The two main findings of this work are the following: i) when the joining material is not purely brittle, several ring shaped joined samples with decreasing ring width should be prepared and tested, until a purely linear behaviour of the torsion curve versus angle curve is obtained, to obtain the shear strength; ii) when the adhesive is inside the joined volume, its elastic modulus may be lower than what measured on a bulk, un-constrained adhesive.

4.2.2.2. Adhesive: Hysol

This work aims to assess the shear strength values of adhesively joined ceramics (SiC, Si_3N_4) and steel in case of an elasto-plastic (ductile) joining material; comparing Torsion test with different shear tests commonly employed (A4PB, SLO).

On the basis of an experimental campaign and an analytical model, this work tries to shed some light on the assessment of the shear strength in case of an elasto-plastic (ductile) joining material. Logically, the different testing techniques, if correctly applied, should give the same result of shear strength of the joining material under examination.

Thus, if the torsion test with hourglass specimens is adopted, the experimental strategy to deal with the effect of plasticity is using hollow specimens (TDHG) with increasing inner diameter until the obtained strength (simply evaluated as in elastic regime) converges to a constant value. The validity of such approach is supported by the analytical model proposed.

Alternatively, the same model can be used to evaluate the shear strength by fitting the measured moment-rotation curve with the analytical one. In this way, also the shear modulus can be obtained. Obviously, all these expedients become unnecessary in case of a brittle joining material, exhibiting linear behavior until failure, as the calculation of the strength can be obtained by the torsion elastic formula. However, in such a case the stress concentration at the outer radius (Re) due to the hourglass shape cannot be neglected to obtain the true shear strength. It is also worth noting that in such a case the use of a hollow torsion specimen brings no advantage and, conversely, the defects possibly introduced by the manufacturing process may alter the results.

The consideration expressed on torsion can be of help in deciding the testing procedure fit to the case under examination.

4.2.2.3. Adhesive: Araldite

To confirm what has been discovered in the previous two paragraphs on the shear strength of elasto-plastic (ductile) joining materials, a third epoxy adhesive was studied for comparison.

Adhesive joined steel substrates were tested in Torsion and size independent shear strength results were calculated for full- and ring-joined hourglass samples. Fracture surfaces after torsion were analysed, revealing a completely cohesive failure (fracture propagation only inside the adhesive).

Furthermore the elastic properties of the adhesive were evaluated with nano-indentatio and impulse excitation technique. With this analysis, Araldite showed the same behaviour of DP490 adhesive, with elastic modulus values slightly lower for the material inside the joint when compared with the same test on a bulk specimen.

Finally, 5 different joining materials (2 glass-ceramics and 3 adhesives) were tested in Torsion. Different sample size and different testing temperatures were compared. Elasto-plastic behaviour of joining materials was studied, with the help of modelling too.

For all studied materials it was possible the calculation of a shear strength value, derived from Torsion testing, that can be used for design purposes for the intended application.

Advanced joined materials development and their shear strength evaluation for aerospace, energy and structural applications

Stefano De la Pierre des Ambrois